Structural Analysis of Monomeric Isocitrate Dehydrogenase from *Corynebacterium glutamicum*

A Thesis Submitted to the College of

Graduate Studies and Research

In Partial Fulfillment of the Requirements

For the Degree of Master of Science

In the Department of Biochemistry

University of Saskatchewan

Saskatoon

By

Fumie Imabayashi

Keywords: protein crystallography, conformational changes, mutagenesis

© Copyright Fumie Imabayashi, September 2004. All rights reserved.

Permission to Use

In presenting this thesis in partial fulfilment of the requirements for a Postgraduate degree from the University of Saskatchewan, I agree that the Libraries of this University may make it freely available for inspection. I further agree that permission for copying of this thesis in any manner, in whole or in part, for scholarly purposes may be granted by the professor or professors who supervised my thesis work or, in their absence, by the Head of the Department or the Dean of the College in which my thesis work was done. It is understood that any copying or publication or use of this thesis or parts thereof for financial gain shall not be allowed without my written permission. It is also understood that due recognition shall be given to me and to the University of Saskatchewan in any scholarly use which may be made of any material in my thesis.

Requests for permission to copy or to make other use of material in this thesis in whole or part should be addressed to:

Head of the Department of Biochemistry

University of Saskatchewan

Saskatoon, Saskatchewan S7N 5E5

Abstract

In this research project, structural aspects of monomeric NADP+-dependent isocitrate dehydrogenase from *Corynebacterium glutamicum* (CgIDH) are investigated together with site-directed mutagenesis and fluorescence spectroscopy studies. CgIDH, one of the enzymes of the Krebs cycle, catalyzes the decarboxylation of isocitrate into α-ketoglutarate, which in some bacteria and plants regulates the flow of carbon into either the Krebs cycle or the glyoxylate

bypass depending on the available carbon source. The structure of CgIDH complexed with Mg2+ has been determined at 1.75 Å resolution using X-ray crystallography. In contrast to the closed conformation of published structures of monomeric NADP+-dependent IDH from *Azotobactor vinelandii* complexed with either isocitrate-Mn2+ or NADP+, the structure of CgIDH complexed with Mg2+ demonstrates the open conformation. The superimposed structure of CgIDH complexed with Mg2+ onto the structures of AvIDH complexes reveals that Domain II is rotated ~24° or ~35º, respectively, relative to Domain I when isocitrate-Mn2+ or NADP+ is bound, resulting in the closure of the active site between the two domains. Fluorescence spectroscopic studies support the proposal that the presence of isocitrate or NADP+ could mediate the conformational changes in CgIDH.

In addition, three CgIDH mutants (S130D, K253Q, and Y416T) were created based on the structural analysis and previous mutagenesis studies of homodimeric NADP+-dependent IDH. Both the specific activities and the fluorescence spectra of these CgIDH mutants elucidate the roles of these active site residues in CgIDH catalysis. It has been suggested that the conformational changes observed in the presence of the substrate(s) may regulate enzymatic activity in CgIDH, in contrast to homodimeric NADP+-dependent IDH in *Escherichia coli*, where the phosphorylation cycle controls activity. It is also presumed that both Lys253 and Tyr416 may play critical roles in CgIDH activity, as do the equivalent residues in homodimeric IDH from porcine heart mitochondria. Similar structural features and conformational changes among monomeric CgIDH and homodimeric NADP+-dependent IDH enzymes suggest the phylogenetic relationships among various monomeric and homodimeric NADP+-dependent IDH from different sources.

ACKNOWLEDGEMENTS

I would like to express my heartfelt gratitude to my supervisor, Dr. Louis T. J. Delbaere. From the undergraduate, he has provided the great opportunities to pursue my interests in the research. I am extremely grateful to Dr. Delbaere for allowing me to work on a wide range of the research techniques.

I would like to thank the members of my Advisory committee and all of the Faculty members of the Department of Biochemistry. Your helpful suggestions and encouragement have been greatly appreciated.

Financial support has been provided from the Saskatchewan Synchrotron Institute and from the CHIR grant to Dr. Delbaere.

I wish to thank all members of the BioCARS facility at the Advanced Photon Sources (APS) (Argonne, IL, U.S.A.) for technical support with regard to the X-ray diffraction data collection. I would like to thank Doug Olson at Mass Spectrometry Unit and the technicians of the Oligo Synthesis and of the DNA sequencing Units for their technical support.

I wish to express thank to all of our lab members for their support. Dr. Sanjukta Aich did the early work on monomeric IDH project. She has provided numerous laboratory techniques and helpful discussions through the entire research for this thesis. Dr. Lata Prasad taught me a practical computational crystallography. Yvonne Leduc did inventory organization of our lab facilities and provided technical suggestions.

I would also like to thank all of the graduate students in the Department of Biochemistry for their friendship. I wish to express a special thank to Tricia for her friendship.

I would like to thank my sister, Yoko, for her graphic work in this thesis. I really thank my mother and father, who have been always supported and encouraged me across the sea.

With love,
To mom and dad, Masako and Tetsuo,
And my sister, Yoko,
You taught me to learn and to practice,
And to my dearest dogs,
You inspired the nature and life.

Table of Contents

List of Tables

List of Figures

List of Abbreviations

A	absorbance
ATP	adenosine triphosphate
AvIDH	*Azotobactor vinelandii* isocitrate dehydrogenase
ASU	asymmetric unit
CCP4	Collaborative Computing Project Number 4
CNS	Crystallography and NMR system
CgIDH	*Corynebacterium glutamicum* isocitrate dehydrogenase
DTT	dithiothreitol
EcIDH	*Escherichia coli* isocitrate dehydrogenase
EDTA	ethylenediaminetetraacetic acid
GST	glutathione S-transferase
HcIDH	Human cytosolic isocitrate dehydrogenase
I	intensity
IC	internal conversion
IBP	isosbestic point
IDH	isocitrate dehydrogenase
IMDH	isopropylmalate dehydrogenase
IPTG	isopropyl -D-thiogalactopyranoside
Isocitrate	trisodium-DL-isocitrate
LB	Luria Bertani
M2+	metal divalent cation
T_m	melting temperature
MPD	2-methyl-2,4-pentanediol
MS	mass spectrometry
MR	molecular replacement
MES	2-morpholineethanesulfonic acid
MOPS	3-[N-morpholino] propane sulfonic acid
NAD+	nicotinamide adenine dinucleotide, oxidized form
NADP+	nicotinamide adenine dinucleotide phosphate, oxidized form

NADPH	nicotinamide adenine dinucleotide phosphate, reduced form
PAGE	polyacrylamide gel electrophoresis
PCR	polymerase chain reaction
PEG	polyethylene glycol
PEG 2000 MME	polyethylene glycol 2000 monomethyl ether
pH	negative logarithm of the hydrogen ion concentration
SDS	sodium dodecyl sulfate
TEA	triethanolamine
TEMED	N,N,N',N'-tetramethylethylene-diamine
Tris	tris-[hydroxymethyl]aminomethane
UV	ultra violet

Chapter 1 Introduction

1.1 Isocitrate dehydogenase (IDH)

1.1.1 General properties

Isocitrate dehydrogenase (IDH) is one of the enzymes involved in the Krebs cycle. This enzyme catalyzes the oxidative decarboxylation of 2R, 3S-isocitrate with $NAD(P)^+$ to yield α-ketoglutarate, CO_2 and NAD(P)H. This catalytic reaction requires a divalent metal cation such as Mg^{2+} or Mn^{2+}.

$$\text{Isocitrate} + NAD(P)^+ \leftrightarrow \alpha\text{-ketoglutarate} + CO_2 + NAD(P)H$$

Because isocitrate is decarboxylated at the β-carbon position to yield carbon dioxide, and because $NAD(P)^+$ is reduced to NAD(P)H, IDH belongs to the β-decarboxylating dehydrogenase family of enzymes. The amino acid sequences of IDH enzymes show less than 10% identity to other dehydrogenases except isopropylmalate dehydrogenase (IMDH), which is 23% identical to IDH. Because of this low identity to other dehydrogenases, it is believed that IDH has evolved differently from other dehydrogenases (Chen and Gadal, 1990).

The IDH enzymes are divided into two groups, NAD^+- and $NADP^+$-dependent, based on the coenzyme specificity. NAD^+-dependent IDH (EC 1.1.1.41) is hetero-oligomeric and is found only in eukaryotes, whereas $NADP^+$-dependent IDH (EC 1.1.1.42) is ubiquitously present in both prokaryotes and eukaryotes. In general, NAD^+-dependent IDH has a larger molecular mass than $NADP^+$-dependent IDH, e.g. the $NADP^+$-dependent pig heart enzyme is a tetramer of 340 kDa molecular mass, and incidentally catalyzes an irreversible reaction (Chen and Gadal, 1990). The reaction catalyzed by NAD^+-dependent IDH is allosterically regulated by AMP, citrate and its catalytic products (NADH and α-ketoglutarate). On the other hand, $NADP^+$-dependent IDH catalyzes the same reaction in a reversible manner but no allosteric control has been identified (Chen and Gadal, 1990). $NADP^+$-dependent IDH is further classified into homodimeric and monomeric structural forms. While most prokaryotes and eukaryotes have a homodimeric $NADP^+$-dependent IDH with two identical subunits of 40-50 kDa, a few bacteria, including *Vibrio* species (Ochiai *et al*., 1979; Fukunaga *et al*., 1992; Steen *et al*., 1998), *Mycobacterium bovis* (Florio *et al*., 2002), *Azotobactor vinelandii* (Suzuki *et al*., 1995; Sahara *et al*., 2002) and *Corynebacterium glutamicum* (Eikmanns *et al*., 1995) contain a monomeric form of $NADP^+$-dependent IDH.

1.1.2 Proposed reaction mechanism

According to the proposed catalytic mechanism (Figure 1.1) (Hurley *et al*., 1991; Stoddard and Koshland, 1993), the hydroxyl group of isocitrate is first deprotonated by an enzymatic general base. The resultant hydride is then removed and transferred to $NAD(P)^+$ so that NAD(P)H is produced. Next, the intermediate, S-oxalosuccinate, is decarboxylated at the β-carboxyl group. This intermediate associated with IDH releases carbon dioxide and then is protonated to generate α-ketoglutarate.

1.1.3 Biological roles

The catalytic regulation of IDH plays an important role because isocitrate is a common intermediate for both the Krebs cycle and the glyoxylate bypass in plants and in some bacteria (Chen and Gadal, 1990). In the Krebs cycle, the oxidative decarboxylation of isocitrate is catalyzed by IDH to produce α-ketoglutarate. Isocitrate lyase, on the other hand, mediates the conversion of isocitrate into glyoxylate in the glyoxylate bypass (Figure 1.2). The glyoxylate bypass is the essential metabolic pathway to produce glucose from acetyl-CoA when acetate is the only carbon source available for growth. Some bacteria and plants possess this pathway in their mitochondria and in the glyoxysome, so that these organisms can adapt their metabolic processes, depending on the carbon sources available for their growth (Chen and Gadal, 1990).

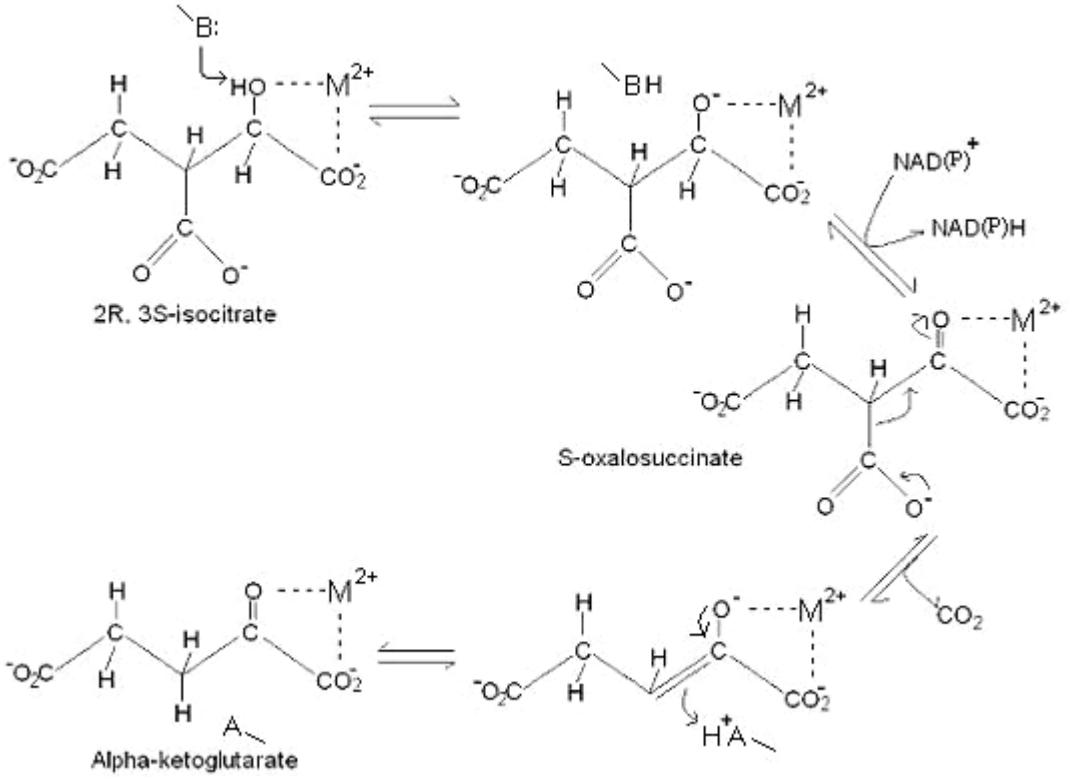

Figure 1.1 The proposed reaction mechanism of $NAD(P)^+$-dependent IDH (Hurley *et al*., 1991; Stoddard and Koshland, 1993).

$NAD(P)^+$-dependent IDH converts 2R, 3S-isocitrate into α–ketoglutarate as well as $NAD(P)^+$ into NAD(P)H and releases CO_2. The half-arrows represent the direction of the catalytic reaction and the release of products (NADPH and CO_2), and the curved arrows indicate the movements of electrons in the reaction. A general base (B) and a general acid (A) are from the enzyme. The coordination of the divalent metal cation (M^{2+}) is drawn as a dashed line.

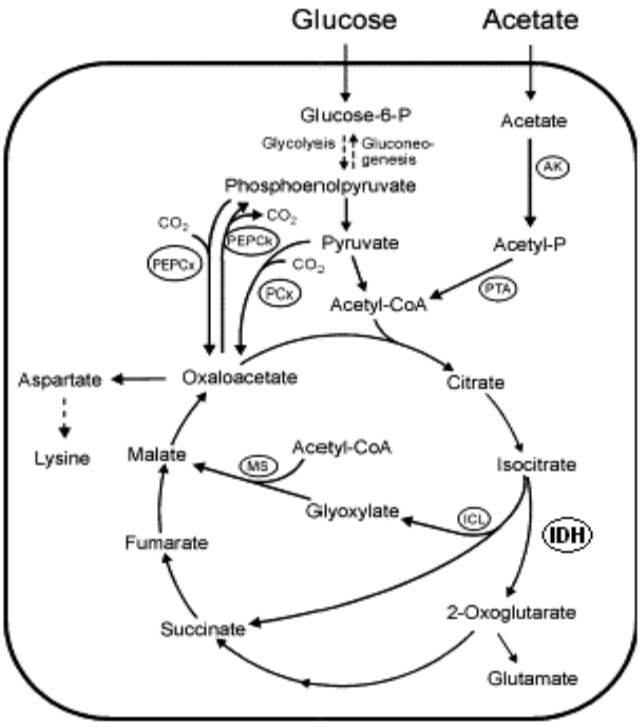

Figure 1.2 Central metabolism in some bacteria and in plants during growth on glucose and acetate.

Both the Krebs cycle and the glyoxylate bypass during growth on glucose and acetate, respectively, are illustrated. The dashed arrows represent metabolic pathways including several reactions, and the solid arrows show single reactions. The enzymes involved in the reaction are abbreviated and indicated in the circles. AK, acetate kinase; PTA, phosphotransacetylase, IDH, isocitrate dehydrogenase; ICL, isocitrate lyase; MS, malate synthase; PEPCK, phosphoenolpyruvate carboxykinase; PCx, pyruvate carboxylase; PEPCx, phosphoenolpyruvate carboxylase. Adapted from Gerstmeir *et al*., 2003.

Both NAD(P)H and α-ketoglutarate as the end products of the IDH catalysis are essential not only for energy production but also for the biosynthesis of other cellular components in higher organisms. Whereas NAD^+-dependent forms of IDH participate in energy production via the electron transport system within the mitochondrial matrix, the function of the $NADP^+$-dependent forms of IDH is not fully understood. It has been suggested that $NADP^+$-dependent IDH could be involved in the biosynthesis of glutamate and other cellular compounds (Chen and Gadal, 1990).

Recently, an anti-oxidant effect of $NADP^+$-dependent IDH has been suggested based on results showing that the number of surviving *E. coli* cells after ionizing radiation were reduced in the absence of IDH (Lee *et al*., 1999). The inactivation of $NADP^+$-dependent IDH by nitric oxide has also been reported (Lee *et al*., 2002; Yang *et al*., 2002). Cardiac mitochondrial $NADP^+$-

dependent IDH has also been shown to be modified by the lipid peroxidation product and inactivated *in vivo* and *in vitro* (Benderdour *et al*., 2003). These studies proposed that the $NADP^+$-dependent IDH would play a role in a cellular defence mechanism against oxidative stress-induced damage because NADPH produced from IDH catalysis is a critical requirement for the reduction of free radicals.

1.2 Homodimeric $NADP^+$-dependent IDH from *Escherichia coli* (EcIDH)

1.2.1 General properties

$NADP^+$-dependent IDH in *Escherichia coli*, (EcIDH) is a homodimer with molecular mass of ~45 kDa for each subunit and is encoded by the 1.9 Kb *icd* gene. It has been studied extensively in terms of its kinetic properties, mutagenesis, and structural analysis. Among the 416 residues in each polypeptide chain of this enzyme, serine 113 was identified at the active site and as the crucial residue for the regulation of EcIDH activity (LaPorte and Koshland, 1983). The topology of the solved EcIDH structure revealed the absence of a typical nucleotide ($NADP^+$)-binding site that is often observed in other $NADP^+$-dependent dehydrogenases (Hurley *et al*., 1989).

Regulation of EcIDH activity plays an essential role in *E. coli* to adapt the metabolic pathways, to the available carbon source (Holms and Nimmo, 1982). In the presence of glucose, the Krebs cycle, via EcIDH activity, prefers to produce catabolites and energy in the form of ATP and NADPH, required for the biosynthesis of other cellular components. In some bacteria and in plants, however, when growing on acetate as a sole carbon source, the glyoxylate bypass is utilized to prevent the loss of carbons from acetate so that acetate carbons are used for synthesis of further cellular constituents (Figure 1.2). Because these two different enzymes require the same substrate, the competition between EcIDH and isocitrate lyase toward isocitrate determines the direction of flow of isocitrate. From kinetic studies, the Michaelis-Menten constant (K_m) values for EcIDH and isocitrate lyase were 8 μM and 600 μM, respectively (LaPorte *et al*., 1985), indicating that EcIDH exhibits a much higher affinity toward isocitrate than does isocitrate lyase. In other words, EcIDH can bind to isocitrate effectively even at a low concentration of isocitrate, but isocitrate lyase requires a high concentration of isocitrate. Hence, EcIDH has to be inactivated and then lose its higher affinity toward isocitrate, so that isocitrate

lyase is able to utilize isocitrate in the glyoxylate bypass. Therefore, EcIDH is the key enzyme which contributes major control over the flow of isocitrate into either the Krebs cycle or the glyoxylate bypass for bacterial growth, depending on the available carbon source (Holms and Nimmo, 1982; LaPorte *et al*., 1985).

1.2.2 Phosphorylation cycle for regulation of catalytic activity

Phosphorylation as a means of regulation of EcIDH activity was first proposed as an example of protein phosphorylation, in which the specific endogenous substrate for the protein kinase had been identified (Garnak and Reeves, 1979). When *E. coli* was grown on acetate, EcIDH activity was significantly decreased, and EcIDH became phosphorylated (Garnak and Reeves, 1979; Reeves and Malloy, 1982). It has been suggested that inactivation of EcIDH via phosphorylation might switch on the glyoxylate bypass by isocitrate lyase so that bacteria can grow in the presence of acetate (Reeves and Malloy, 1982). This hypothesis was further supported by a study that showed that neither lower expression nor overproduction of IDH appeared to disturb *E. coli* growth on acetate (Garnak and Reeves, 1979). This indicated that a constant level of EcIDH activity could be maintained by converting EcIDH into the inactive form via a phosphorylation cycle. Such adaptation is probably dependent on growth conditions.

The phosphorylation of EcIDH occurs at a single serine residue, Ser113, according to various kinetic studies and structural analysis (Thorsness and Koshland, 1987; Hurley *et al*., 1989; Dean and Koshland, 1993). This serine residue was mutated to Ala, Cys, Thr, Tyr, Glu, and Asp, in order to determine the role of the functional group of its side chain and its impact on the phosphorylation cycle of EcIDH. The introduction of a negatively-charged side chain (Glu, Asp) completely inactivated EcIDH, whereas a neutral side chain lowered its catalytic activity (Thorsness and Koshland, 1987). Phosphorylated EcIDH was also detected only when the residue at position 113 was serine (Thorsness and Koshland, 1987). These results confirm that EcIDH would be inactivated when either a negatively-charged side chain or phosphorylation of the Ser residue was introduced at this position.

Two residues, Tyr160 and Lys230, at the active site in EcIDH have been also suggested as essential residues that interact with the β-carbon of isocitrate to release CO_2 during decarboxylation (Lee *et al*., 1995). When Tyr160 was substituted by phenylalanine, the catalytic activity of this mutant was reduced by 250-fold (Lee *et al*., 1995). Furthermore, mutation of

Lys230 to methionine lowered both the catalytic activity and the affinity toward isocitrate by 100-fold and 500-fold, respectively (Lee *et al*., 1995). In addition, decarboxylation of oxalosuccinate was not detected for this mutant, suggesting a role for Lys230 in both substrate binding and decarboxylation (Lee *et al*., 1995).

1.2.3 Structural studies

1.2.3.1 Isocitrate-Mg^{2+}complex

The first EcIDH structure (PDB; 5ICD) solved to 2.5 Å resolution revealed that the topology of this EcIDH dimer was different from the other known dehydrogenase structures (Hurley *et al*., 1989, 1990). The tertiary structure consisted of three domains for each subunit, a large domain, a small domain, and a clasp-like domain (Figure 1.3). The large domain spanned residues 1-124 and 318-416 and contained both the N and C termini, which formed eight α-helices (a-d and j-m) and five β-strands (A-E), respectively. The small domain consisted of residues 125-157 and 203-317 with a typical α/β sandwich structure, formed from four α-helices (f-i) and six β-strands (F-L). The clasp-like structure was formed from one α-helix (e) and two β-strands (M-N) corresponding to residues 158-202. This clasp region in the EcIDH dimer structure is unique because it is composed of two α-helices and four-stranded anti-parallel β-strands, of which one α-helix and two β-strands are donated by each of two subunits, indicating that this unique clasp region would play a role for the dimer interlock. The proposed phosphoserine residue, Ser113, was also identified to lie on the protein surface at the edge of the pocket between two domains, suggesting that this residue would be accessible to IDH kinase/phosphatase (IDHK/P) in the EcIDH phosphorylation cycle (Hurley *et al*., 1989, 1990).

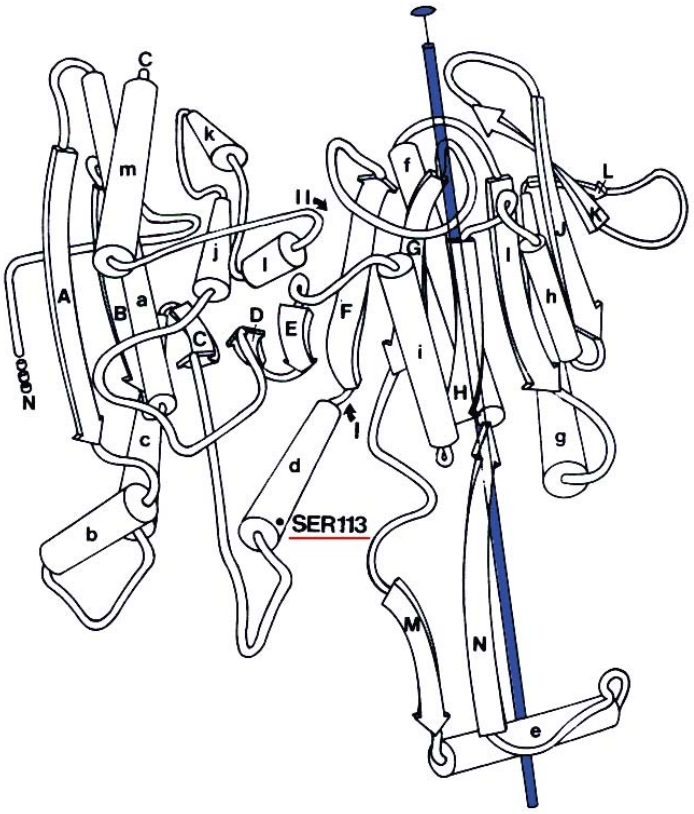

Figure 1.3 Overall structure of one subunit of EcIDH.

The cylinders labelled with lower case letters represent α–helices; the arrows form β-strands labelled with capital letters; and the string indicates the random coils of the structure. The phosphoserine residue, Ser113, is underlined in red. The blue stick shows the two-fold axis present in the dimer. Adapted from Hurley *et al*., 1989, 1990.

The structure of EcIDH complexed with isocitrate and Mg^{2+} (PDB; 5ICD) has also been determined to 2.5 Å resolution (Hurley *et al*., 1991). The divalent metal cation, Mg^{2+}, was coordinated by Asp307, Asp283′ (the prime represents a residue from the second subunit of the dimer), and two water molecules in an octahedral arrangement. The Mg^{2+} cation was also coordinated to the α-carboxylate and the α-hydroxyl oxygen of isocitrate in order to stabilize the negative charge formed on the hydroxyl oxygen when isocitrate is converted to α–ketoglutarate during decarboxylation and dehydrogenation. Isocitrate is bound at the pocket between the large and small domains of each subunit, and hydrogen bonds are formed between isocitrate and Ser113, Arg119, Arg129, Arg153, Tyr160 and Lys230′ (Figure 1.4). While five water molecules interacted with isocitrate-Mg^{2+}, Asn115 was also a possible candidate to interact with isocitrate. Compared to the IMDH structure (Wallon *et al*., 1997), Ser113 and Asn115 appeared to be

unique residues that interact with the γ–carboxylate of isocitrate, indicating the substrate specificity of EcIDH.

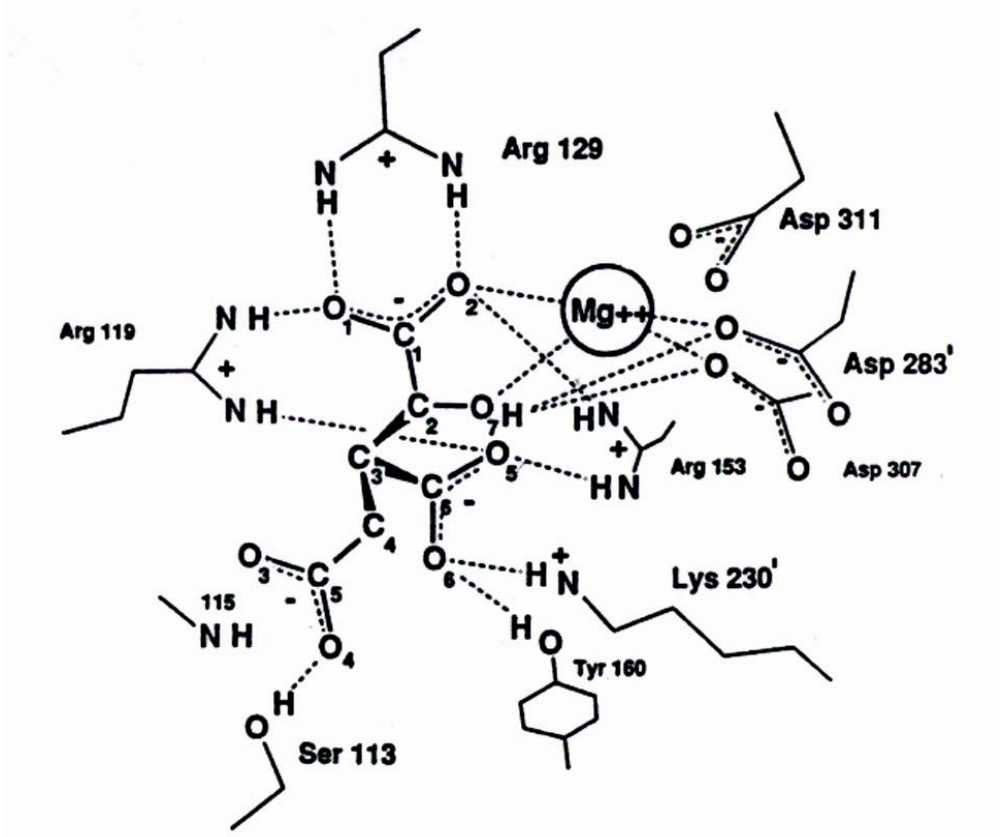

Figure 1.4 The active site in the structure of EcIDH complexed with isocitrate-Mg^{2+}.
The side chains and isocitrate were observed at the cleft of the two subunits in the EcIDH structure. The solid lines represent the side chains of the residues and isocitrate at the active site. Possible hydrogen bonds or salt bridges are shown as dashed lines. The residues labelled with a prime symbol indicate a residue from the second subunit. Adapted from Hurley *et al*., 1991.

1.2.3.2 $NADP^+$ complex

The 2.5 Å resolution structure of EcIDH complexed with $NADP^+$ (PDB: 9ICD) identified the $NADP^+$ binding site that is located at the interdomain cleft (Hurley *et al*., 1991). The adenine moiety appeared to form hydrogen bonds with Asn352, Tyr391, and His339 whereas the 2'-phosphate hydrogen bonded to Tyr345, Tyr391 and Arg395 as well as to Arg292′ from the second subunit (Figure 1.5). These residues at the $NADP^+$ binding site are not conserved as well as those at the isocitrate binding site between EcIDH and IMDH. In terms of topological folds,

the $NADP^+$-binding site in the EcIDH structure seems to be distinct from the nucleotide-binding sites observed in the other dehydrogenase structures, supporting the hypothesis that the evolution of EcIDH could be different from the other decarboxylating dehydrogenases (Hurley *et al*., 1991).

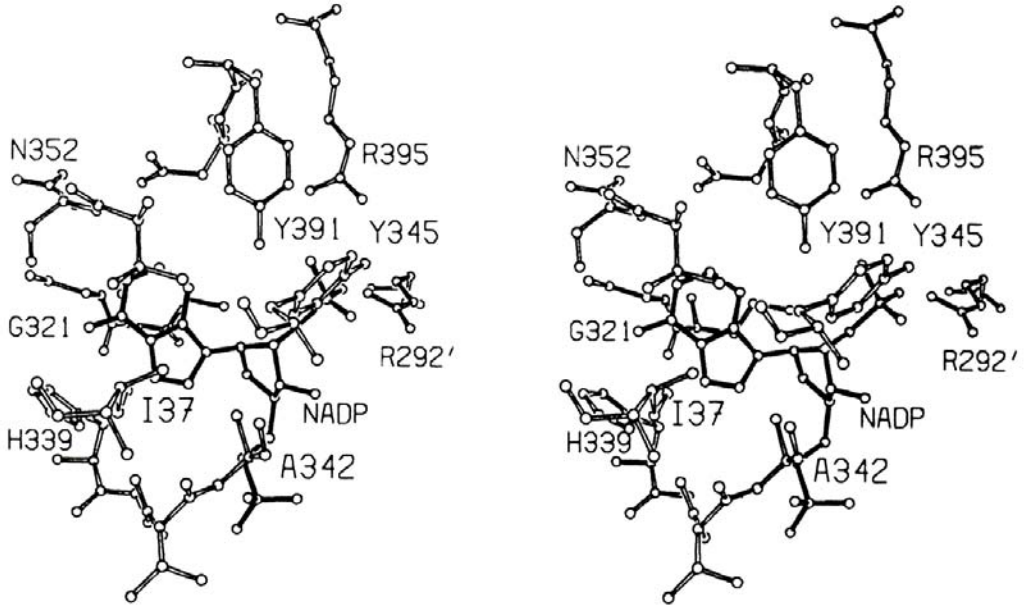

Figure 1.5 Stereo diagram of the $NADP^+$ binding site in the structure of EcIDH complexed with fragments of $NADP^+$.

The solid bonds represent well-ordered fragments of $NADP^+$ (2'-phosphate and adenine moieties), and the protein residues are drawn with open bonds. Residues from the second subunit are labelled with a prime symbol. Adapted from Hurley *et al*., 1991.

1.2.3.3 Isocitrate-Ca^{2+} and $NADP^+$ complex

When Mg^{2+} was substituted by Ca^{2+}, EcIDH catalytic activity was reduced by a factor of 2.5×10^{-3} without a change in the K_m values for the substrates (Mesecar *et al*., 1997). The EcIDH structure in complex with isocitrate-Ca^{2+} and $NADP^+$ has been determined to 1.9 Å resolution (PDB; 1AI2). The substitution of Mg^{2+} by Ca^{2+} caused a rearrangement of water molecules resulting in the formation of an 8-coordination geometry for Ca^{2+} and its relocation compared to the position of Mg^{2+}. This allowed Ca^{2+} to interact with a water molecule that hydrogen bonded to the carbonyl oxygen atom of Thr338 (Figure 1.6). These changes resulting from the substitution of the divalent cation also adjusted the positions of isocitrate and $NADP^+$ so that the distances from active site residues and the dihedral angles for $NADP^+$ and isocitrate are altered,

resulting in lower catalytic activity. From these differences observed between isocitrate-Mg^{2+} and -Ca^{2+} bound EcIDH structures, it can be concluded that small structural alterations of the enzyme and substrates may play an important role in catalytic activity.

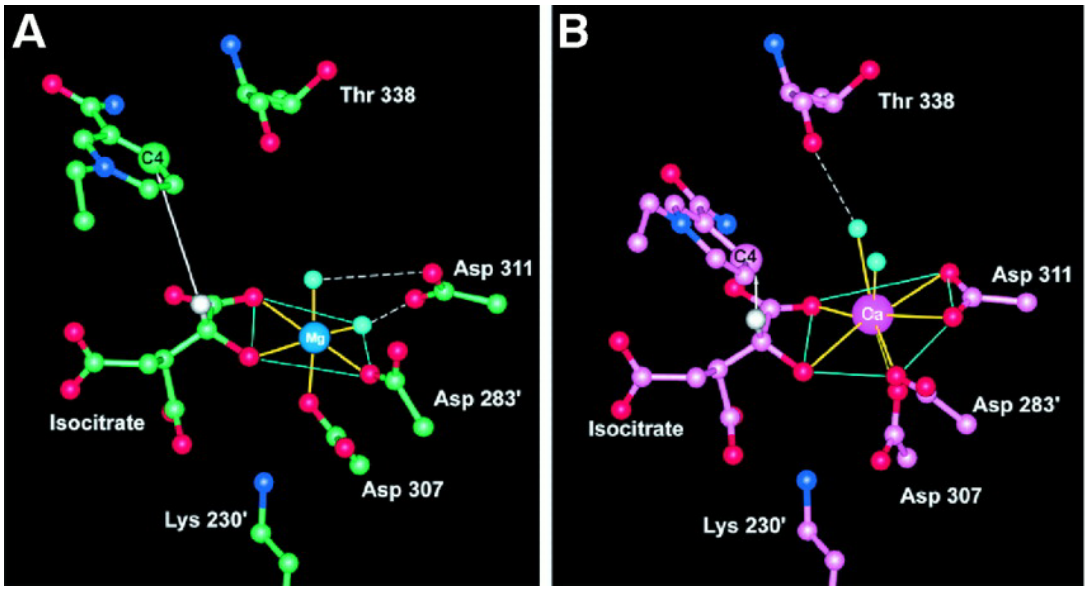

Figure 1.6 Coordination geometry of Mg^{2+} and Ca^{2+} ions bound in the structure of EcIDH complexed with isocitrate and $NADP^+$.

(A) The Mg^{2+} ion (blue sphere) is coordinated with octahedral geometry. (B) The 8-coordination of the Ca^{2+} ion (purple sphere) was observed in the EcIDH structure complex with isocitrate, Ca^{2+} and $NADP^+$. The yellow lines show the possible coordinations of the metal cations. The white dashed lines represent hydrogen bonds. C4 is the carbon atom of $NADP^+$; the light green coloured spheres are water molecules. Adapted from Mesecar *et al*., 1997.

1.2.3.4 IDH kinase/phosphatase (IDHK/P) complex

The phosphorylation cycle of dimeric $NADP^+$-dependent IDH in *E. coli* is catalysed by a bifunctional enzyme, isocitrate dehydrogenase kinase/phosphatase (abbreviated as IDHK/P). This enzyme is homodimeric with a molecular mass of ~68 kDa for each subunit and is encoded by a single gene, *aceK* (Cortay *et al*., 1988). Because mutation in the *aceK* gene increased the EcIDH activity by 3-fold, and because the loss of the IDHK/P activity decreased *E. coli* growth on acetate, IDHK/P was considered as a rate-limiting catalyst in the phosphorylation cycle of EcIDH (Stueland *et al*., 1988; LaPorte, 1993)

Although attempts to co-crystallize of IDH and IDHK/P were not successful, a new different EcIDH crystal structure was solved and refined to 2.42 Å resolution (PDB; 1SJS) (Finer-Moore *et al*., 1997). This structure showed that the large domain was rotated by ~16˚ with respect to the

small domain and the clasp region of the subunit (Figure 1.7). Such an open conformation would allow IDHK/P to access Ser113 more easily for the phosphorylation of EcIDH. This newly observed conformation is quite similar to the one observed in the IMDH structure (Finer-Moore *et al*., 1997). Disruption of the $NADP^+$-binding site due to the open conformation was also observed, suggesting that $NADP^+$ prefers to bind to EcIDH in a closed conformation. It is hypothesized from these two different conformational forms of EcIDH that the equilibrium state between the energetically similar open and closed conformations may make this enzyme flexible for phosphorylation or dephosphorylation by IDHK/P in a reversible manner (Finer-Moore *et al*., 1997).

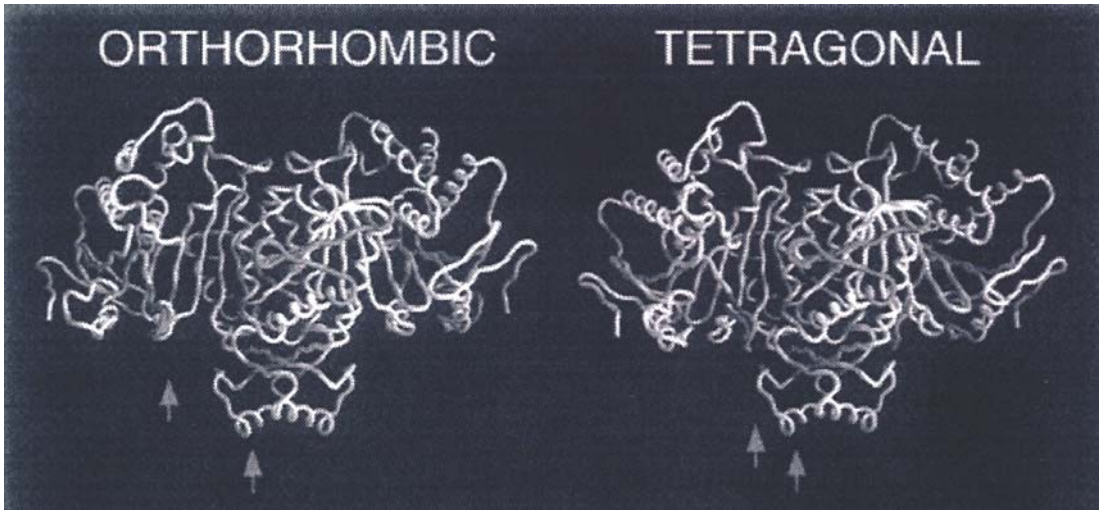

Figure 1.7 Two conformations for the structures of EcIDH in the absence and the presence of isocitrate-Mg^{2+}.

The orthorhombic form on the left-side of the figure represents the open conformation of the EcIDH structure solved from the crystal that was unsuccessfully co-crystallized with IDHK/P. The tetragonal form is the closed form of the EcIDH structure in the presence of isocitrate-Mg^{2+}. The left arrow denotes Ser113, and the right arrow, Asn232. The transition between the open and closed conformations causes a movement of Ser113 with respect to Asn232, as evident in this figure. Adapted from Finer-Moore *et al*., 1997.

1.2.3.5 α-Ketoglutarate and Ca^{2+} complex

It has been proposed that EcIDH undergoes conformational changes upon binding of substrate(s) since soaking the substrate-free EcIDH crystals in a solution containing isocitrate, Mg^{2+}, and $NADP^+$ immediately destroyed the crystals (Stoddard and Koshland, 1993). The structure of EcIDH complexed with α-ketoglutarate and Ca^{2+} was determined to 2.7 Å resolution

(PDB; 1IKA) (Stoddard and Koshland, 1993). Although α-ketoglutarate was bound at the active site in a similar manner to isocitrate, the structure of this complex was different from the other structures of EcIDH complexed with isocitrate-Ca^{2+} and $NADP^+$ and those complexed with isocitrate-Mg^{2+}. In the structure of EcIDH complexed with α-ketoglutarate and Ca^{2+}, Ca^{2+} shifted by ~1 Å in distance from Ser113 compared to the Mg^{2+} in the isocitrate-Mg^{2+} complex, so that the Ca^{2+} was coordinated by α-ketoglutarate, Asp283, Asp307, Asp311, and two water molecules, resulting in a modified interaction between the metal ion and α-ketoglutarate at the active site. The major difference observed in this structure was the formation of a hydrogen bond between Tyr160 and Asp307. The Tyr160 that had bound to isocitrate in the Mg^{2+} complex shifted by more than 2.5 Å in the structure of EcIDH complexed with α-ketoglutarate and Ca^{2+} and formed a new hydrogen bond to Asp307, which induced the movements of the surrounding backbone regions, especially at the interdomain and the active sites. These rearrangements observed in the structure of EcIDH complexed with α-ketoglutarate and Ca^{2+}, indicate that a local shift of EcIDH could be induced upon substrate binding, during the conversion of isocitrate to α-ketoglutarate.

1.2.3.6 S113E mutant complex with isopropylmalate, Mg^{2+} and $NADP^+$

Inactivation of EcIDH by a Ser113 to Glu mutation is consistent with the evidence that phosphorylated EcIDH is inactive due to the introduction of the negative charge at this position (Thorsness and Koshland, 1987). The S113E mutant structure has been solved in complex with isopropylmalate, Mg^{2+} and $NADP^+$ to 2.0 Å resolution (PDB; 1HJ6) (Doyle *et al*., 2001). This mutant structure is globally similar to other EcIDH structures, except that the interdomain hinge region and the loop of residues 255-263 are altered. Compared to the S113E mutant structure in the absence of substrate (PDB; 7ICD) (Hurley *et al*., 1990), a rigid body movement of one domain relative to the other was observed in this structure of the S113E mutant EcIDH complexed with ligands. Although such a conformational change is relatively small, the interdomain hinge angles are altered to cause the reorientation of the side chains at this region. Since the active site lies at this interdomain hinge, the N-terminal end of the active site d-helix (Figure 1.3) is tilted, and new hydrogen bonds among Asn115, Val116, and the mutated Glu113 are formed. The positions of the backbone atoms at the loop and helix regions of the $NADP^+$ binding site are shifted toward the catalytic site so that the binding of $NADP^+$ would be possibly stabilized even in the presence of isopropylmalate (Figure 1.8). The upward shift of the loop

connecting the $NADP^+$ and isocitrate binding sites was also observed, suggesting that conformational flexibility at this region plays a role in EcIDH catalytic activity (Doyle *et al*., 2001).

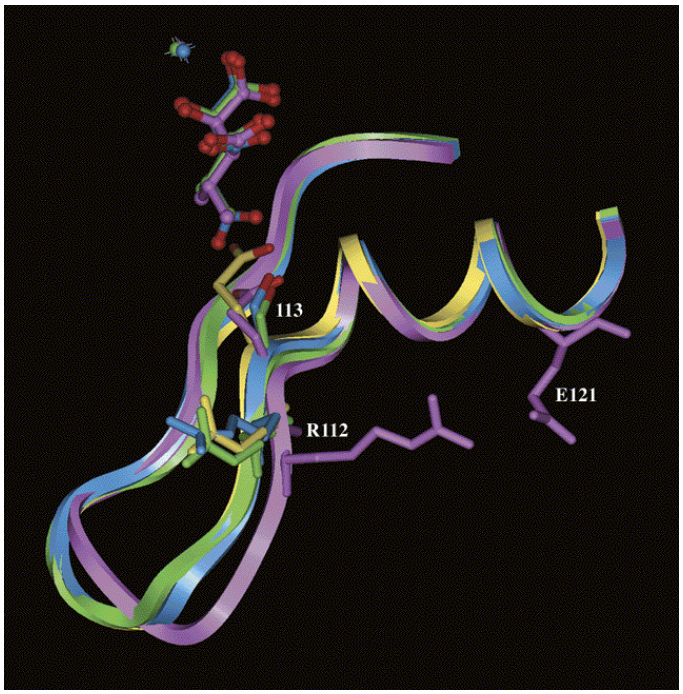

Figure 1.8 Comparisons of the active site in the structures of the complexes of EcIDH.
Four EcIDH structures; Ser113Glu mutant complexed with isopropylmalate, Mg^{2+} and $NADP^+$ (abbreviated as IPM·IDH^{S113E}) (purple), Apo-Ser113Glu (yellow), the Tyr160Phe mutant EcIDH complexed with isocitrate (blue) and the wild-type EcIDH complexed with isopropylmalate, Mg^{2+}, and $NADP^+$ (green) are overlaid at their catalytic sites. Ligands and Mg^{2+} are shown in ball-and-stick rendering, and residues 112 and 113 (and residue 121 for IPM·IDH^{S113E}) are shown in stick rendering. Adapted from Doyle *et al*., 2001.

1.3 Isopropylmalate dehydrogenase (IMDH)

1.3.1 Crystal structures of IMDH

Another closely related dehydrogenase to EcIDH in terms of amino acid sequence and topology is IMDH which catalyses the dehydrogenation and decarboxylation of 2-isopropylmalate to 2-oxoisocaproate and requires NAD^+ and Mn^{2+}. The amino acid sequence alignment between EcIDH and IMDH from *E. coli* (EcIMDH) shows 23% identity, and both enzymes are homodimeric. The substrate-free crystal structure of EcIMDH has been solved to 2.06 Å resolution (PDB; 1CM7) (Wallon *et al*., 1997). It has a non-crystallographic 2-fold axis

relating the two identical subunits, each with two domains, and two subunits are linked by a ten-stranded anti-parallel β–sheet. The large domain is formed from the N- and C-termini residues (1-105 and 256-363), and the small domain from residues 106 to 255. The active site is located between the two domains with residues donated by the two subunits. These topological features are similar to those found in EcIDH.

In addition, both open and closed conformations have been reported for the crystal structure of IMDH from *Salmonella typhimurium* (StIMDH) (PDB; 1CNZ) (Wallon *et al*., 1997). The closed conformation of StIMDH complexed with Mn^{2+} and SO_4^{2-} appeared more similar to the active, closed conformation of EcIDH rather than to the open conformation found in other IMDHs, indicating that the closed conformation in IMDH is indeed the active form. The divalent metal cation in the StIMDH complex is also coordinated in an octahedral geometry by Asp227', Asp255, Asp251, two water molecules and the sulfate ion (Figure 1.9). The sulphate ion further interacts with Tyr145 and Lys195, which are equivalent to Tyr195 and Lys350 at the active site in EcIDH. Based on these structural features, it is suggested that both homodimeric IDH and IMDH belong to the same dehydrogenase family.

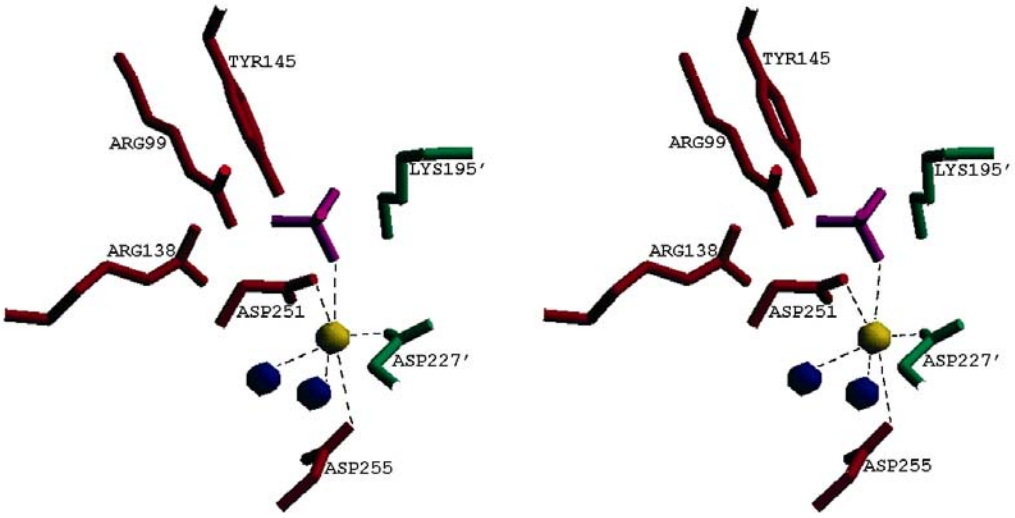

Figure 1.9 Stereo diagram of the structure of StIMDH complexed with Mn^{2+} and SO_4^{2-}.
SO_4^{2-} ion (SO_4) is located near the non-leaving carboxylate of the substrate. Mn^{2+} ion (yellow sphere) is hexa-coordinated by three Asp residues (red stick bonds), SO_4^{2-} (pink), and two water molecules (blue spheres), as the dashed lines indicate. The residues from the second subunit, are indicated by green stick bonds. This diagram was produced using Setor (Evans, 1993).

1.4 Homodimeric $NADP^+$-dependent IDH from porcine heart mitochondria (PmIDH)

1.4.1 General properties

In porcine heart, homodimeric $NADP^+$-dependent IDH enzymes are present in both the cytoplasm and mitochondria. These two forms share 70% sequence identity and are homodimeric with a molecular mass of 47 kDa per subunit. Cytosolic IDH possesses an anabolic function by generating NADPH for the reductive biosynthesis of the long-chained and unsaturated fatty acids (Belfiore and Iannello, 1995). The function of mitochondrial $NADP^+$-dependent IDH in mammals is not clearly understood; however, it seems to have a catabolic role in energy production and to be involved in the control of the oxidative damage (Jo *et al*., 2001).

Even though porcine heart mitochondrial $NADP^+$-dependent IDH (PmIDH) is homodimeric like that of *E. coli*, amino acid sequences between mammalian and prokaryotic homodimeric $NADP^+$-dependent IDH have only 16% sequence identity (Haselbeck, 1992). Also, the phosphorylation of PmIDH has not been reported to date. Therefore, the relationship between mammalian and prokaryotic homodimeric IDH enzymes has been investigated by structural and various mutagenesis studies.

1.4.2 Structural studies

The structure of PmIDH complexed with isocitrate-Mn^{2+} has been solved to 1.85 Å resolution (PDB; 1LWD) (Ceccarelli *et al*., 2002). The structure shows a well-conserved active site in comparison with those of prokaryotic and eukaryotic dimeric $NADP^+$-dependent IDHs. The metal ion is coordinated with two aspartate residues, two water molecules and two oxygens from isocitrate in an octohedral manner, similar to the EcIDH structure (Figure 1.10). One side chain at the active site also seemed to act as a base as occurs in EcIDH (Figure 1.1). Ser95 is identified as analogous to Ser113 in *E. coli*, and is located at the C-terminal end of the d-helix, the so-called “phosphorylation loop” (Figure 1.3).

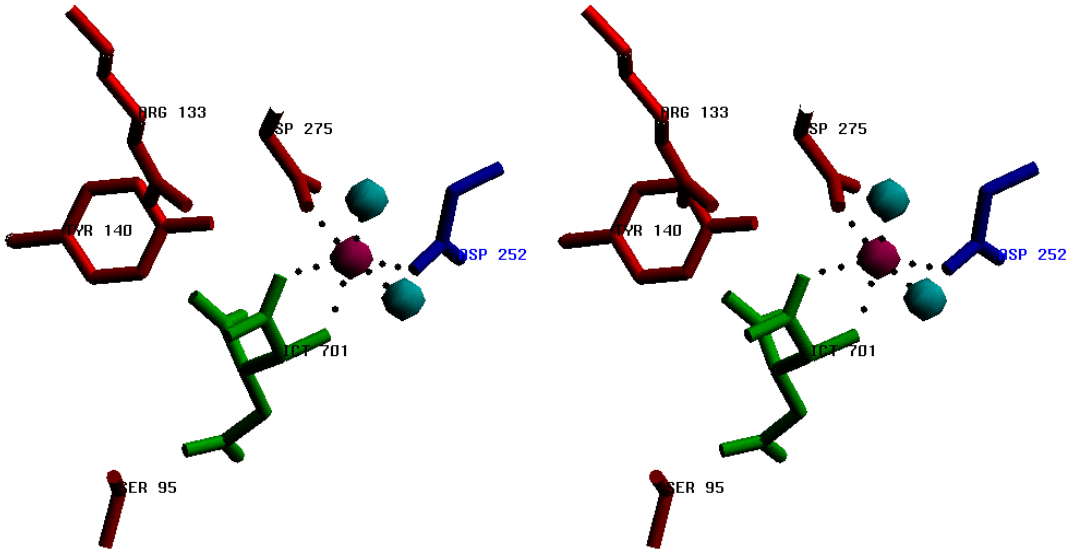

Figure 1.10 Coordination geometry of isocitrate-Mn^{2+} at the active site of PmIDH.

Mn^{2+} (pink sphere) is coordinated in the octahedral manner by Asp252′ (blue), Asp275 (red), two water molecules (light blue spheres) and two oxygens of isocitrate (green). The coordination is indicated by dashed lines, and the blue coloured residue is from the other subunit. This figure was produced from the use of Setor.

Major differences between PmIDH and EcIDH were found at the inter-subunit surface (Ceccarelli *et al*., 2002). While anti-parallel α-helices were stacked on top of the four-stranded anti-parallel β-sheets at the clasp region in EcIDH, four β-strands from each subunit, instead of the α-helices, produced the eight-stranded anti-parallel β-barrel at the clasp region in the structure of PmIDH complexed with isocitrate- Mn^{2+} (Figure 1.11). Moreover, the predicted $NADP^+$-binding site based on the structural alignment suggested that the $NADP^+$-binding site in PmIDH could be similar to that in EcIDH, except for two residues (Tyr345 and Tyr349 in EcIDH, and His315 and Lys375 in PmIDH, respectively) that would interact with the 2'-hydroxyl-bound phosphate. These residues provide hydrogen bonds to the oxygen atoms of the 2'-phosphate. When His315 was mutated to Gln, the K_m value for $NADP^+$ increased by 40-fold, supporting the proposal that this residue is involved in $NADP^+$-binding (Huang and Colman, 2002). Structural analysis of the $NADP^+$-binding site with the structures of other complexes of PmIDH is still required to establish a more detailed mechanism of PmIDH.

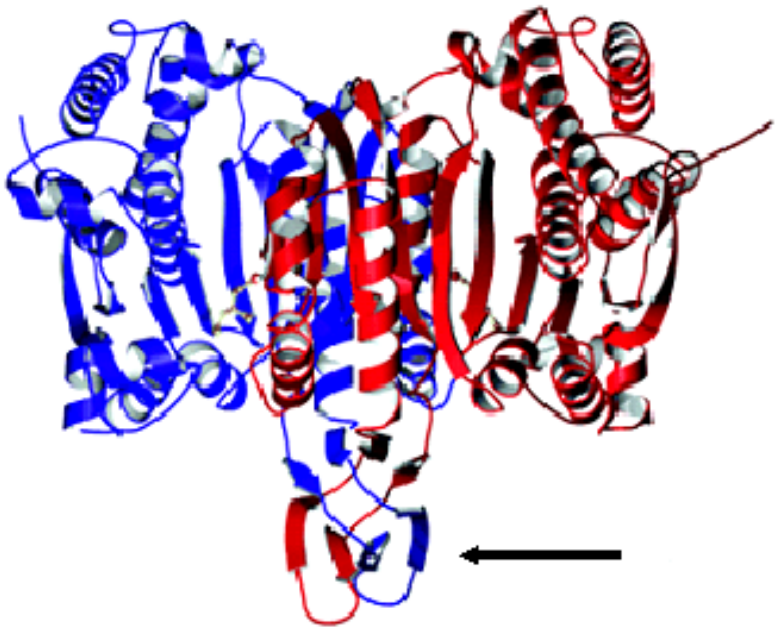

(A)

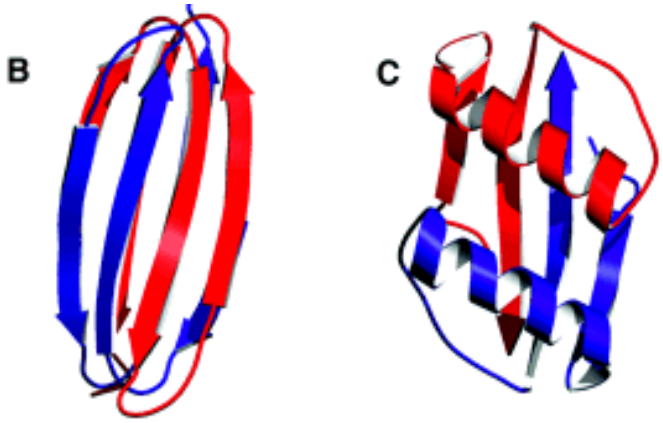

Figure 1.11 Ribbon diagrams of the structure of PmIDH and comparing the clasp regions of PmIDH and EcIDH.

(A) The red and blue ribbons represent one subunit and the other, respectively in the structure of PmIDH complexed with isocitrate (white-yellow) and Mn^{2+} (orange). The clasp region is indicated by an arrow. (B) The clasp region of PmIDH is formed from eight β-strands, of which one set of four β-strands is donated from one subunit (red) and one set from the other (blue). (C) The clasp region of EcIDH consists of anti-parallel α-helices laid on top of four β-strands. One set of one α-helix and two anti-parallel β-strands are donated from one subunit (red) and one set from the other (blue). Adapted from Ceccarelli *et al*., 2002.

1.4.3 Mutagenesis studies

Based on the structure of PmIDH, Lys212 and Tyr140 were selected for mutagenesis since these residues are located close to bound isocitrate (Kim *et al*., 2003). Mutations of Lys212 to

glutamate, tyrosine, or arginine exhibited only 0.01-9.0% of the specific activity of the wild-type enzyme. Similarly, each of the Tyr140 mutants was nearly inactivated when Tyr140 was mutated to phenylalanine, threonine, glutamate, or lysine. It has been proposed that Lys212 and Tyr140 are critical in PmIDH catalytic activity (Kim *et al*., 2003).

Three other aspartate residues at the catalytic site, Asp252, Asp275 and Asp279, have been studied to elucidate their roles in PmIDH (Huang *et al*., 2004). In the PmIDH structure, Asp252 and Asp275 coordinate Mn^{2+} along with two water molecules and two oxygen atoms of isocitrate, while Asp279 appears to link indirectly to Mn^{2+}. When Asp252 and Asp275 have been separately mutated in PmIDH to His, their affinities for isocitrate and Mn^{2+} and their catalytic activities were significantly reduced, indicating that these Asp residues could be essential for the binding of isocitrate and Mn^{2+} (Huang *et al*., 2004). On the other hand, the D279H mutant showed lower affinity toward $NADP^+$ rather than toward isocitrate and Mn^{2+}, suggesting a role for this residue in coenzyme binding (Huang *et al*., 2004).

1.5 Human cytosolic homodimeric $NADP^+$-dependent IDH (HcIDH)

1.5.1 General properties

Human cytosolic $NADP^+$-dependent IDH (HcIDH) is homodimeric with a molecular mass of 46.7 kDa for each subunit. Unlike mitochondrial $NADP^+$-dependent IDHs, HcIDH possesses a peroxisomal target sequence at its C-terminus that allows it to localize in the peroxisomes and to provide the NADPH required for the β–oxidation of fatty acids (Belfiore and Iannello, 1995; Yoshihara *et al*., 2001). This enzyme has also been reported to play a cellular defence role against oxidative damage (Lee *et al*., 2002). As is the case with PmIDH, possible enzymes equivalent to *E. coli* IDHK/P have not been found in the human genome, and phosphorylation of HcIDH has not been reported to date.

1.5.2 Structural studies

1.5.2.1 $NADP^+$, isocitrate, and Ca^{2+} complex

The homodimeric HcIDH structure consists of three domains with an overall structure similar to the other known homodimeric structures of EcIDH and PmIDH (Xu *et al*., 2004). The active site is also found at the hydrophilic region between the small and large domains of the same

subunit (Figure 1.12). Like PmIDH, two layers of four stranded anti-parallel β-sheets form the clasp domains of two subunits. The major difference between HcIDH and EcIDH is observed at the small cleft located between the small and large domains. While this small cleft is mainly hydrophilic in EcIDH, it consists of both hydrophobic and hydrophilic residues in HcIDH. This feature suggests that this small cleft could be involved in the function and regulation of HcIDH.

The structure of HcIDH in complex with $NADP^+$, isocitrate, and Ca^{2+} was solved and refined to 2.41 Å resolution (Xu *et al*., 2004). There are two homodimeric molecules with four sets of $NADP^+$, isocitrate, and Ca^{2+} per asymmetric unit. This structure revealed that isocitrate interacts with Thr77, Ser94, Arg100, Arg109, Arg132, Tyr139, and Asp275 from one subunit and with Lys212, Thr241 and Asp252 from the adjacent subunit, in addition to interacting with three water molecules, $NADP^+$, and Ca^{2+}. These interacting residues are similar to those found in the PmIDH structure as well as in EcIDH, indicating that the catalytic residues are well conserved among prokaryotic and eukaryotic $NADP^+$-dependent IDH enzymes.

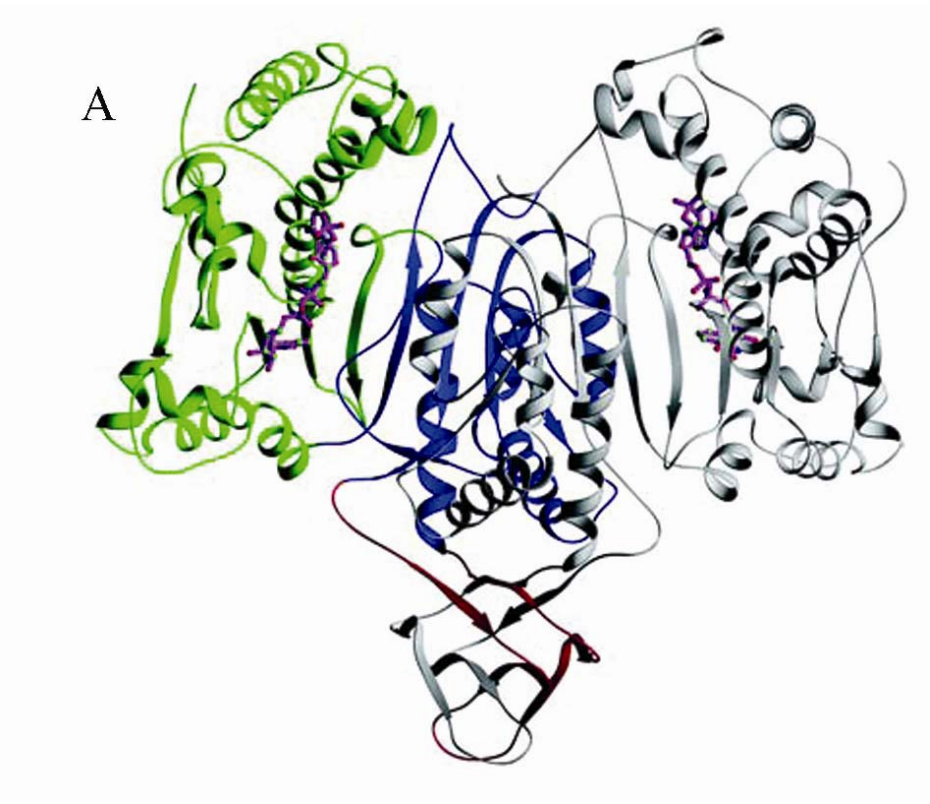
A

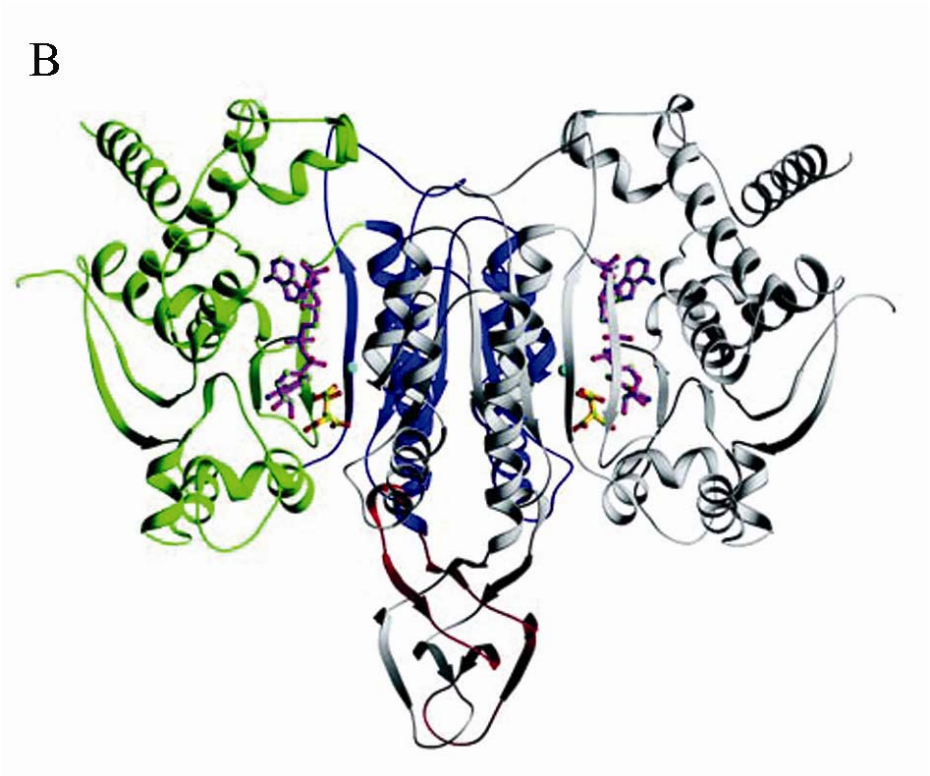
B

Figure 1.12 Ribbon diagrams of two HcIDH structures.
(A) The overall structure of HcIDH complexed with $NADP^+$ exhibits an open conformation. (B) The overall structure of HcIDH complexed with isocitrate- Ca^{2+} and $NADP^+$ shows a closed conformation. The large domain, the small domain, and the clasp region of one subunit of HcIDH are shown in green, blue, and red, respectively, while the second subunit is drawn in grey. Isocitrate (yellow gold), $NADP^+$ (purple) and Ca^{2+} (a sky blue sphere) are bound at the active site. Adapted from Xu *et al*., 2004.

1.5.2.2 $NADP^+$ complex

The structure of HcIDH in complex with only $NADP^+$ was also solved up to 2.7 Å resolution (Xu *et al*., 2004). In this structure, $NADP^+$ was found to interact with residues at the active site of the large domain that is close to the isocitrate-binding site. The adenine moiety of $NADP^+$ interacts with His309, Val312, Arg314, His315, Thr327 and Asn328 in both hydrophobic and hydrophilic manners (Figure 1.13). The 2'-phosphate group forms salt bridges with Arg314 and His315. Because Tyr345, Tyr391 and Arg395 interact with the 2'-phosphate of $NADP^+$ in EcIDH, it is proposed that Arg314 and His315 determine the specificity of the $NADP^+$ binding in HcIDH. Indeed, mutagenesis studies in PmIDH supported this hypothesis since the mutation at the equivalent His315 reduced the affinity of PmIDH toward $NADP^+$ (Huang and Colman, 2002).

Compared to the structure of HcIDH in complex with $NADP^+$, isocitrate, and Ca^{2+}, the structure of HcIDH in complex with $NADP^+$ was observed to be in a more open conformation (Xu *et al*., 2004). Whereas the former structure was very similar to other known $NADP^+$-dependent IDH structures containing substrate(s), the $NADP^+$ complex structure is a unique, open conformation in an inactive form (Figure 1.14). Detailed analysis of these structures shows that Asp279 interacts via hydrogen bonds with Ser94, Thr77 and Asn96 at the active site in the $NADP^+$ complex structure. These interactions appear to prevent the occurrence of the closed conformation and thus binding of isocitrate, since Ser94 has been identified not only as an interacting residue with isocitrate, but also as the analogous residue to the key residue (Ser113) in EcIDH. The active site is also widely open in the structure of HcIDH complexed with $NADP^+$, resulting in inactivation of this enzyme.

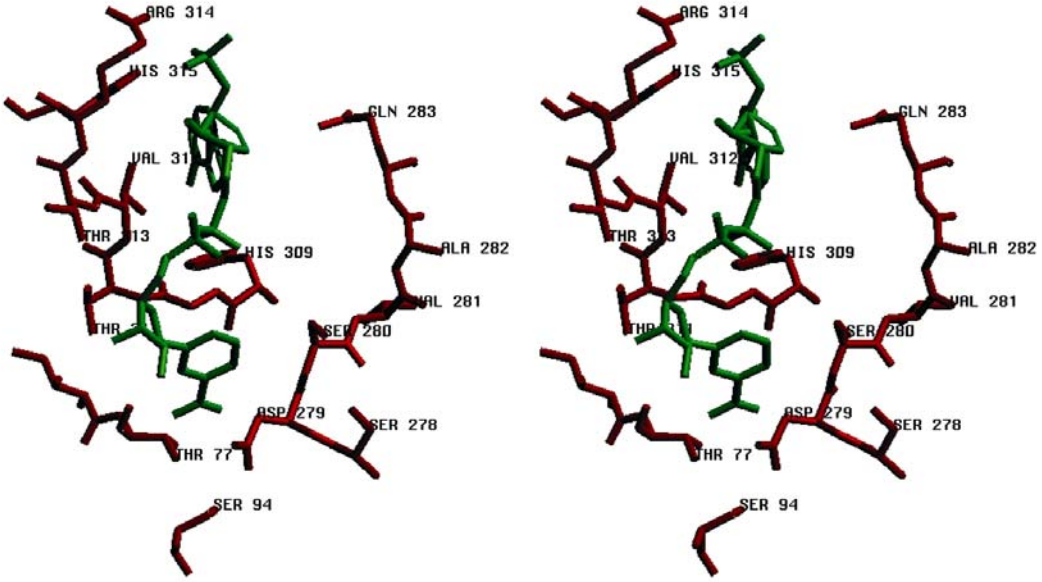

Figure 1.13 Stereo diagram of the $NADP^+$ binding site in HcIDH.
$NADP^+$ (green) is coordinated by the labelled residues (red stick bonds) (Xu *et al*., 2004). This figure was produced from Setor.

From these structural studies, it has been proposed that two inter-convertible conformational states of similar energy exist in mammalian $NADP^+$-dependent IDH (Xu *et al*., 2004). The closed conformation seems to be induced by the hinge movements of the clasp and of the small domain with respect to the large domain when isocitrate binds to the catalytic site of the enzyme. It is suggested that inter-conversion between these conformational states in HcIDH could regulate its catalytic activity and would play a role in its function since similar conformational changes to control its enzymatic activity were also observed in EcIDH during the phosphorylation cycle.

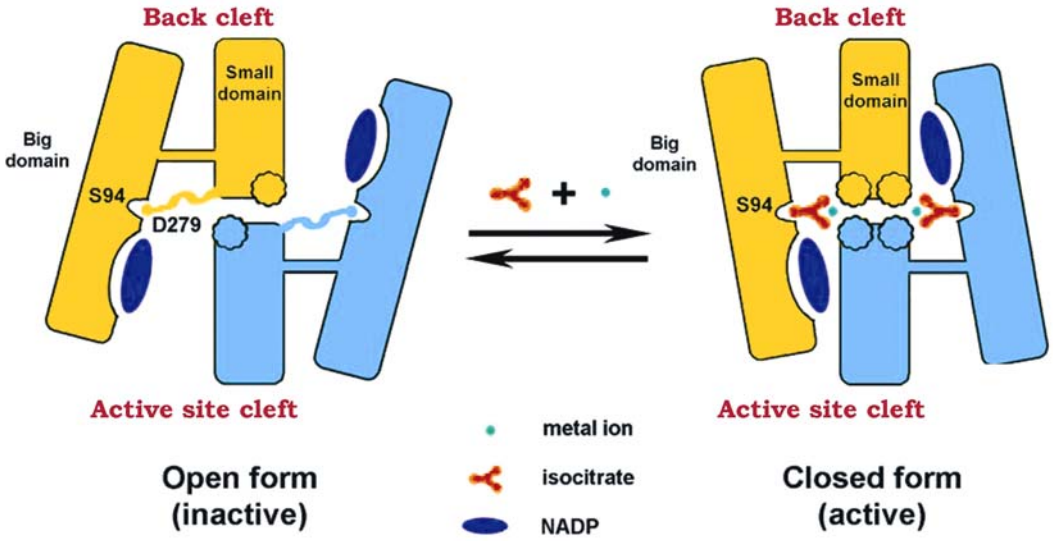

Figure 1.14 Schematic illustration of the conformational changes in HcIDH.

The domains are drawn as coloured rectangular boxes to show the one subunit (yellow) and the other (blue). Small circles attached to the small domain represent Asp279 (D279) and Gln277 residues. The ribbon shows Asp279 interacting with Ser94 (S94) in the open form. Adapted from Xu *et al*., 2004.

1.6 Monomeric $NADP^+$-dependent IDH

1.6.1 General properties

Monomeric $NADP^+$-dependent IDH is found in a few bacteria such as *A. vinelandii* (Suzuki *et al*., 1995 ; Sahara *et al*., 2002), *C. glutamicum* (Eikmanns *et al*., 1995), and *Vibrio* species (Ochiai *et al*., 1979 ; Fukunaga *et al*., 1992; Steen *et al*., 1998). No cross-reactivity against antibodies has been observed between homodimeric and monomeric $NADP^+$-dependent IDH although both forms catalyze the identical reaction (Chen and Gadal, 1990). The molecular mass of monomeric $NADP^+$-dependent IDH is ~80 kDa. There is less than 10% identity between amino acid sequences of homodimeric and monomeric $NADP^+$-dependent IDH enzymes. These studies suggest that two different forms of $NADP^+$-dependent IDH could have evolved separately. On the other hand, partial sequence alignment revealed that the catalytic residues between homodimeric and monomeric $NADP^+$-dependent IDH are fairly conserved, indicating the possibility that one single unit of monomeric IDH could function similarly to two subunits of homodimeric IDH (Chen and Yang, 2000).

1.6.2 Structural studies of monomeric $NADP^+$-dependent IDH structure from *A. vinelandii* (AvIDH)

1.6.2.1 Isocitrate-Mn^{2+} complex

The relationship between homodimeric and monomeric $NADP^+$-dependent IDH had not been discussed until the first monomeric IDH structure at 1.8 Å resolution was published (PDB; 1ITW) (Yasutake *et al*., 2002). The crystal structure of monomeric IDH from *A. vinelandii* (AvIDH) revealed the presence of two distinct domains within the single polypeptide. A small domain (Domain I) is formed from both the C- and N-terminal regions and corresponds to the large domain (Domain A) in EcIDH. On the other hand, a large domain (Domain II) contains two symmetrically arranged Greek Key motifs and is homologous to the small domain (Domain B) and the clasp region (Domain C) of EcIDH (Figure 1.15). The presence of the pseudo 2-fold axis only in Domain II of AvIDH is also similar to the crystallographic 2-fold found in EcIDH, indicating the partial duplication of the common gene during the evolution to maintain the spatial form for the identical catalytic reaction (Yasutake *et al*., 2002).

The cleft formed between Domain I and II in the AvIDH structure creates the active site in a similar manner to the two subunits of homodimeric IDH (Figure 1.16). Although there are two active sites in EcIDH, the second catalytic site is absent in AvIDH because of the lack of the equivalent domain that would correspond to Domain A' of the second subunit in EcIDH. From the comparison of the catalytic site of AvIDH onto one of the catalytic site of EcIDH, Ser132 in AvIDH was found to be analogous to Ser113 in EcIDH. In AvIDH, hydrogen bonds are formed between isocitrate and Ser132 as well as the other equivalent residues such as Asn135, Arg139, Arg145, Arg547, Tyr420 and Lys255 (Figure 1.16). The active site residues in AvIDH are completely conserved among monomeric IDH enzymes from other sources and are homologous with the active site of homodimeric $NADP^+$-dependent IDH from numerous sources (Yasutake *et al*., 2002). These similarities implied that monomeric and homodimeric forms of $NADP^+$-dependent IDH could have possibly evolved from a common ancestral protein even though their primary structures are not significantly identical (Yasutake *et al*., 2002).

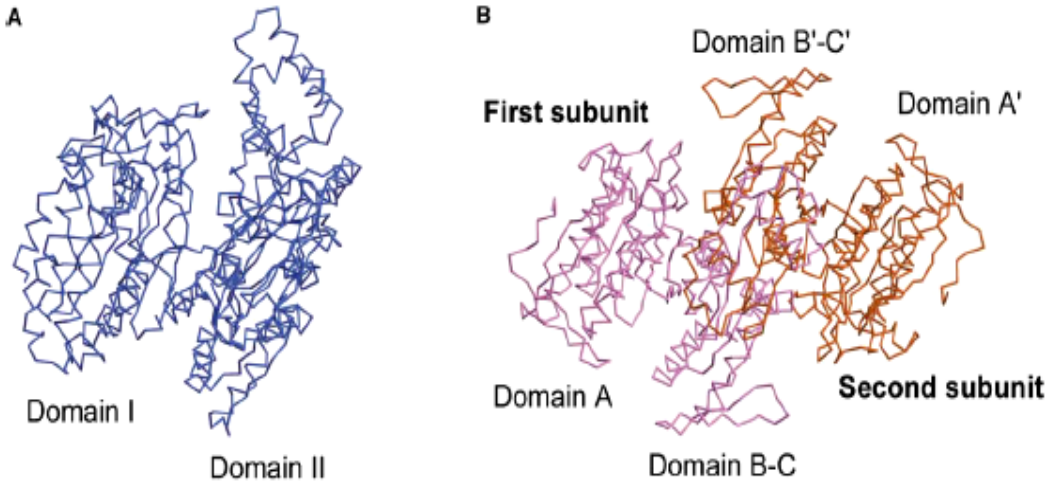

Figure 1.15 Schematic illustration of the tertiary structures of (A) AvIDH and (B) EcIDH.
(A) AvIDH consists of Domain I and II. (B) The first and second subunits in EcIDH are coloured in pink and orange, respectively. The domains in the second subunit in EcIDH are indicated with the prime symbol. Adapted from Yasutake *et al*., 2002.

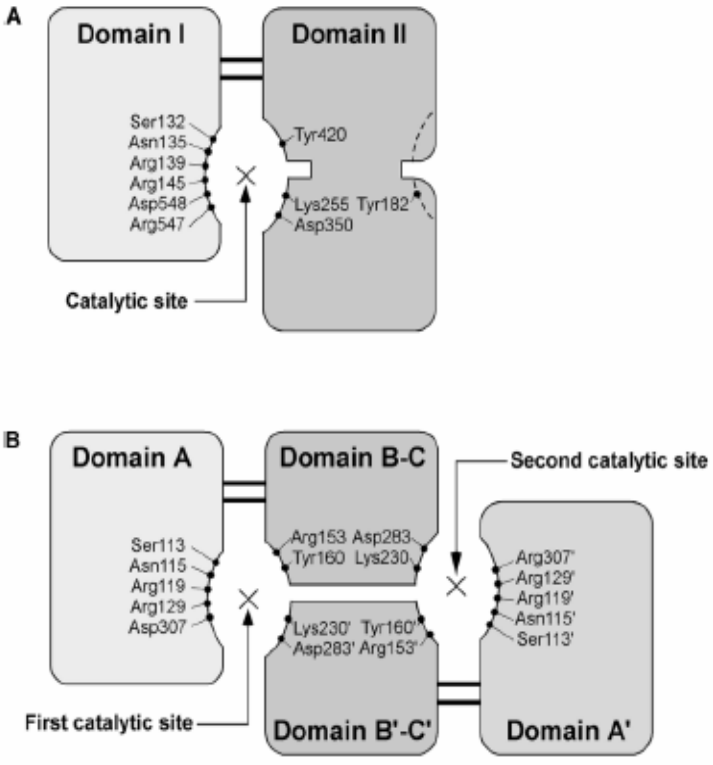

Figure 1.16 Schematic illustration of the catalytic sites in AvIDH and EcIDH.

The cross (×) represents the catalytic site(s) found in (A) AvIDH and in (B) EcIDH. Functionally corresponding residues are drawn as black spheres. Residues and domains from the second subunit in EcIDH are indicated by the prime symbol. Adapted from Yasutake *et al*., 2002.

1.6.2.2 $NADP^+$ complex

The structure of AvIDH complexed with $NADP^+$ has been also solved to 3.2 Å resolution (PDB; 1J1W) (Yasutake *et al*., 2003). Even though the enzyme was originally crystallized from solution containing isocitrate-Ca^{2+} and $NADP^+$, possibly due to the inhibition of the AvIDH by Ca^{2+}, only $NADP^+$ was present in the structure (Figure 1.17). The $NADP^+$ binding site was observed at the active site cleft when $NADP^+$ interacted directly with the residues from the small domain and both its adenine and nicotinamide ring were in the anti-conformation (Figure 1.18). Hydrogen bonds were formed between adenine and the residues His589, Arg600, Asp602, and Arg649. The diphosphate moiety has van de Waals contacts with Gly684, Ser585 and Ala586. The nicotinamide ribose moiety formed hydrogen bonds with Ser585, Ser87 and Asn85. These residues interacting with $NADP^+$ are conserved among various monomeric IDH enzymes, but their equivalents are not found in EcIDH. Thus, monomeric AvIDH has a unique $NADP^+$-binding site which is distinct from homodimeric IDH.

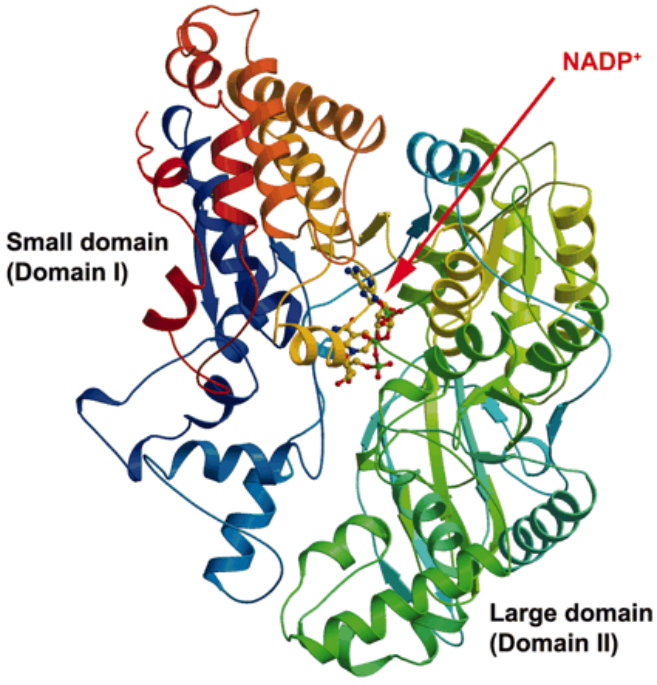

Figure 1.17 Ribbon diagram of AvIDH complexed with $NADP^+$.

$NADP^+$ is represented as sticks-and-balls bound at the cleft in AvIDH. The α-helices of the AvIDH structure are drawn as ribbons; the β-sheets are drawn as arrowed-ribbons; and the random coils are illustrated as strings. Adapted from Yasutake *et al*., 2003.

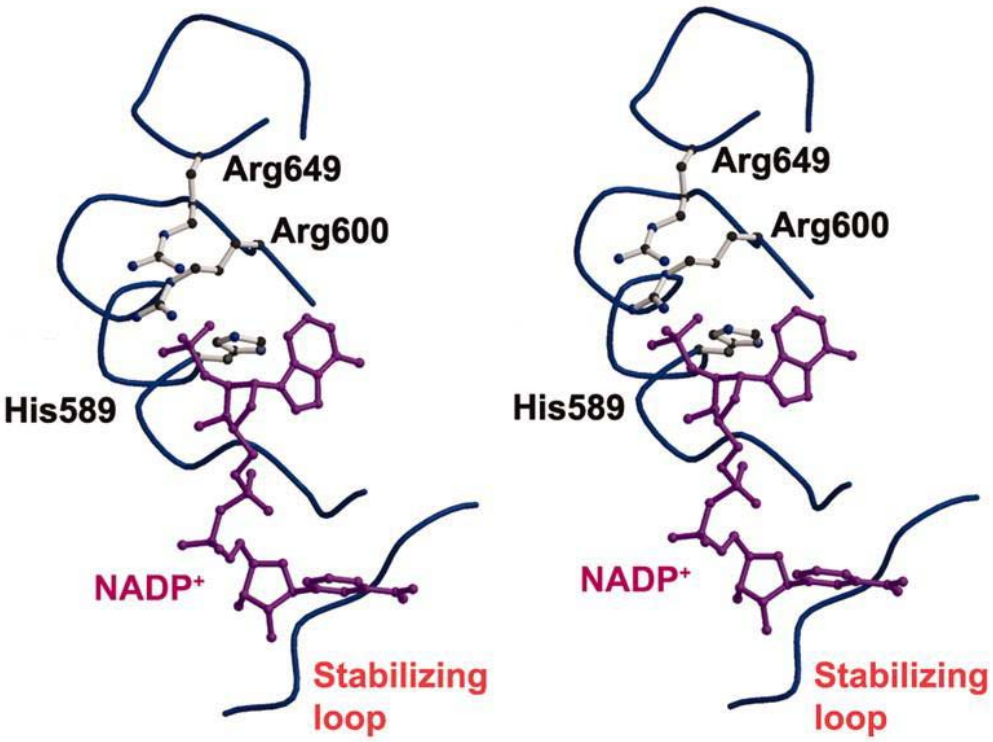

Figure 1.18 Stereo diagram of the $NADP^+$ binding site in AvIDH.
The blue loop represents the backbone of the protein. Three residues that interact with $NADP^+$ (purple) are drawn with sticks-and-balls. Adapted from Yasutake *et al*., 2003.

The detailed structure of AvIDH complexed with $NADP^+$ also revealed that the hydrogen-bonding network between water molecules and Asp350 is well ordered and provides a proton acceptor for isocitrate at the active site, similar to that provided in the homodimeric PmIDH structure (Yasutake *et al*., 2003). In addition, a residue, analogous to His589, at the $NADP^+$-binding site of AvIDH is present in PmIDH. These structural observations suggest that monomeric IDH may be more closely related to mammalian homodimeric IDH rather than to prokaryotic homodimeric IDH.

1.6.3 Monomeric $NADP^+$-dependent IDH from *C. glutamicum*

1.6.3.1 Industrial importance of *C. glutamicum*

A gram-positive, non-pathogenic bacterium, *C. glutamicum*, is known as an amino acid producing organism since it is widely used in industry for the large scale production of amino acids, such as lysine and glutamate, for animal nutrition (Jetten *et al*., 1994). Annually, ~1 000 000 tons of L-glutamate and ~450 000 tons of L-lysine are produced from these industrial *C. glutamicum* strains (Kalinouski *et al*., 2003).

This bacterium can grow on either glucose or acetate as the sole carbon source. One of the unique features of this bacterium as an industrial amino acid producer is the presence of a lysine specific export carrier (Bröer and Krämer, 1991). When the normal feedback inhibition of aspartate kinase by lysine during lysine synthesis is impaired, not only is this enzyme deregulated by the increased concentration of lysine, but also the activity of the lysine specific export carrier is increased (Bröer and Krämer, 1991). As a consequence, massive production and secretion of lysine can be achieved from this bacterium. Various metabolic pathways have been studied to understand the mechanisms of amino acid production in *C. glutamicum* (Gerstmeir *et al*., 2003; Kiefer *et al*., 2004). The whole genome for the wild type strain of *C. glutamicum* has been reported (Ohnishi *et al*., 2002).

1.6.3.2 The *icd* gene from *C. glutamicum*

Because *C. glutamicum* can grow on glucose or acetate, IDH is a key candidate enzyme to control the carbon flux at the branch point between the Krebs cycle and the glyoxylate bypass depending upon the carbon source available. The *icd* gene encoding monomeric $NADP^+$-dependent IDH from *C. glutamicum* has been identified and cloned into a shuttle vector of *E. coli* and *C. glutamicum*, named pEK (Eikmanns *et al*., 1995). There is only a single *icd* gene with 3595 base-pairs present in *C. glutamicum*, the product of which is one single monomeric $NADP^+$-dependent IDH (CgIDH). It was previously found that CgIDH activity is independent of the bacterial growth substrate and growth phase, but is likely involved in controlling the branch point between the Krebs cycle and the glyoxylate bypass. No enhanced secretion of glutamate was observed from the recombinant strain although CgIDH activity increased by about 10-fold. On the other hand, a mixture of oxaloacetate and glyoxylate significantly reduced CgIDH activity. It is suggested that CgIDH is not the rate-limiting enzyme for glutamate production but it is sensitive in some way to oxaloacetate and glyoxylate and could indirectly regulate the branch point between the Krebs cycle and the glyoxylate bypass (Eikmanns *et al*., 1995).

1.6.3.3 Kinetic properties of CgIDH

Although the overall sequence alignment has less than 10% identity between monomeric and homodimeric IDH, the partial sequence alignment suggested that the active sites would be conserved between monomeric and homodimeric IDH enzymes (Chen and Yang, 2000). According to kinetic studies on both EcIDH and CgIDH, CgIDH had higher catalytic activity and specificity for $NADP^+$ than did EcIDH. In a separate experiment, Lys253 was mutated to methionine, based on the partial sequence alignment. The activity of this mutant enzyme was not detectable, indicating that Lys253 could be involved in the reaction catalyzed by monomeric IDH (Chen and Yang, 2000).

1.7 Research Objectives

The objectives of my research were to express, purify, crystallize and solve the detailed X-ray structure of monomeric CgIDH as a substrate-free form and/or as a complex with its substrate(s). The X-ray crystallographic study of a protein is a powerful approach to obtain a three-dimensional structural model that can establish the detailed catalytic and functional mechanism of the enzyme.

Preliminary purification and crystallization of CgIDH were successfully performed in our laboratory as well as initial X-ray diffraction studies (Bai *et al*., 1999; Audette *et al*., 1999). It was planned to use the structure as a basis for mutagenesis to further explore the mechanism and the functions of monomeric IDH. The detailed mechanism of CgIDH catalysis should also help elucidate how monomeric IDH controls the branch point between the Krebs cycle and the glyoxylate bypass in some bacteria and plants.

Chapter 2 Materials and Experimental Procedures

2.1 Materials

2.1.1 Reagents and supplies

Chemical reagents, enzymes, chromatographic, microbacterial and crystallographic supplies used for this project and names and addresses of suppliers are listed in Tables 2.1 and 2.2.

Chemical reagents	**Supplier**
Acrylamide;Bisacrylamide solution (30%, 29:1)	Bio-Rad Laboratories
Adenosine triphosphate (ATP)	Sigma-Aldrich
Agarose, electrophoresis grade	GIBCO BRL
Ammonium persulfate	Bio-Rad Laboratories
Coomassie-Brilliant Blue R250	Kodak
Dithiothreitol (DTT)	Sigma-Aldrich
Ethidium bromide	Sigma-Aldrich
Ethylenediaminetetraacetic acid (EDTA)	BDH/VWR International Ltd.
Ethylene glycol	Fluka/ Sigma-Aldrich
Glutathione (reduced form)	Sigma-Aldrich
Glycerol	BDH/VWR International Ltd.
Isopropyl -D-thiogalactopyranoside (IPTG)	Sigma-Aldrich
Magnesium chloride ($MgCl_2$)	BDH/VWR International Ltd.
2-methyl-2,4-pentanediol (MPD)	Fluka/ Sigma-Aldrich
2-morpholineethanesulfonic acid (MES)	Sigma-Aldrich
3-[N-morpholino] propane sulfonic acid (MOPS)	Sigma-Aldrich
Nicotinamide adenine dinucleotide phosphate, oxidized form ($NADP^+$)	Sigma-Aldrich
Nitrogen (liquid)	Praxair
Phenol: Chloroform: Isoamylalcohol (25:24:1)	Sigma-Aldrich
Polyethylene glycol (PEG) 400	Fluka/ Sigma-Aldrich
PEG 2000 monomethyl ether (MME)	Fluka/ Sigma-Aldrich
Sodium dodecyl sulfate (SDS)	Sigma-Aldrich

Triethanolamine (TEA)	Sigma-Aldrich
N,N,N',N'-Tetramethylethylene-diamine (TEMED)	Amersham Biosciences
Tris-[hydroxymethyl]aminomethane (Tris)	BDH/VWR International Ltd.
Trisodium-DL-isocitrate	Sigma-Aldrich

Enzymes	**Suppliers**
*EcoR*I	Amersham Biosciences
*Sal*I	Amersham Biosciences
*Dpn*I	Stratagene
Taq™ DNA polymerase	Novagen
T4 DNA ligase	Novagen
Pfu Turbo™ DNA ligase	Stratagene
RNase	Amersham Biosciences
PreScission™ protease	Amersham Biosciences

Chromatographic supplies	**Supplier**
Red Sepharose CL-6B	Amersham Biosciences
Glutathione Sepharose 4B	Amersham Biosciences

Microbiological supplies	**Supplier**
Bacto™-agar	BD
Tryptone peptone	BD
Bacto™-yeast extract	BD

Crystallographic supplies	**Suppliers**
Additive screening	Hampton
Cryoloops	Hampton
Dow Corning High Vacuum Grease	VWR International Ltd.
Glass capillaries	Hampton
Silica Hydrogel ™	Hampton

24-Well VDX Plates	Hampton

Table 2.1 Chemical reagents, enzymes, chromatographic, microbacterial and crystallographic supplies used in this project.

Suppliers	**Address**
Amersham Biosciences	Amersham Biosciences, Baie d'Urfe, QC, Canada
Bio-Rad Laboratories	Bio-Rad Laboratories Ltd., Mississauga, ON, Canada
BD	BD Biosciences Canada, Mississauga, ON, Canada
BDH/VWR International Ltd.	VWR International Ltd., Mississauga, ON, Canada
Fluka/ Sigma-Aldrich	Sigma-Aldrich Canada Ltd., Oakville, ON, Canada
GIBCO BRL	Web Scientific Ltd., Cheshire, England, UK.
Hampton	Hampton Research, Laguna Niguel, CA, USA.
Kodak	Eastman Kodak Company, Rochester, NY, USA.
Novagen	EMD Biosciences, Madison, WI, USA.
Praxair	Praxair, Saskatoon, SK, Canada
Sigma-Aldrich	Sigma-Aldrich Canada Ltd., Oakville, ON, Canada
Stratagene	Stratagene co., La Jolla, CA, USA.

Table 2.2 Names and addresses of suppliers.

2.1.2 Plasmid vectors

The protein expression vector, pGEX6p-1, was obtained from Amersham Biosciences. This vector is ~5.5 Kbp and consists of the *Lac*I ^{q} gene, an ampicillin resistance gene, a *taq* promoter, a glutathione encoding gene, protease cleavage sites, and a multiple cloning site (MCS).

2.1.3 Bacterial strain

E. coli DH5α and BL21 strains were obtained from GIBCO BRL, and competent cells were prepared by the methods described elsewhere in the literature. The *E. coli icd*$^{-}$ strain, EB106, was generously provided by the *E. coli* genetic stock center (Yale University). The XL1-Blue super-

competent cells were included in the Quickchange® site-directed mutagenesis kit purchased from Stratagene.

2.1.4 Bacterial growth media

Bacterial growth media were prepared as described by Miller (Miller, 1972). Luria Bertani (LB) medium contained 10 g tryptone peptone, 10 g NaCl and 5 g Bacto^{TM}-yeast extract per liter of distilled water. The medium was autoclaved at 125 ˚C and 18 psi. For preparation of LB agar plates, 15 g/L of Bacto^{TM}-agar was added to the liquid media prior to autoclaving. After autoclaving and cooling down media to room temperature, either ampicillin (100 μg mL^{-1}) or kanamycin (30 μg mL^{-1}) was added as described below.

2.2 Purification of monomeric NADP^{+}-dependent IDH from *C. glutamicum*

2.2.1 Bacterial growth

The *C. glutamicum* cells that harbored the plasmid *p*EK*icd*ES, containing the *icd* gene, were inoculated in 5mL of LB medium containing kanamycin (30 μg mL^{-1}) and shaken at 30 °C overnight. The overnight culture was transferred to and incubated in 500 mL of medium and shaken at 30 °C overnight. The growth culture was harvested through centrifugation at 6 000 ×g at 4 °C for 20 min. The cell pellet was stored at -80 °C (Bai *et al*., 1999).

2.2.2 Ammonium sulfate fractionation

The harvested cell pellet was re-suspended in Buffer A [25 mM 2-morpholineethanesulfonic acid (MES), pH 6.2, 2.5 mM $MnSO_4$, and 2.5 mM DTT] and disrupted by ultrasonication at 50 W (5 × 1 min bursts with 6 min intervals). The sonicated solution was centrifuged at 12 000 ×g at 4 °C for 20 min. The supernatant containing IDH was transferred to a fresh tube, and activity assay was performed on the crude extract. The cell lysis and activity assay steps were repeated ten times until no activity was detected in the crude extract. In this way, the maximum amount of IDH could be obtained from the crude extract. Ammonium sulfate (35% to 80% cut) at room temperature in solid form was added to the pooled crude extract while stirring on ice. The mixture was centrifuged at 12 000 ×g at 4 °C for 20 min after incubation on ice for 30 min. The

pellet was dissolved in a minimal volume of Buffer A and dialyzed against the same buffer overnight.

2.2.3 Affinity chromatography purification

The dialyzed protein solution was loaded on a pre-equilibrated Red Sepharose CL-6B affinity column with Buffer A containing 20 mM NaCl, and then the column was washed with 10× the bed volume of Buffer A containing 0.15 M NaCl. Monomeric IDH protein was then eluted with Buffer A containing 4 mM trisodium-DL-isocitrate. The fractions containing high enzymatic activity were pooled together and their purity was checked by 8% SDS polyacrylamide gel electrophoresis (PAGE). The pooled fractions were dialyzed against Buffer A. Following concentration of IDH using an UltraFree Amicon centrifuge tube (Millipore), 2.5 mM DTT and 10% glycerol were added and the concentrated protein solution was stored at -80 ºC.

2.3 Crystallization of substrate-free and coenzyme-bound enzyme

2.3.1 Crystallization trials

A crystal is defined as a regular array of molecules exhibiting a consistent packing arrangement (Weber, 1997). Theoretically, a crystal grows only at the metastable phase, the region above the solubility curve and below the supersolubility curve in the phase diagram (Figure 2.1). Both the concentration and the solubility parameters of a protein, such as pH and precipitant concentration, affect the phases of the protein. Protein crystals will dissolve in the unsaturated phases, whereas nucleation and crystal growth compete in the labile phase of the supersaturation region (Weber, 1997). In the metastable phase, the activation energy of protein molecules favour the solid phase while the other precipitants remain in soluble forms, resulting in crystal growth. In short, the protein crystal grows through the time-course specific, interior aggregation of a protein in solution via a kinetic process when the protein concentration and the solubility parameters meet at the metastable phase (Figure 2.2).

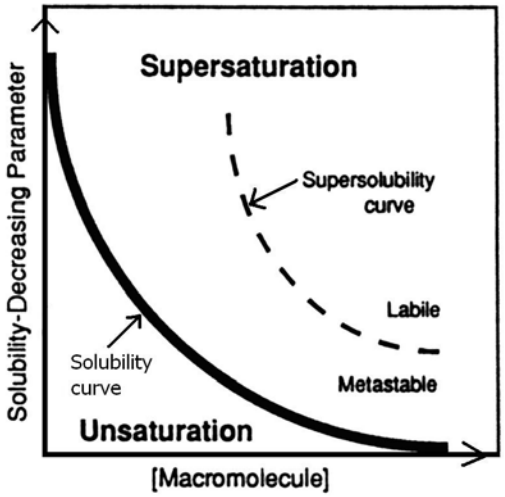

Figure 2.1 Phase diagram of protein crystallization.

The solubility curve (solid) divides the phase space into unsaturated region (Unsaturation) and supersaturated region (Supersaturation). The supersaturated region is further divided into the labile and the metastable phases by the supersolubility curve (dashed). Adapted and modified from Weber, 1997.

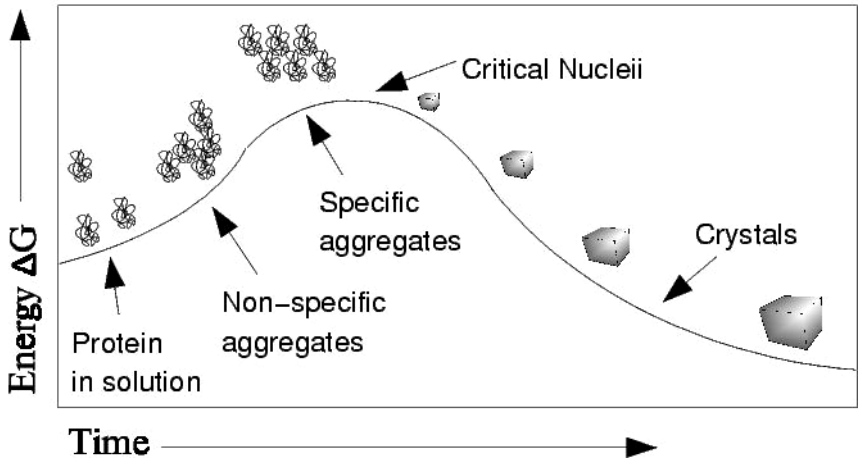

Figure 2.2 The kinetic process of crystallization.

The process of crystal growth is schematically illustrated along an energy (ΔG) vs. time course. The clear crystal is drawn as a cube whereas the non-crystal form of protein is illustrated as coils. Adapted from the website: http://www-structmed.cimr.cam.ac.uk/Course/Crystals/Theory/phases.html.

There are five categorized methods for crystallization: bulk crystallization, vapour diffusion, dialysis, free interface diffusion, and batch. Among these methods, vapour diffusion was mainly used for the crystallization of CgIDH. This crystallization method is a time-dependent saturation of the protein solution via vapour equilibration between a protein-containing droplet and a

reservoir. As water vapour diffuses from the protein-containing droplet to the reservoir, supersaturation of the protein solution will be achieved, and so nucleation and protein crystal growth occur simultaneously (Weber, 1997; Ducruix and Giegé, 1999).

CgIDH was crystallized by the hanging-drop vapour diffusion method at room temperature under the conditions previously described by Audette *et al.* (1999). Reservoir solution was made of 25% polyethylene glycol (PEG) 2000 monomethyl ether (MME), 0.1 M Tris-HCl (pH 7.3), and 0.2 M $MgCl_2$, while the drop consisted of 1 μL of CgIDH at a concentration of 5 mg mL^{-1} and 1 μL reservoir solution. A CgIDH crystal with dimensions 0.3 × 0.1 × 0.05 mm was obtained within a week.

Three additive and detergent screening kits from Hampton Research were used to optimize the crystallization conditions (Sousa, 1995). Various small molecules were added to the protein-containing droplet on a plastic cover slip, since such additives are likely able to manipulate specific interactions with the macromolecule and possibly to obtain better quality and/or size of crystals.

Direct interface crystallization in a glass capillary using agarose gel or Silica Hydrogel™ (Hampton Research) was also attempted to obtain a crystal supported in a gel matrix, which would be directly frozen in a stream of nitrogen, without exposing the crystal to air (Garcia-Ruiz *et al*., 2001; Lopez-Jaramillo *et al*., 2001).

2.3.2 Cryo-crystallography

X-rays are parts of the electromagnetic spectrum with energy of 4×10^{3}-10^{4} $kJmol^{-1}$. A protein crystal is highly hydrated (30-75% solvent) and very fragile. Thus, a protein crystal can be easily damaged and even destroyed by prolonged exposure to X-rays during the diffraction data collection. Hence, a protein crystal is required to be frozen and it is diffracted at ~100 K under a cold nitrogen stream resulting in less decay and destruction of the protein molecules. If an untreated hydrated protein crystal is frozen directly, on the other hand, ice formation increases the volume of solvent content damaging the orderly packing of molecules within the protein crystal. Therefore, addition of a cryoprotectant is used to protect a protein crystal during flash cooling and from X-ray damage during diffraction (Ducruix and Giegé, 1999; Robert *et al*., 1999). A proper cryoprotectant is critical to minimize any damage to the crystal from liquid nitrogen freezing and to achieve high resolution with low crystal mosaicity.

One single cryoprotectant, such as ethylene glycol, glycerol, or mineral oil, is generally used to permeate a protein crystal (Hope, 1988; Garman and Schneider, 1997). Another method is to replace a high molecular weight polyethylene glycol (PEG) precipitant with a low molecular weight PEG400 which serves as a precipitant and a cryoprotectant, and it can be easily combined with another cryoprotectant due to its high viscosity. A two-step cryocrystallographic procedure has also been suggested, in which a crystal is permeated with a diffusible cryoprotectant and then transferred to an immiscible oil (Kwong and Liu, 1999; Riboldi-Tunnicliffe and Hilgenfeld, 1999). Since the excess cryoprotectant around a crystal could be removed by passing the crystal through the immiscible oil, better resolution and lower crystal mosaicity of the crystal diffraction could be achieved. Additionally, mixtures, for example of glycerol and 2-methyl-2, 4-pentandiol (MPD), have been reported to work synergistically and give a better diffraction than one individual cryoprotectant alone (Fremont *et al*., 1996).

For CgIDH crystals, various cryoprotectants, such as 5-25% glycerol, MPD, ethylene glycol and PEG400, mixed with reservoir solution were prepared and examined by the flash cooling method in order to optimize the cryocrystallographic conditions for successful diffraction data collection. Because CgIDH crystals tend to crack when exposed to the air, the crystals were soaked in a series of mixtures of reservoir and glycerol solutions from 10 to 25% (v/v) in 5% (v/v) increments, followed by transfer to light paraffin oil. Two cryoprotectant mixtures, glycerol and MPD, and glycerol and ethylene glycol, at different ratios of each of cryoprotectants were also tested.

2.4 Data collection and processing

When x-rays are diffracted by a protein crystal, the intensity and the position of the diffracted beam are measured. When an incoming X-ray at a certain wavelength (λ) hits a crystal, X-rays are re-emitted from the planes of the crystal as reflections and recorded as diffraction spots by a detector. The diffracted x-rays scatter in all directions as a form of electromagnetic energy released from the electrons of each molecule in the crystal. The resultant diffraction data consist of differences of individual amplitudes of the scattered waves diffracted by the crystal.

According to Bragg's Law (Bragg, 1913), for constructive interference to occur, the integral multiple of the wavelength of the X-ray (λ) is equal to twice the distance (d) between two lattice planes, multiplied by the sine of the diffraction angle (θ) (Formula 2.1).

$$n\lambda = 2d_{hkl}\sin\theta_{hkl} \qquad \text{Formula 2.1}$$

Reflection indices, *hkl,* determine the reflecting planes, and the diffraction angle (θ_{hkl}) is the angle between the reflecting plane and the incident X-ray beam (Figure 2.3). Bragg's law tells us that d-spacing of the crystal is reduced as the diffraction angle is increased at constant wavelength. In other words, the diffraction pattern is sensitive to the diffraction angle and spacing of the planes of a crystal.

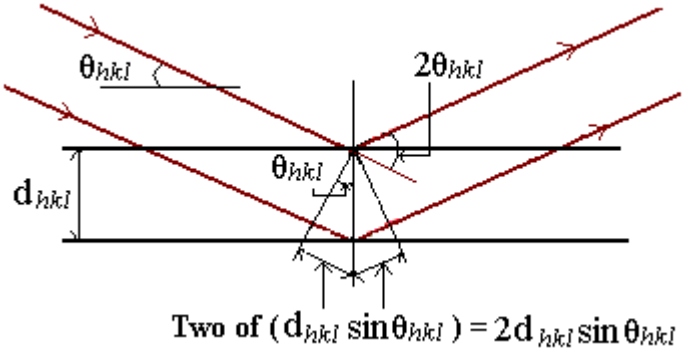

Figure 2.3 Schematic illustration of Bragg's Law.
Both the incoming x-rays and the reflection from the adjacent planes are drawn as red arrows. Two lattice planes are drawn as thick black lines, which re-emit electrons when the x-ray strikes. The reflection angle and the perpendicular distance between two reflection planes are illustrated as θ_{hkl} and d_{hkl}, respectively. Modified from Otwinowski and Minor, 1997.

The periodic arrangement of the collected diffraction pattern is mathematically related in a reciprocal manner to the actual crystal lattice (Otwinowski and Minor, 1997). The process to establish the periodicity of a diffraction pattern is done by a peak search. Then, the diffraction pattern is mapped from the peak search onto its reciprocal space so that the diffraction angles can be estimated. Based on the diffraction patterns determined from the peak search, the periodicity of the reciprocal lattice in the direction of the vector is searched automatically through a computational program in a process called autoindexing. This process finds the integer values of one index (*h*, *k*, or *l*) that are equivalent to the real-space vectors of the crystal because the reciprocal lattice space is represented as a vector that is normal (perpendicular) to the Bragg

planes with the inverse amplitude of the actual d-spacing within the crystal. As Bragg's Law indicates, the inverse proportional relation between the diffraction angles and the d-spacing of the crystal at a constant wavelength means that the reciprocal space depends on the unit cell dimensions of the crystal. The three independent vectors, which would index almost all of the observed peaks, obtained from autoindexing are used to find the best unit cell dimensions of the crystal (Otwinowski and Minor, 1997).

The unit cell is defined as the smallest unit that makes up one crystal by simple translation in three dimensions. Each unit cell is formed from *a*, *b*, and *c* dimensions along x, y, and z axes respectively at α, β, and γ angles in three-dimensional space (McRee, 1993). In other words, a crystal is made up of the repetitions of the unit cell. These arrangements of the lattice points in space are classified into 14 space lattices called Bravais Lattices (Table 2.3).

The predicted unit cell dimensions from autoindexing are refined as the crystal and detector orientation parameters are fixed for each processed diffraction image since these parameters are slightly changed from one image to another during a rotation-based diffraction data collection. This process is done by integration, and further refinement, using the fixed unit cell dimensions, is performed by scaling (Otwinowski and Minor, 1997).

Diffraction data sets for three CgIDH crystals were collected on Beamline 14ID-B at the Advanced Photon Sources (APS), Argonne National Laboratory, in March 2003. Each data set was collected from a single CgIDH crystal on a MAR CCD detector at 100 K. Diffraction images from the flash-cooled crystal were taken at 1° increments per frame (10 s exposure per frame) for a 180° total rotation of the *phi* axis.

Crystal System	Bravais Type(s)	External Minimum Symmetry	Unit Cell Properties
Triclinc	*P*	None	*a, b, c, α, β, γ*
Monoclinic	*P, C*	One 2-fold axis, parallel *b* (*b* unique)	*a, b, c, 90, β , 90*
Orthorhombic	*P, I, F*	Three perpendicular 2-folds	*a, b, c, 90, 90, 90*
Tetragonal	*P, I*	One 4-fold axis, parallel *c*	*a, a, c, 90, 90, 90*
Trigonal	*P, R*	One 3-fold axis	*a, a, c, 90, 90, 120*
Hexagonal	*P*	One 6-fold axis	*a, a, c, 90, 90, 120*

Cubic	*P, F, I*	Four 3-folds along space diagonal	*a, a, ,a, 90, 90, 90*

Table 2.3 The classification of the Bravais Lattices.

The five Bravais types are primitive (*P*), centered (*C*), face-centered (*F*), body-centered (*I*), and primitive rhombohedral (*R*). The unit cell properties include the unit cell axes (*a, b, c*) and the angles (*α, β, γ*). The fixed angles in the crystal system (90, 120) are written in degrees. Adapted from International Tables for X-ray Crystallography, Volume I Symmetry Groups (Edited by Norman, H.F.M., and Lonsdale, K., 1967).

A single crystal of CgIDH complexed with Mg^{2+} diffracted to 1.75 Å and belonged to space group *C*2, with unit cell dimensions of *a* =129.0 Å, *b*= 52.7 Å, *c*= 124.0 Å, and *β* = 108.9º. There was one molecule of monomeric IDH per asymmetric unit (ASU) with a solvent content of 50.3 % and a Matthews coefficient (V_M) of 2.43 $Å^3$ Da^{-1} (Matthews, 1968). The diffraction data were indexed and integrated with the program HKL2000 (Otwinowski and Minor, 1997) and scaled with the program SCALA (Otwinowski and Minor, 1997). In addition, crystals of CgIDH in complex with either NAD^+ or $NADP^+$ diffracted to 2.10 Å and 2.04 Å, respectively, and their data sets were collected and processed as above. Both crystals belonged to the same space group, *C*2, as is the CgIDH crystal in complex with Mg^{2+} but with different unit cell dimensions. Unit cell dimensions were *a* =128.9 Å, *b*= 52.7 Å, *c*= 235.3 Å, and *β* = 103.5º for the NAD^+-complex and *a* =128.4 Å, *b*= 52.5 Å, *c*= 234.4 Å, and *β* = 102.8º for the $NADP^+$-complex. In 2004, diffraction data were collected at the APS to 2.5 Å resolution from a CgIDH crystal co-crystallized with isocitrate and NAD^+. This crystal again belonged to space group *C*2 with unit cell dimensions *a* =129.1 Å, *b*= 52.5 Å, *c*= 241.5 Å, and *β* = 108.5º. The diffraction data collection statistics for these four CgIDH crystals are summarized in Table 2.4.

CgIDH crystal complex	Mg^{2+}	$NADP^+$	NAD^+	Isocitrate-NAD^+
Wavelength (Å)	0.99	0.90	0.90	0.90
Resolution limit (Å)	50-1.75 (1.81-1.75)	50-2.04 (2.11-2.04)	50-2.10 (2.18-2.10)	50-2.50 (2.59-2.50)
Space group	*C*2	*C*2	*C*2	*C*2
Unit cell dimensions	*a* = 129.0 Å, *b*= 52.7 Å, *c*= 124.0 Å, and β = 108.9°	*a* = 128.4 Å, *b*= 52.5 Å, *c*= 234.4 Å, and β = 102.8°	*a* = 128.9 Å, *b*= 52.7 Å, *c*= 235.3 Å, and β = 103.5°	*a* = 129.1 Å, *b*= 52.5 Å, *c*= 241.5 Å, and β = 108.5°
# of observed reflections	151387	168976	141208	80182
# of unique reflections	79292	98067	90030	51709
Completeness (%)	99.2 (95.6)	93.2 (98.6)	85.3 (76.1)	86.3 (84.3)
I/σ	8.4 (1.66)	9.2 (4.40)	7.7 (2.15)	11.6 (4.40)
R_{symm}	0.072 (0.343)	0.087 (0.352)	0.087 (0.458)	0.153 (0.407)

Table 2.4 Summary of diffraction data for CgIDH crystals complexed with various substrate(s).

Statistical parameters after scaling are listed. Values in brackets are those for the highest resolution shell. R_{symm} was calculated by $R_{symm}=\Sigma |I-\langle I\rangle|/\Sigma I$, where I = individual measured intensity and $\langle I\rangle$ = average of symmetry-related intensities.

2.5 Solution and refinement of the CgIDH structure

2.5.1 Molecular replacement

From diffraction data, only indices (*h k l*) and intensities of the reflection are measured. Phases are, however, required to solve the structure. Intensity (I) is proportional to the square of the amplitude of the structure factor ($|\boldsymbol{F}_{hkl}|$) and is a real number. The structure factor ($\boldsymbol{F}_{hkl}$), on

the other hand, is the summation of the scattering factors of atoms and is a complex number derived from:

$$F_{(h,k,l)} = \sum_{j=1}^{atoms} f_{(j)} \exp\left[2\pi \cdot i(hx_{(j)} + ky_{(j)} + lz_{(j)})\right]$$

Formula 2.2

where the scattering factor ($f_{(j)}$) of atom (j) is dependent on the kind of atom and the diffraction angle of the corresponding reflection. From the structure factors, the electron density is generated using a Fourier transform. The Fourier transform refers to the mathematical operation to transform the electron density into structure factors. In other words, the diffraction pattern is the Fourier transform of the electron density, and the structure factor amplitudes, but not phases, are obtained from the collected diffraction data. This lack of phase information is called the"phase problem" in X-ray crystallography. To solve the phase problem, the initial phases to start the model are required (McRee, 1993).

Molecular replacement (MR) is one of the phase techniques to determine the initial phases of a crystal structure from a known structure that has at least 30-40% amino acid sequence identity to the unknown structure (Brünger, 1997). The known structure (search model) is first rotated and then translated within the unit cell of the target crystal until the best fit was found between the observed and calculated diffraction data. Instead of comparing the structure factors, the summation of the square of the structure amplitudes with all phase angles equal to zero (known as Patterson functions) are used in MR. A Patterson peak is a measure of the vector between two atoms within the unit cell, and there are two types of Patterson vectors involving atoms of a molecule; self-Patterson and cross-Patterson vectors. The self-Patterson vectors are short intra-molecular vectors to tell us the orientation of a molecule at the three rotation angles (α, β, γ) in the unit cell and are used during the rotation search. A higher peak solution in the rotation function usually corresponds to a better solution for the rotation search. If the possible solution peak is much higher than the other peaks, it indicates a correct solution. The cross-Patterson vectors, on the other hand, are inter-molecular vectors that provide information about the exact position of the atoms in the symmetry-related molecules within the unit cell in the translation search. The translation search is done along three translation axes (x, y, z). Three criteria, packing of the atoms, the R value and the correlation coefficient, are examined to determine the correct solution. The best solution should have a lower R value and a high correlation coefficient

with the least overlapping of the atoms in the unit cell. As a consequence, six parameters (three rotation angles and three translation axes) to place the search model into the unit cell of the crystal are determined and are further refined to start the model rebuilding and refinement since the amino acid residues may still form unique, variable conformations which differ from the search model (Brünger, 1997).

The first structure of CgIDH complexed with Mg^{2+} was solved by MR using the program CNS (Brünger *et al.*, 1998) with the isocitrate-Mn^{2+} bound AvIDH structure (PDB; 1ITW) used as its search model. Due to the presence of two domains in the search model, the rotational orientation and the translational position for each domain were determined individually at first. The well-fitted domain with the higher correlation coefficient was fixed and the position of the other domain was searched. As a consequence, with the finding of the second domain, the correlation coefficient improved dramatically from 0.286 to 0.502. After relocating each domain using equivalent positions, the solved structure was examined with TURBO-FRODO (Roussell *et al*., 1990) and the domains were confirmed to be properly located in the unit cell without any overlapping of each other. For the rigid-body refinement, one domain was fixed as a reference to optimize the relative positions of the two domains in the asymmetric unit of the unit cell, and an R_{cryst} value of 0.433 was obtained after rigid-body refinement (McRee, 1993).

2.5.2 Initial refinement

Refinement is the adjusting process of the atomic positions and B factors of the structure so that the calculated structure factors ($\boldsymbol{F}_{cal}$) will resemble the observed structure factors ($\boldsymbol{F}_{obs}$). Not only the protein molecules but also any ligands and solvent (water) molecules in the structure are adjusted during the refinement. The refinement is monitored by the crystallographic R value (R_{cryst}) and by the cross-validation R value (R_{free}) (Brünger, 1992) (Formula 2.3 and 2.4). Approximately 5-10% of the observed reflections ('$_T$' set of reflections) are randomly chosen and separated from the rest of the reflections to be used in the calculation of R_{free}. While the R_{cryst} is dependent on the completeness, the resolution limit, and the accuracy of the diffraction data and the refinement process, R_{free} can help validate the model entirely based on the diffraction data.

$$R_{cryst} = (\Sigma\, |\boldsymbol{F}_{obs} - \boldsymbol{F}_{cal}|) / \Sigma\, |\boldsymbol{F}_{obs}| \qquad \text{Formula 2.3}$$

$$R_{free} = (\Sigma_T\, |\boldsymbol{F}_{obs} - \boldsymbol{F}_{cal}|) / \Sigma_T\, |\boldsymbol{F}_{obs}| \qquad \text{Formula 2.4}$$

Using the initial phases from the MR solution, the electron density map is calculated by the Fourier transform (Formula 2.5).

$$\rho_{(x,y,z)} = \frac{1}{V}\sum_{h}\sum_{k}\sum_{l}\left|F_{(h,k,l)}\right|\exp\left[-2\pi \cdot i(hx + ky + lz - \alpha_{(h,k,l)})\right]$$

Formula 2.5

Where V is the volume of the unit cell, $|\boldsymbol{F}_{(h,k,l)}|$ is the structure factor amplitude of the reflection (*hkl*), x, y, and z are the coordinates of a point in the unit cell, and $\boldsymbol{\alpha}_{(h,k,l)}$ is the phase angle of any particular reflection (*hkl*). The starting model of the unknown structure will be modified according to the electron density map. The new electron density map is subsequently generated from the Fourier transformation after every cycle of refinement, resulting in a higher correlation between the calculated structure factors and the observed structure factors.

The initial refinement was performed using CNS (Brünger *et al.*, 1998). Approximately 10 % of the reflections were randomly selected to calculate the R_{free} value. Simulated annealing is a refinement process using molecular dynamics (Brünger, 1990). Because the potential energy of a molecule is proportional to a given temperature, the energy barrier of the atom is overcome computationally by increasing the temperature and assigning the potential energy at the high temperature. The assigned potential energy is then minimized as the temperature cools down step by step (slow-cooling); therefore, the atoms are relocated by their thermal motion and their dynamic behavior. The initial simulated annealing at 2.0 Å resolution improved R_{cryst} and R_{free} significantly to become 0.339 and 0.377, respectively. Then, a B-factor refinement was performed resulting in 0.319 and 0.351 for R_{cryst} and R_{free}, respectively. After energy minimization, the values to start the first modeling were R_{cryst}= 0.315 and R_{free}= 0.348. The electron density maps were generated using CNS after a cycle of initial refinement (Read, 1986). In order to reduce model bias that is often present when MR is used to solve a structure, an omit map was generated by a simulated annealing SIGMAA weighted omit map method using 7.5% of the total number of reflections randomly selected for every cycle (Bhat, 1988; Hodel *et al*., 1992).

2.5.3 Manual modeling of the structure

Using TURBO-FRODO software (Roussell *et al*., 1990), the structure was manually adjusted by fitting each atom into the electron density map as well as examining other parameters of the

protein structure. For instance, the average bond distance between the Cα and the C of the main chain is ~1.53 Å, and the average bond distance between the C and the N of the main chain is ~1.33 Å. A Ramachandran plot also provides information about the dihedral angles (phi and psi angles) of the main chain to help monitor the accuracy of the protein structure (Ramakrishnan and Ramachandran, 1965). After replacing the amino acid residues from the AvIDH search model with the ones present in CgIDH, R_{cryst} and R_{free} were improved to 0.274 and 0.306, respectively. Water molecules were automatically picked using a CNS sub program (Brünger *et al.*, 1998). Approximately 200 water molecules were picked and confirmed with TURBO-FRODO to fit into the newly generated 2***F***o-***F***c map. After further refinement, the water molecules with B-factors above 40 $Å^2$ were deleted. From the subsequent difference map (***F***o-***F***c), some additional water molecules were manually added. Manual building of the structure followed by the simulated annealing, B-factor refinement, and generation of the electron density map were repeated. The electron density for Mg^{2+} was observed in both 2***F***o-***F***c and ***F***o-***F***c maps. The coordination of this cation was obtained from the Hetero-compound Information Center in Uppsala (HIC-UP), Sweden (Kleywegt and Jones, 1998) and was included in further refinement. The final R_{cryst} and R_{free} were 0.22 and 0.23, respectively, at 1.75 Å resolution, after checking the structure using the PROCHECK (Laskowski *et al*., 1996) from the CCP4 package (CCP4, 1994) and doing further adjustments.

2.5.4 Calculation of the rotation angle

In order to calculate a rotation angle between one domain of the structure and the equivalent domain of the other structure, two structures were first superimposed at one domain, using LSQKAB from the CCP4 package (Kabsch, 1976; CCP4, 1994). Then, another domain of the rotated structure was superimposed onto the subsequent domain of the other structure while the structural polar chi angle was set at the value obtained from the previous rotation. The structural polar chi angle from the second rotation corresponds to the rotation angle of the equivalent domain between two structures (CCP4, 1994)

2.6 Site-directed mutagenesis of CgIDH

2.6.1 Cloning the *icd* gene from *C. glutamicum* into an *E. coli* expression vector

2.6.1.1 Isolation of the plasmid DNA through ‘mini-prep’

The plasmid DNA was purified by either the manual ‘mini-prep’ method (Birnboim and Doyle, 1979) or using the Wizard® *Plus* SV Minipreps DNA purification kit (Promega). The isolated colony was inoculated into 5 mL LB medium containing 100 μg mL^{-1} ampicillin and shaken at 37 °C overnight. The cells were harvested by centrifugation at 5 000 ×g for 20 min. In the manual ‘mini-prep’ method, the harvested cells were resuspended into 100 μL of the lysis buffer [25 mM Tris-HCl (pH 8.0), 50 mM glucose, and 10 mM EDTA]. Then, 200 μL of a freshly prepared alkaline solution [0.2 N NaOH, and 1% SDS] was added and mixed with the cell lysis solution. The mixture was incubated on ice for 5 min and then neutralized by adding 150 μL of neutralization solution [3 M potassium acetate], so that the plasmid DNA could be separated from the other cell components. After centrifugation of the mixture at 11 000 ×g for 10 min, the supernatant contained plasmid DNA whereas the cell debris precipitated. The plasmid DNA was extracted by adding an equal volume of a phenol:chloroform:isoamyl alcohol (25:24:1) solution. The mixture was vortexed and centrifuged at 12 000 ×g for 2 min. The upper aqueous layer was carefully transferred to a fresh tube. A two volume of ice-cold 95% ethanol was added to the supernatant and the plasmid DNA was precipitated by flash cooling the mixture at -80 °C. The plasmid DNA was then washed twice with 70% ethanol and dried at room temperature. The dried plasmid DNA was re-suspended into TE buffer [10 mM Tris-HCl (pH 8.0) and 1 mM EDTA] containing 20 μg mL^{-1} RNase.

The Wizard® *Plus* SV Minipreps DNA purification kit (Promega) was used, in which all solutions and spin columns were provided. The harvested cells were resuspended and lysed in cell re-suspension and lysis solutions, respectively. Then, alkaline phosphatase was added and the mixture was incubated at room temperature for 5 min. After adding the neutralization solution, the mixture was centrifuged at 10 000 ×g for 10 min. The supernatant was carefully applied to a spin column. The plasmid DNA bound to the membrane of the spin column, so that only plasmid DNA was eluted with nuclease-free water after washing the column with ethanol. The purified plasmid DNA was stored at -80 °C.

2.6.1.2 Polymerase chain reaction (PCR)

The cloning of the *icd* gene into an *E. coli* expression vector is schematically illustrated in Figure 2.4. Two primers, named as IDH-U, 5′d(CAGCCAAGGGAATTCATGGCTAAG) and

IDH-D, 5′d(CCTTGTCGACGTCGACGCTGAGTG), were designed to newly introduce *EcoR*I and *Sal*I sites at amino- and carboxy-termini of the coding region for *C. glutamicum* IDH (the *icd* gene). These primers were synthesized by Dr. F. Georges laboratory of the Plant Biotechnology Institute (PBI), Saskatoon, Saskatchewan. The coding regions were amplified by the polymerase chain reaction (PCR) using pEK*icd*ES1 (a generous gift from J. Eikmanns at Universität Ulm, Germany) as a template. Fifty µL of the PCR mixture containing 800 ng of template DNA (pEK*icd*ES1), 0.2 µmol of each primer, 0.2 mM dNTPs mix, 5 units of Nova*Taq*^{TM} DNA polymerase and 1× PCR buffer containing 1.5 mM $MgCl_2$ (Novagen) was carried for 30 thermal cycles. Each thermal cycle involved denaturation at 94 ºC for 1 min, annealing at 53 ºC for 1 min 40 s, and polymerization at 71 ºC for 2.5 min. An extra denaturation at 94 ºC for 3 min and polymerization at 71 ºC for 3 min was added to initiate and terminate the thermal cycles, respectively. The PCR product was obtained through phenol:chloroform:isoamyl alcohol extraction followed by ethanol precipitation previously described. The isolated PCR product was digested with *EcoR*I and *Sal*I restriction enzymes and run on 1% agarose gel. The digested DNA with the corresponding size was excised from the gel and extracted using Quantum Prep^{TM} Freez ‘N Squeeze DNA gel extraction spin column (Bio-Rad Laboratory).

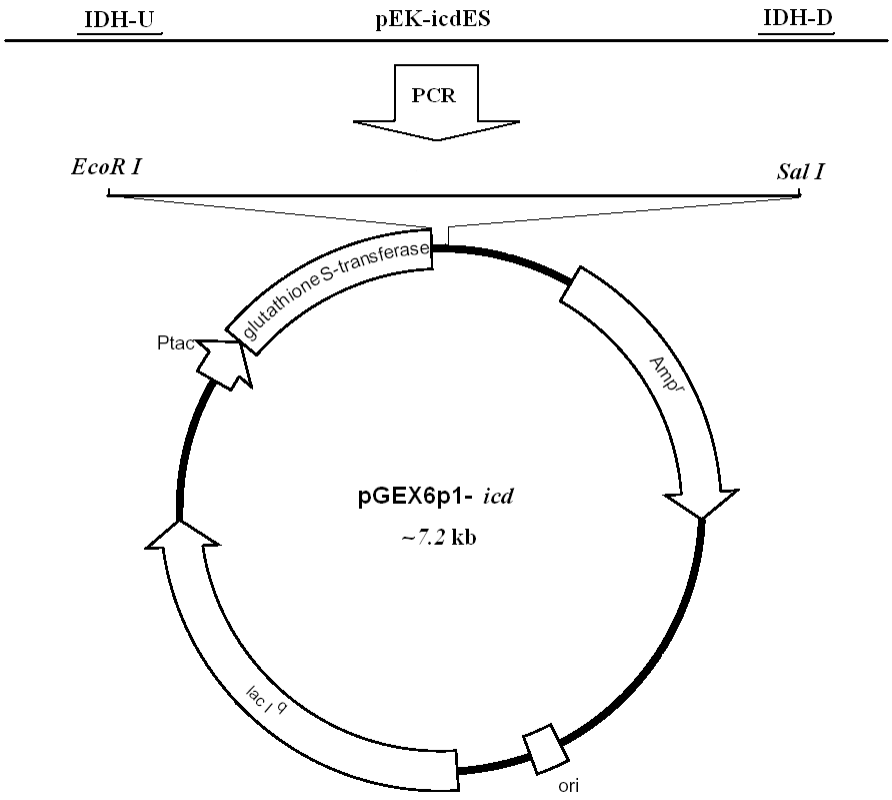

Figure 2.4 Schematic illustration of cloning the *icd* gene into an *E. coli* expression vector.

The *icd* gene was amplified from the template plasmid (*p*EK-icdES) using the upstream (IDH-U) and downstream (IDH-D) primers. The PCR created two restriction enzyme cleavage sites (*EcoR*I and *Sal*I). The amplified gene was inserted into the pGEX6p1 protein expression vector that consists of an origin (ori), a *Lac*I^q gene (lac I^q), a *taq* promoter (P_{tac}), a GST tag (glutathione S-transferase), and an ampicillin resistance gene (Amp^r).

2.6.1.3 Ligation of the *icd* gene into the plasmid vector

Using the extracted DNA insert, the ligation mixture containing the isolated DNA insert, the pre-digested *E. coli* expression vector (pGEX6p1), 0.2 mM ATP, 1 mM DTT, 1× reaction buffer and 4 units of T4 DNA ligase (Novagene) was incubated at 12 ºC overnight. Then, 2 µL of the ligation mixture was added to 100 µL of *E. coli* DH5α competent cells and chilled on ice for 30 min. Heat-shock was applied to the transformed cells at 42 ºC for 1 min, followed by cooling on ice for 2 min. To the cell mixture, 400 µL of LB media was added, and the cells were incubated at 37 ºC for one hour (out-growth). The out-grown cells were plated on LB-agar plates containing 100 µg mL^{-1} ampicillin and incubated at 37 ºC overnight. The colonies were

inoculated into 5 mL of LB media at 37 ºC overnight, and the ligated plasmid DNA was isolated using Wizard® *Plus* SV Minipreps DNA purification kit (Promega). The constructed plasmid was sequenced at PBI using a Stretch DNA sequencer (Applied Biosystems), to confirm the insertion of the *icd* gene in the proper reading frame.

2.6.2 Site-directed mutagenesis

Site-directed mutagenesis was performed using the Quickchange® site-directed mutagenesis kit (Stratagene). Three CgIDH mutants were designed based on previous studies on dimeric $NADP^+$-dependent IDH mutants and the partial sequence alignments obtained from crystallographic structures. The analogous residues, Ser113, Lys253, and Tyr416 were altered to aspartic acid, glutamine, and threonine, respectively. The pairs of oligonucleotide primers used to generate each of these three mutants are listed in Table 2.5. These mutagenic primers were synthesized by Dr. F. Georges laboratory of the PBI, Saskatoon, Saskatchewan.

Using each pair of oligonucleotide primers, PCR was carried out in a 50 µL reaction mixture containing 100 ng of 7.3 kb template DNA (pGEX6p1-*icd*), 250 ng of each oligonucleotide, 0.25 mM dNTPs mixture, 2.5 units of *Pfu Turbo*™ DNA polymerase and 1× reaction buffer (Stratagene). Denaturation, annealing, and polymerization were performed at 95 ºC for 50 sec, 60 ºC for 1 min, and 68 ºC for 10 min, respectively, for 18 cycles. Each reaction was initiated with an additional denaturation at 95 ºC for 1min and was terminated at 68 ºC for 7 min after the above 18 cycles of the reaction were completed. The reaction mixture was incubated at 37 ºC for one hour after adding 10 units of *Dpn* I in order to digest the methylated, template DNA. Then, 2 µL of the *Dpn* I digested DNA was transformed into 100 µL of *E. coli* XL1-Blue supercompetent cells by the heat-shock method described above. The outgrown cells were plated and grown on LB agar plates containing 100 µg mL^{-1} ampicillin. Colonies were sub-cultured and the plasmid DNA was isolated using the Promega Wizard® plasmid DNA purification kit described above. These mutants were sequenced at DNA Technologies Unit NRC-PBI using the sequence primer provided from Amersham Biosciences Pharmacia to confirm the successful mutations.

CgIDH mutant	Oligonucleotide primer pairs	T_m (°C)
Ser130Asp	U; 5'd(GCAGCACTGGGTTCACAGCGTCACCCTTAACAGC)3' D; 5'd(GCTGTTAAGGGTGACGCTGTGAACCCAGTGCTGC)3'	79.8
Lys253Gln	U; 5'd(CATCATGGTGGCCTGCAGGTGTGCGGAG)3' D; 5'd(CTCCGCACACCTGCAGGCCACCATGATG)3'	80.2
Tyr416Thr	U; 5'd(GGTCTTGTCATGGGAGCCGGTCTCTTCAGCCTTC)3' D; 5'd(GAAGGCTGAAGAGACCGGCTCCCATGACAAGACC)3'	79.9

Table 2.5 List of oligonucleotide primer pairs used to generate CgIDH mutants.

Each pair of oligonucleotides (U = Upstream; D = downstream) is designed to alter the minimum number of nucleotides to generate the desired mutant. The underlined nucleotides are those that were changed to create the mutated residue. The melting temperature (T_m) was calculated by;

$$T_m = 81.5+0.41\ (\%\ GC)- 675/N -(\%\ mismatch)$$

where % GC is the percentage of GC bases, N refers to the primer length in bases, and % mismatch is calculated simply by (changed bases/ total bases) multiplied by 100 (Nelson and McClelland, 1992).

2.6.3 Purification of CgIDH mutants

2.6.3.1 Protein overexpression

The plasmid containing the *icd* gene mutant was transformed as described above into either 100 µL of *E. coli icd*$^-$ strain EB106 or BL21 competent cells. The transformed cells were streaked on an LB agar plate containing 100 µg mL^{-1} ampicillin and were incubated at 37 ˚C overnight. A single colony was inoculated into 3 mL of LB medium with ampicillin (100 µg mL^{-1}) and shaken at 37 ˚C overnight. The grown culture was then transferred to 200 mL of LB medium containing 1% glucose and ampicillin (100 µg mL^{-1}) and was further incubated at 28 ˚C. When absorbance of the culture reached at OD_{600} = 0.4-0.6, 0.25 mM IPTG was added to induce bacterial growth overnight at 28 ˚C. The cells were harvested by centrifugation at 6 000 ×g for 20 min.

2.6.3.2 Affinity chromatography purification

The wet cell pellet was resuspended in 4 mL of ice-cold 1× PBS buffer [2.7 mM KCl, 10mM Na_2HPO_4, 1.8 mM KH_2PO_4, and 140 mM NaCl (pH 7.3)] and was sonicated at 50 W (5× 1 min bursts with 6 min intervals). The cell homogenate was centrifuged at 12 000 ×g for 20 min. The sonication and centrifugation were repeated two more times. The supernatant (crude extract)

after each centrifugation was transferred to fresh tubes and expression levels of the GST-fused IDH mutants were examined on SDS-PAGE gel. After addition of 5 mM DTT, the crude extract was loaded onto a pre-equilibrated glutathione Sepharose 4B column (Amersham Biosciences) with 1× PBS buffer. The column was washed twice with 10× bed volume of Buffer B [50 mM Tris-HCl (pH7.0), 0.15 M NaCl, and 1mM DTT]. Then, PreScission^{TM} protease diluted 1:25 with Buffer B was applied to the column and incubated at 4 ˚C overnight in order to cleave the GST tag. The enzyme was eluted with Buffer B, followed by glutathione elution Buffer C [10 mM reduced glutathione, 50 mM Tris-HCl (pH 8.0) and 1 mM DTT]. Protein purity at each step was checked by SDS-PAGE.

2.6.3.3 Mass spectrometry (MS)

Mass spectrometry (MS) is used to measure the molecular mass of a compound. MS studies for the purified IDH mutants were performed at the PBI by Doug Olson. The protein molecular weight was determined by linear MALDI-TOF MS. A protein solution containing approximately 10 pico-moles of protein was mixed 1:1 with sinapinic acid as the matrix. The matrix was made up at 20 mgs/ml in 70% acetonitrile and calibrated wit bovine serum albumin.

2.7 Kinetic assays of wild-type and mutant CgIDH

The kinetic characteristics of an enzyme can be determined if the absorbance of an assay solution changes as a substrate is converted into the product by enzyme catalysis. When either the substrate or the product of a catalytic reaction absorbs light of a certain wavelength, the change in the absorbance monitored is related to the rate of catalysis. The rate of catalysis is equivalent to the change in absorbance over the time-course of the reaction, as in the calculation below (Formula 2.6):

$$\text{Rate} = \frac{(\Delta A/\text{min})\ (\text{Assay Volume})}{(\epsilon)\ (\text{Path Length})}$$

Formula 2.6

where (ΔA/min) is the change in absorbance per min, and ε is the extinction coefficient for the product in the assay system. One μmol of product formed per mg of enzyme per minute is termed the specific activity of the enzyme and is calculated by:

Specific Activity = Rate/ [mg of protein used in the assay]

Enzyme assays were performed at room temperature using an Ultraspec 2100 *pro* UV/visible spectrophotometer and the application software, SWIFTII-Methods (Amersham Biosciences). The 1-ml assay solution consisted of 87.4 mM triethanolamine buffer (TEA) pH 7.6, 0.8 mM $MnSO_4$, 1.0 mM isocitrate and 0.5 mM $NADP^+$, unless specific conditions were mentioned (Bai *et al*., 1999). The K_m values for isocitrate and $NADP^+$ have been reported as 5 μM and 4 μM, respectively (Chen and Yang, 2000). For activity assays of wild-type CgIDH, about 1-2 μg of enzyme was used, whereas ~100 μg of the CgIDH mutants were required to examine their activities. A unit of activity is defined as 1 mmol of NADPH formed per minute while ε for NADPH is 6220 M^{-1} cm^{-1}. Absorbance at 340 nm increased as $NADP^+$ was changed into NADPH by CgIDH catalysis, as shown in Figure 2.5.

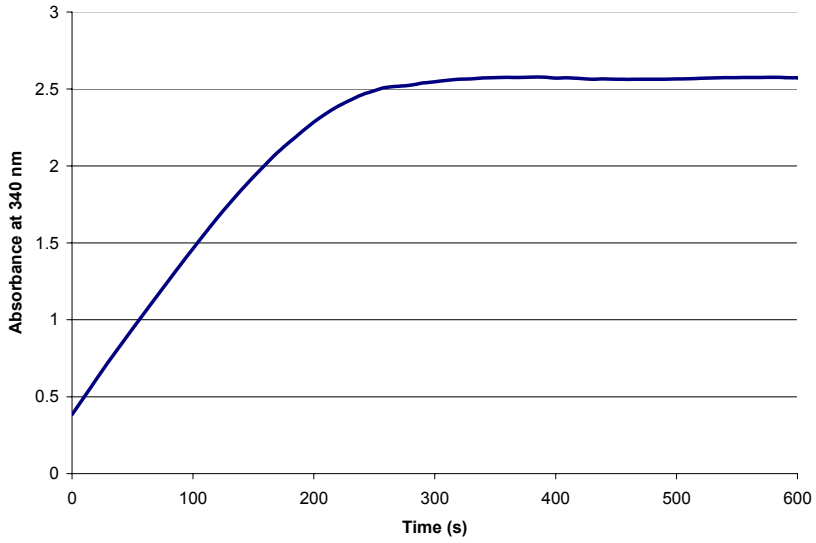

Figure 2.5 A typical plot for CgIDH activity.

The absorbance at 340 nm was increased over a time-course as $NADP^+$ was converted to NADPH by CgIDH catalysis. About 1.5 μg of CgIDH was used to obtain its catalytic activity.

2.8 Fluorescence spectroscopic studies on CgIDH

Fluorescence is the property of certain molecules (known as fluorophores) to absorb light at one wavelength and emit light at a longer wavelength (reviewed in Eftink and Shastry, 1997). When a fluorophore absorbs light energy, it is usually excited to a higher vibrational energy level in the excited state (Figure 2.6). The subsequent rapid relaxation to the lowest vibrational energy

level is termed internal conversion (IC) and occurs in a pico-second or less. IC is the radiationless transition (heat) between energy levels of the same spin state. If the photon emission occurs between the same spin states, this radiative process is called fluorescence. Due to the relaxation of energy in the excited state, the detected fluorescence emission has lower energy than the detected absorption. This difference in energy between fluorescence and absorption is called the Stokes shift.

Three aromatic amino acid residues in proteins, Trp, Tyr and Phe, have distinct absorption and emission wavelengths and can contribute to the intrinsic fluorescence of a protein. The dominant intrinsic fluorophore, Trp, has much stronger fluorescence and higher quantum yield than the other two aromatic amino acid residues. Its fluorescence can be selectively excited at 295-305 nm and can be observed at 330-350 nm. Trp fluorescence is very sensitive to its local environment. Typically, Trp residues that are exposed to water, have maximal fluorescence at a wavelength of about 340-350 nm, whereas for totally buried Trp residues fluorescence occurs at about 330 nm. Any changes in fluorescence emission spectra of a protein are related to a conformational change, a subunit association, substrate binding, denaturation, or anything that affects the local environment surrounding the indole ring of the Trp residue. Also, Trp appears to be uniquely sensitive to collisional quenching, either by externally added quenchers such as acrylamide, or by neighboring protonated acidic groups such as Asp or Glu in the protein. Hence, fluorescence spectroscopy is a useful technique to monitor the local side chain environment and dynamics of a protein in solution (reviewed in Eftink and Shastry, 1997).

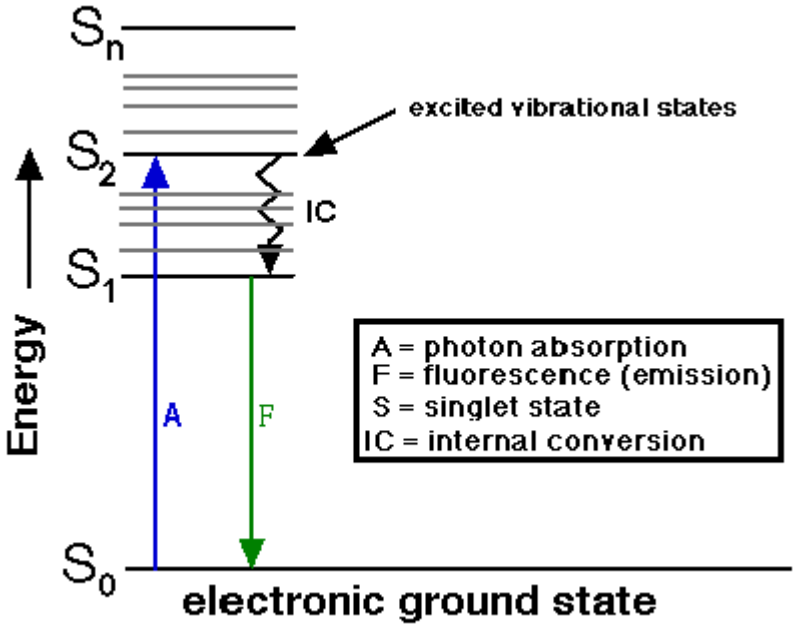

Figure 2.6 A Jablonski diagram describing absorption and emission of light.

Fluorescence activity can be schematically illustrated with a Jablonski diagram, which describes how electrons in fluorophores are excited from the ground state (S_0) into higher electronic energy states (S_1, S_2, and Sn), and then how these excited molecules emit photons and fall back into lower energy states. Modified from website: http://www.shsu.edu/~chemistry/chemiluminescence/JABLON.GIF

Prior to fluorescence spectroscopic studies, absorption spectra studies were conducted using the Ultraspec 2100 *pro* UV/Visible spectrophotometer (Amersham Bioscience), in order to verify the presence of an interaction between CgIDH and its substrate(s) before excitation. Interactions between CgIDH and its substrate(s) before excitation can be monitored by any changes in the absorption spectra. The absorption spectrum for CgIDH was observed between 250 nm to 500 nm before and after adding its substrate(s).

In this research, fluorescence spectroscopic studies were performed at room temperature using the fluorescence spectrometer F-2500 (Hitachi). A KAC buffer [25 mM 3-[N-morpholino] propane sulfonic acid (MOPS) pH 7.3, 5 mM $MgCl_2$, 100 mM NaCl and 1mM DTT] was used as a dilution and a reference buffer. Setting excitation wavelength at 297 nm with 10 nm excitation emission slits, fluorescence spectra were measured at 310-550 nm. No fluorescence was observed by the KAC buffer, isocitrate or $NADP^+$ by itself at 250-350 nm. The changes in maximum fluorescence emission from Trp residues within the protein in the absence and

presence of the substrate(s) were recorded. About 30-50 μg mL^{-1} of protein was used to obtain the fluorescence spectra.

Chapter 3 Results

3.1 Modified purification of monomeric IDH from *C. glutamicum*

For protein crystallization, typically a protein purity of 95 % or higher is recommended. In order to achieve such high purity, an effective protein purification strategy uses a minimum number of steps. Monomeric IDH from *C. glutamicum* (CgIDH) was previously purified with three different chromatography steps after sonication and ammonium sulfate fractionation. Among these chromatography steps, gel filtration was the least effective because of the lowest purity improvement (Bai *et al*., 1999). The anion exchange step with Mono Q HR 10/10 appeared to give the highest purity. This step, however, was difficult and time-consuming since concentration of the pooled protein fractions was required before applying to the column and it required desalting of the collected protein fractions after passing through the column. Affinity chromatography, on the other hand, was the most specific and quick method for CgIDH purification since only $NADP^+$-dependent proteins bind to this column. Therefore, gel filtration and anion-exchange chromatography were omitted after ammonium sulfate fractionation. Ammonium sulfate fractionation was an important step to reduce the volume of crude extract from the repeated sonication so that an adequate volume of protein solution could be applied to the affinity column. The purity from this two-step purification method was still close to 95% according to SDS-PAGE (Figure 3.1), and CgIDH crystals were successfully obtained after using this protein purification strategy.

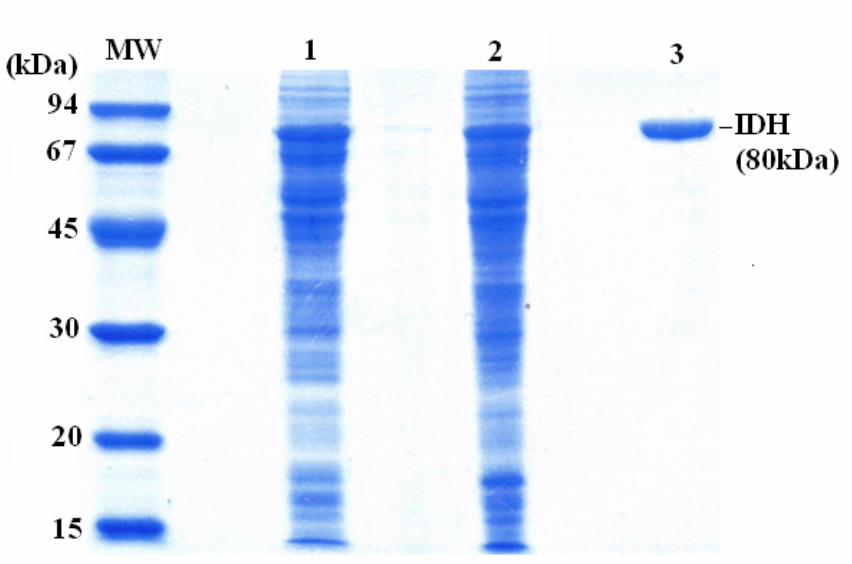

Figure 3.1 SDS-PAGE of CgIDH.

Proteins are stained with Coomassie Blue on the 8% SDS-PAGE. The molecular mass marker (MW) is at the left-end. Approximately 5 μg of protein solution was loaded per lane. Lane 1 for crude extract, Lane 2 for protein solution after the ammonium sulfate fractionation, and Lane 3 for purified CgIDH after Red Sepharose CL-6B affinity chromatography. The approximate molecular mass of CgIDH is 80 kDa as indicated.

3.2 Crystallization

3.2.1 Crystallization in the absence and presence of substrate(s)

Purified CgIDH at a concentration of 5 mg ml^{-1} was crystallized by the hanging-drop vapour diffusion method at room temperature under the conditions previously described (Audette *et al*., 1999). Although an IDH crystal with 0.3 × 0.1 × 0.05 mm dimensions was obtained within a week (Figure 3.2A), the crystal spontaneously started cracking soon after it was exposed to air or several weeks after it appeared (Figure 3.2B).

From the additive screening trials, some additives such as sucrose, glucose, MPD, and ethylene glycol seemed to improve crystal stability (Figure 3.2C) while most inorganic ions had less effect on crystallization. The presence of a substrate (isocitrate or $NADP^{+}$) or an inhibitor (e.g. malate) could stabilize crystals but usually produced a cluster of crystals (Figure 3.2D). Lower concentrations of protein reduced crystal growth rate but a single crystal was only occasionally obtained after a year (Figure 3.2E).

In addition to vapour diffusion crystallization, direct interface crystallization in a capillary using agarose gel or Silica Hydrogel™ was attempted. The problems with this method, however, were the difficulties to observe crystals in a glass capillary and to mount one on the goniometer head for diffraction. Therefore, either successful additives or lower protein concentrations 3-5 mg mL^{-1} were used to produce crystals of consistent quality.

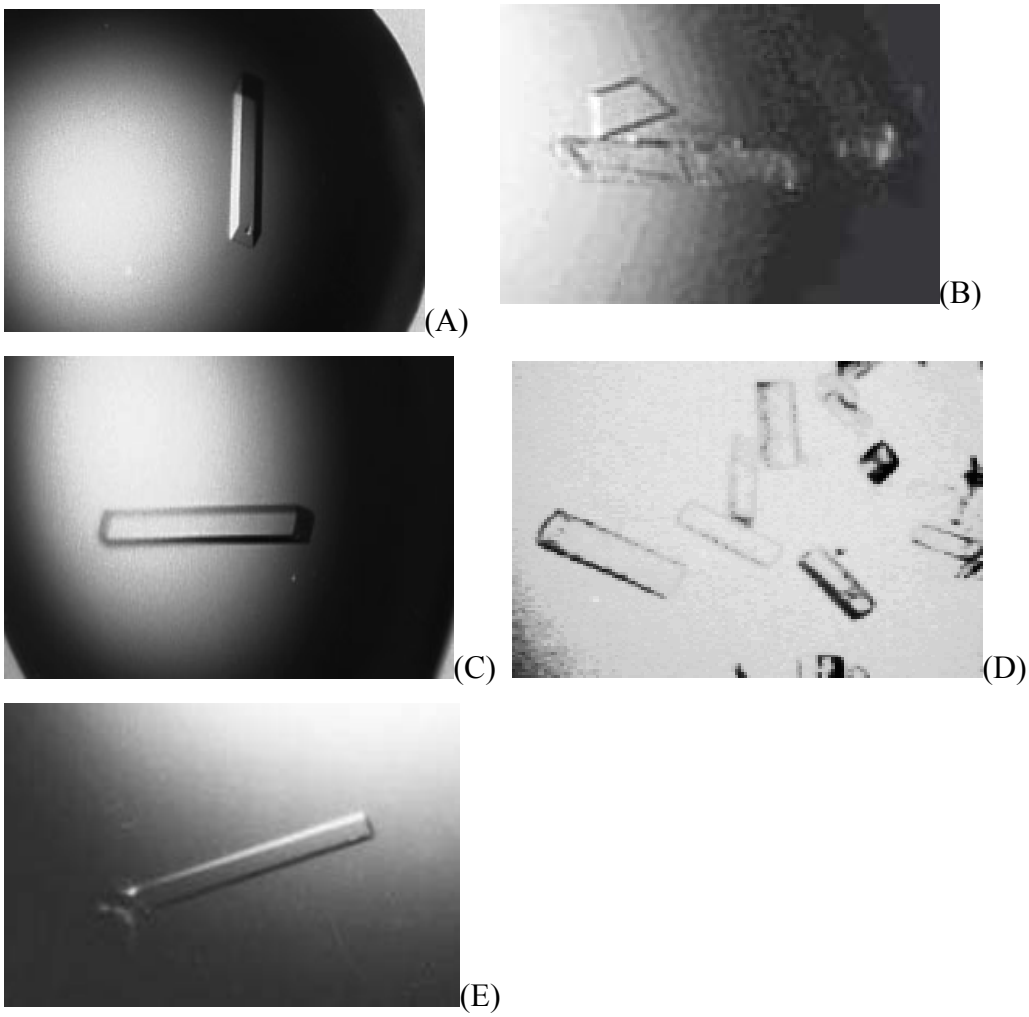

Figure 3.2 CgIDH crystals.

(A) A single crystal of CgIDH complexed with Mg^{2+} was obtained under the conditions previously described (Audette *et al*., 1999). (B) The crystal cracked after a few weeks or when it was exposed to the air. (C) A single CgIDH crystal obtained with 6 % sucrose as an additive. (D) Clusters of CgIDH crystals complexed with NAD^+ obtained under the same conditions as (A) but with 2.5 mM NAD^+. (E) A single CgIDH crystal obtained from a lower concentration of protein after crystallization for a year.

3.2.2 Cryo-crystallography

Various cryoprotectants were prepared and examined by a flash cooling method in order to optimize the cryocrystallographic conditions for successful diffraction data collection from CgIDH crystals. The challenge was that, to date, no CgIDH crystal had given diffraction data better than 3.0 Å resolution nor acceptable crystal mosaicity. High crystal mosaicity makes it difficult to distinguish the diffraction spots from background noise, and thus to determine reflection intensities from which the structure factors are calculated. Due to high crystal

mosaicity, the preliminary diffraction data sets for CgIDH were not accurate enough to solve the structure. It is not unusual for a protein crystal to diffract poorly due to non-optimal cryo conditions. The first AvIDH structure was, indeed, solved after growing the crystal in the presence of 20 % (v/v) glycerol and then flash cooling the crystal under a nitrogen stream just prior to diffraction, because earlier cryoprotectant trials were unsuccessful (Yasutake *et al*., 2002). For CgIDH crystals, however, optimization of the cryoprotectant was definitely required since it had to be frozen prior to shipping to a synchrotron.

After many trial-and-error attempts, a CgIDH crystal complexed with Mg^{2+} successfully diffracted to 1.75 Å resolution. Rather than one single cryoprotectant, a combination of two cryoprotectants, as well as a combination of a cryoprotectant and light paraffin oil appeared to work synergistically to achieve successful diffraction. Covering the crystal-containing droplet with oil prevented cracking of the crystal when exposed to the air. The use of a slightly smaller loop for mounting a crystal also minimized the volume of cryoprotectant covering the crystal. The successful cryocrystallographic conditions and diffraction results are summarized in Table 3.1 and support the idea that a combination of a cryoprotectant with light paraffin oil and a combination of two cryoprotectants most likely worked synergistically to improve resolution and lower crystal mosaicity.

Cryoprotectant(s)	Oil treatment	Diffraction resolution limit (Å)
20 % MPD	No	3.0-3.5
15 % Glycerol	Yes	2.0
30 % Glycerol	No	3.0
30 % Glycerol	Yes	2.2-2.4

10 % MPD and 20 % Glycerol	No	4.0
10 % MPD and 20 % Glycerol	Yes	2.2
15 % MPD and 10 % Glycerol	No	1.8
15 % MPD and 15 % Glycerol	No	2.3-2.6
A serial soaking of 15 %, 20 % and 30% Glycerol	No	3.0
A serial soaking of 20 % and 30% Glycerol	No	3.0-5.0
A serial soaking of 20 % and 30% Glycerol	Yes	1.7-2.3

Table 3.1 Effects of different cryoprotectants and of light paraffin oil on the Mg^{2+}-complex of CgIDH crystal diffraction.

Oil treatment refers to the condition where light paraffin oil was used to cover the crystal-containing droplet during soaking the crystal in cryoprotectant, to prevent exposure to the air. Diffraction resolution limits were obtained from one to three images of each previously frozen crystal at the APS.

3.3 The structure of CgIDH in complex with Mg^{2+}

3.3.1 Quality of the final structure

The structure of CgIDH in complex with Mg^{2+} was solved and refined to a resolution of 1.75 Å. There are four symmetry related CgIDH molecules well packed in the unit cell (Figure 3.3). Each molecule of CgIDH in the refined crystal structure consists of 735 amino acid residues (of a total of 738 in the CgIDH sequence). Electron density was not observed for the first N-terminal residue and for the last two C-terminal residues. There are 235 water molecules refined in the final structure. One divalent metal ion, Mg^{2+}, was observed adjacent to Asp346. The structure was analyzed by the program PROCHECK from the CCP4 package (Laskowski *et al*., 1993; CCP4, 1994). The final R_{crys} and R_{free} values were 0.226 and 0.245, respectively. The average B factors for protein atoms, water molecules, and Mg^{2+} were 30.7 $Å^2$, 29.4 $Å^2$, and 18.5 $Å^2$, respectively; the overall average B factor was 30.4 $Å^2$. A total of 91% of the residues in the CgIDH structure were within the most favoured region of the Ramachandran plot (Figure 3.4) (Ramakrishnan and Ramachandran, 1965). Both Glu13 (φ = 39 and ψ = -124) and Glu418 (φ = 53 and ψ = -136) were in the generously-allowed region but were in excellent density in the 2***F***o-***F***c map, confirming the validity of their unusual dihedral angles. The mean coordinate error from the Luzatti plot analysis was 0.24 Å (Luzatti, 1952). The final refinement statistics are summarized in Table 3.2.

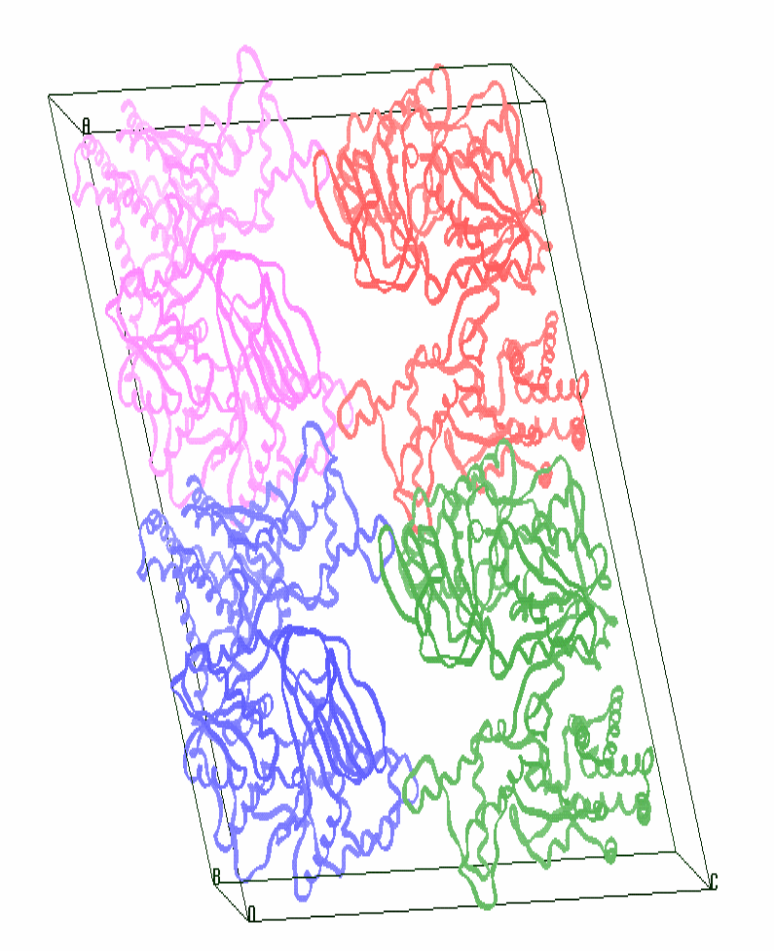

Figure 3.3 Packing of CgIDH molecules in its unit cell.

Four symmetrically related monomeric IDH molecules were packed well within its unit cell. Each equivalent molecule of CgIDH is drawn in different coloured ribbon. This picture was produced from Setor (Evans, 1993).

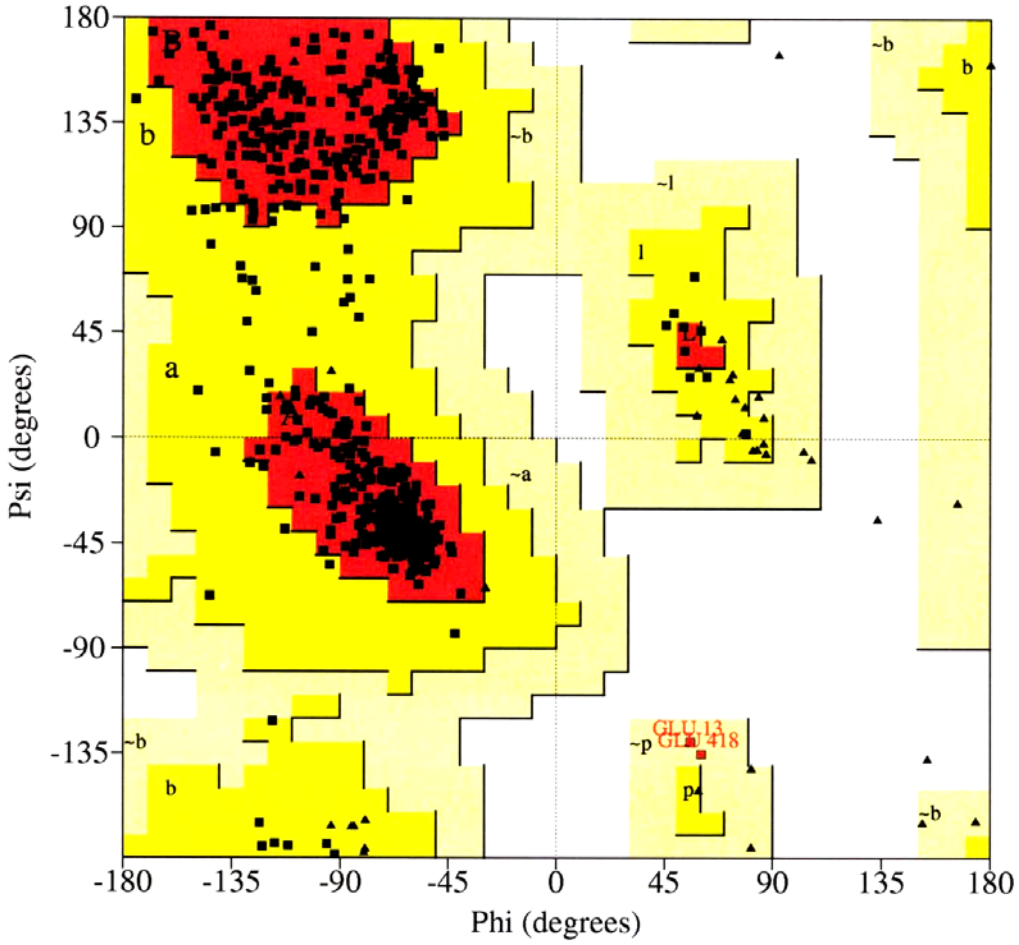

Figure 3.4 Ramachandran plot for the structure of CgIDH complexed with Mg^{2+}.

Every square represents a non-glycine residue in the CgIDH molecule; each triangle is a glycine residue. The red colored region is the most favoured region in the Ramachandran plot (Ramakrishnan and Ramachandran, 1965). The yellow and light-yellow colored areas are the additional and generously allowed regions, respectively. The disallowed region is white. Two red squares labeled as Glu13 and Glu418 are in generously allowed region in the plot, but in the structure, these residues lie in well-defined electron density. The regions labeled as a/~a, b/~b, l/~l, and p/~p correspond to the right-handed α-helices, β-strands, left-handed α-helices, and turns of the structure of a protein, respectively.

Resolution limits (Å)	15-1.75 (1.82-1.75)
No. of reflections	75896 (6563)
R_{cryst}	0.226 (0.322)
R_{free}	0.245 (0.322)
No. of residues	735
No. non-hydrogen atoms	5868
No. water molecules	235
Overall B factor ($Å^2$)	30.4
Average B factor for protein atoms ($Å^2$)	30.7
Average B factor for water molecules ($Å^2$)	29.4
R.m.s.d. from ideal geometry	
Bond distances (Å)	0.005
Bond angles (°)	1.276
Dihedral angles (°)	21.93
Improper angles (°)	0.856
Ramachandran plot regions	
Residues in most favored regions (%)	91.7
Residues in additional allowed regions (%)	8.0
Residues in generously allowed regions (%)	0.3
Residues in disallowed regions (%)	0.0

Table 3.2 Summary of the refinement statistics for a crystal of CgIDH complexed with Mg^{2+}.

The quality of the structure of CgIDH complexed with Mg^{2+} was tested with PROCHECK from the CCP4 package after its final refinement (Laskowski *et al*., 1993; CCP4, 1994). The R_{crys} and R_{free} were calculated from Formulas 2.3 and 2.4 described in Materials and Methods (Page 48). The values in brackets are those for the highest resolution shell.

3.3.2 Overall structural description

The structure of CgIDH complexed with Mg^{2+}consists of two distinct domains like the other monomeric AvIDH structures (Figure 3.5) (Yasutake *et al*., 2002, 2003). The relatively

small domain (Domain I) is formed from 316 amino acid residues from both the N- and C-termini; the larger domain (Domain II) is composed of 422 residues. A cleft region was observed between these two domains and is expected to form the active site as in the other monomeric IDH enzymes. There are 14 α-helices and 6 β-strands in Domain I, and 14 α-helices and 16 β-strands in Domain II. A pseudo 2-fold axis was present only in Domain II, which is analogous to the crystallographic 2-fold axis in the homodimeric IDH structures (Figure 3.6). The equivalent topology to the clasp region that inter-locks two subunits in homodimeric IDH structures is also present in Domain II. All of the residues at the catalytic site that have been described in the structures of AvIDH are donated by the two domains of CgIDH in an asymmetric manner and are located facing the cleft region (Figure 3.7).

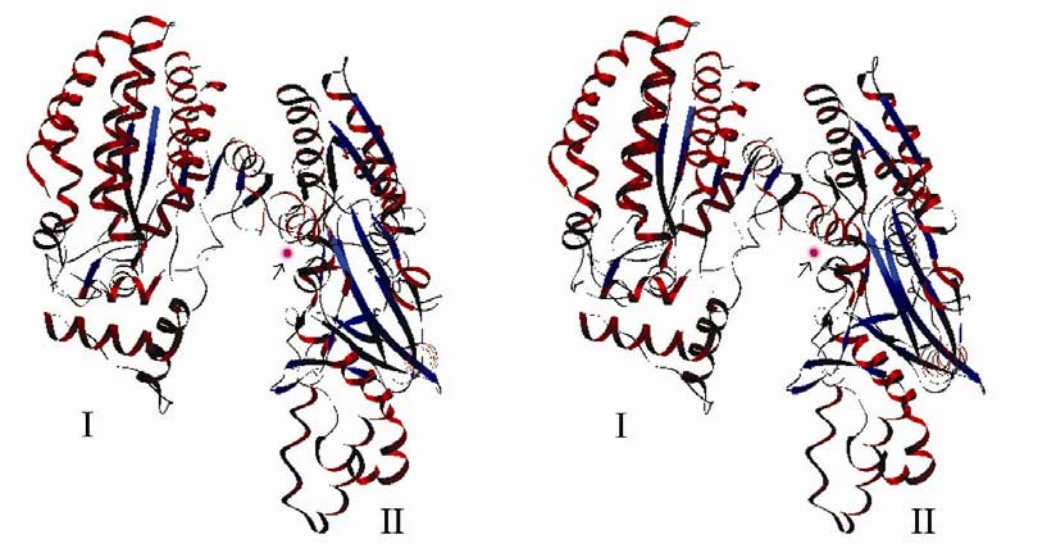

Figure 3.5 Stereo diagram of the overall structure of CgIDH complexed with Mg^{2+}.

The structure of CgIDH complexed with Mg^{2+} is composed of two distinct domains like the structure of AvIDH complexed with isocitrate-Mn^{2+} (Yasutake *et al*., 2002). The blue ribbons represent β–strands; red ribbons are α–helices. Random coils are drawn in black strings, while Mg^{2+} is drawn as a pink sphere and is indicated by an arrow. Domain I and Domain II are indicated as I and II, respectively. This figure was produced using Setor.

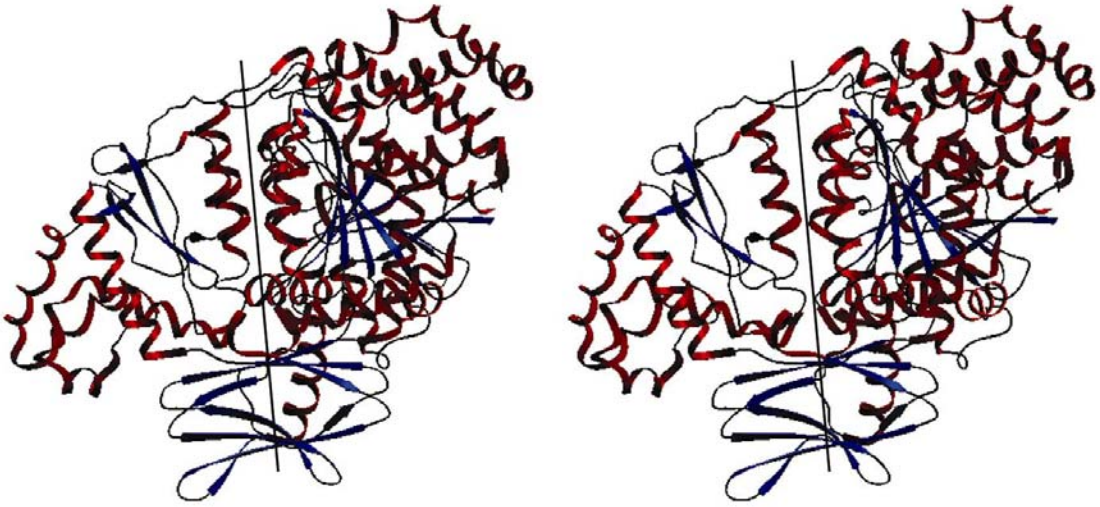

Figure 3.6 Stereo diagram of the pseudo 2-fold axis in Domain II of the structure of CgIDH complexed with Mg^{2+}.

The pseudo 2-fold axis (line) was observed only in Domain II in the structure of CgIDH complexed with Mg^{2+}. This picture was produced from Setor.

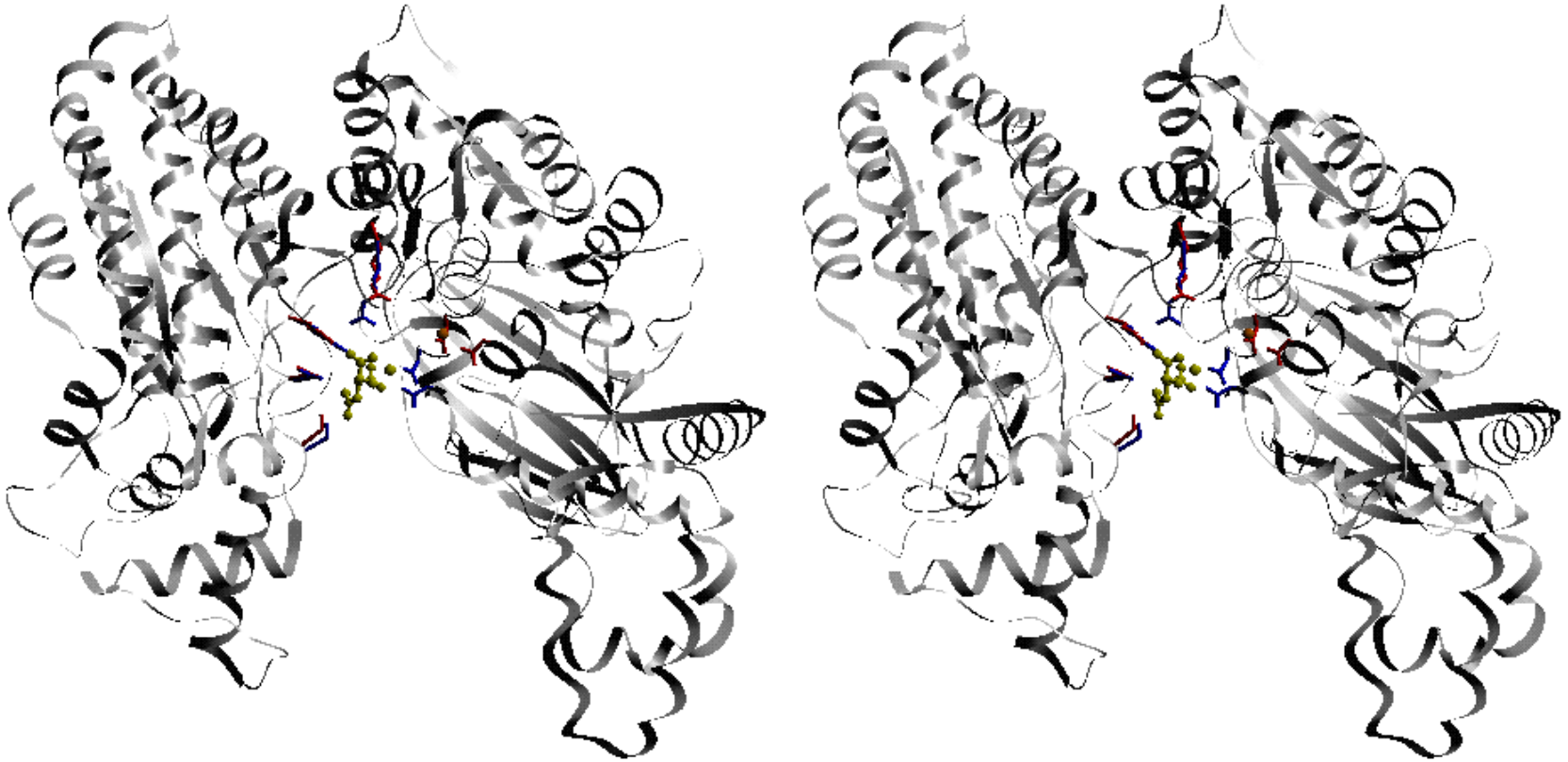

Figure 3.7 Stereo diagram of the active site in the structure of CgIDH complexed with Mg^{2+}.

The structure of CgIDH complexed with Mg^{2+} was superimposed on the structure of AvIDH complexed with isocitrate-Mn^{2+}. The backbone for the structure of AvIDH complexed with isocitrate-Mn^{2+} is not shown, but the active site residues are drawn in blue sticks. The equivalent active site residues in CgIDH to the structure of AvIDH complexed with isocitrate-Mn^{2+} are located at the cleft region between the two domains in the structure. The gray ribbons represent the backbone of CgIDH, while the equivalent active site residues are drawn in red sticks. Isocitrate and Mn^{2+} in the structure of the complex of AvIDH are drawn in yellow sticks and as a yellow sphere, respectively. This picture was produced from Setor.

3.3.3 Coordinates of Mg^{2+} at the active site

$NADP^{+}$-dependent IDH requires a divalent ion for catalysis. Magnesium chloride was added for the crystallization of CgIDH, and it was highly expected that bound Mg^{2+} would be found in the structure. One Mg^{2+} was indeed observed adjacent to Asp346 at the active site in the structure. This cation is coordinated in an octahedral geometry by Asp346 $O^{\delta 1}$, Asp544 $O^{\delta 2}$, Asp548 $O^{\delta 1}$, the carbonyl group of Asp544, and two water molecules (Figure 3.8). The bond distances for each atom to the ion are summarized in Table 3.3. The overall average coordinating distance is 2.22 Å. According to the geometrical data of metal-ligand interaction (Harding, 2001, 2004), the coordination number for Mg^{2+} is commonly six and the average metal-ligand distance is 2.26 Å when a metal is coordinated by carboxylates of Asp or Glu (Harding, 2001). Bound Mg^{2+} in the structure of CgIDH complexed with Mg^{2+} agreed with this accepted value, confirming the bound metal is magnesium ion.

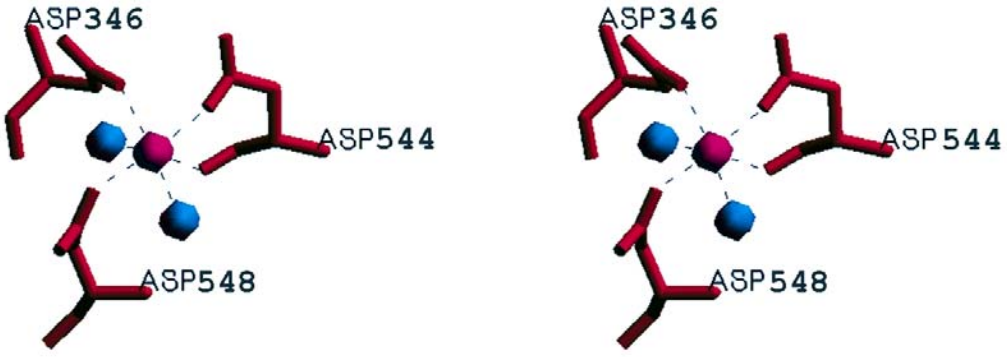

Figure 3.8 Stereo diagram of the coordinating geometry of Mg^{2+} in the CgIDH structure.

Three Asp residues (red) and two water molecules (blue spheres) coordinate Mg^{2+} (pink sphere) in an octahedral manner. The coordinating atoms are connected by dashed lines toward Mg^{2+}.

Coordinating atom	Distance from the Mg^{2+} ion (Å)
Asp346 $O^{\delta 1}$	2.20
Asp544 O	2.21
Asp544 $O^{\delta 2}$	2.17
Asp548 $O^{\delta 1}$	2.18
WAT 1031 O	2.27
WAT 1157 O	2.31

Table 3.3 The coordination distances of atoms with Mg^{2+}.
The distances were obtained from the NEIGHBOURS function on the TURBO-FRODO (Roussell *et al*., 1990).

3.4 Site-directed mutagenesis studies on CgIDH

3.4.1 Purification of the S130D, K253Q, and Y416T CgIDH mutant proteins

Three CgIDH mutants, S130D, K253Q, and Y416T were successfully created and confirmed by DNA sequencing. When the pGEX6p1-*icd* plasmid containing each CgIDH mutant was transformed into either *E. coli* EB106 strain (*icd*$^-$ strain) or BL21 strain, all the mutants were successfully transformed and overexpressed with 0.2 mM IPTG, except the Y416T mutant which could only be purified from the BL21 strain. Since these mutants were expressed with a GST-tag, the GST-tag fused CgIDH could be purified to homogeneity by one-step affinity chromatography while the endogenous *E. coli* dimeric IDH, which lacked the tag, could be excluded. Hence, all the CgIDH mutants were expressed in *E. coli* BL21 rather than in EB106, in order to apply a consistent purification method for all the mutants. GST-tag free CgIDH mutant was purified using glutathione Sepharose 4B chromatography and the on-column cleavage of the GST-tag with PreScission^{TM} protease (Figure 3.9). It should be noted that the specific activity of the CgIDH mutants could only be measured after their purification because of the presence of endogenous *E. coli* dimeric IDH in the crude extract, which catalyzes the same assay reaction.

The GST-tag also appeared to interfere with CgIDH activity, so only SDS-PAGE could be used to verify the purification progress for these mutants.

From SDS-PAGE, it was estimated that the purity of each mutant was approximately 90% (Figure 3.10). Each mutant was further tested by MS analysis to determine the precise molecular mass of each mutant.

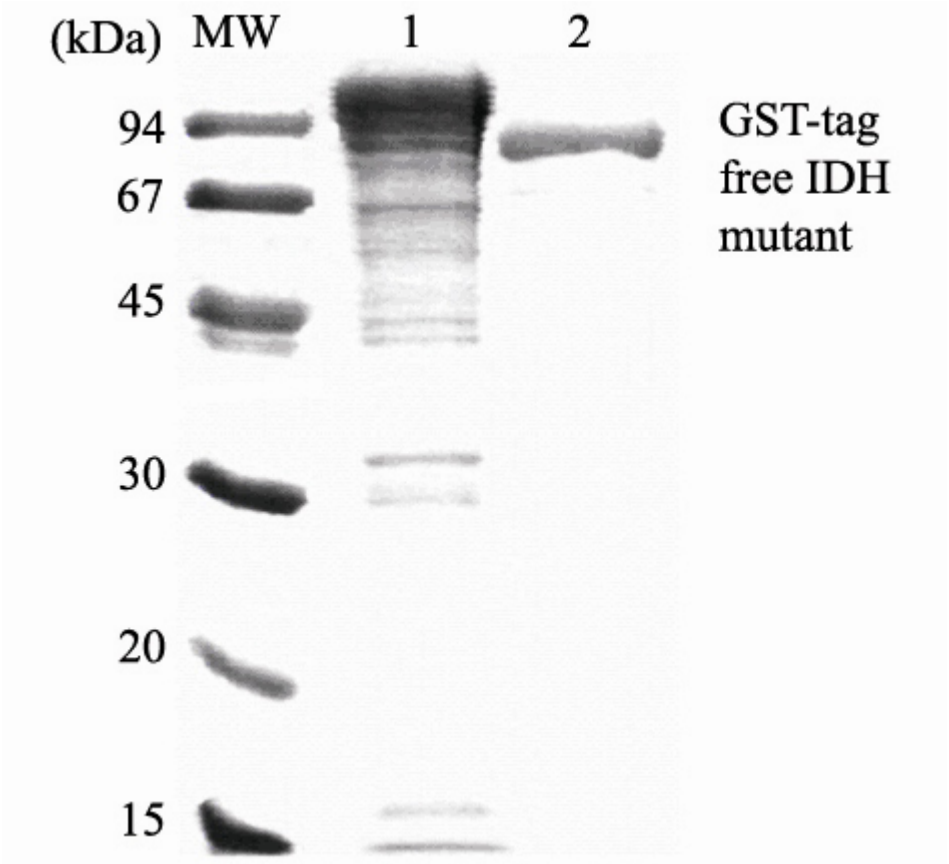

Figure 3.9 SDS-PAGE of the Y416T CgIDH mutant from *E. coli* BL21.

The GST-tag fused Y416T CgIDH mutant with its molecular mass of about 110 kDa was over-expressed in *E. coli* BL21 cells and was purified by affinity chromatography. Lane 1 for crude extract, and Lane 2 for purified CgIDH mutant after glutathione Sepharose 4B affinity chromatography and removal of GST-tag. The approximate molecular mass of this CgIDH mutant is 80 kDa after the GST-tag was cleaved. Approximately 5 μg of protein solution per lane was run on an 8% SDS-PAGE.

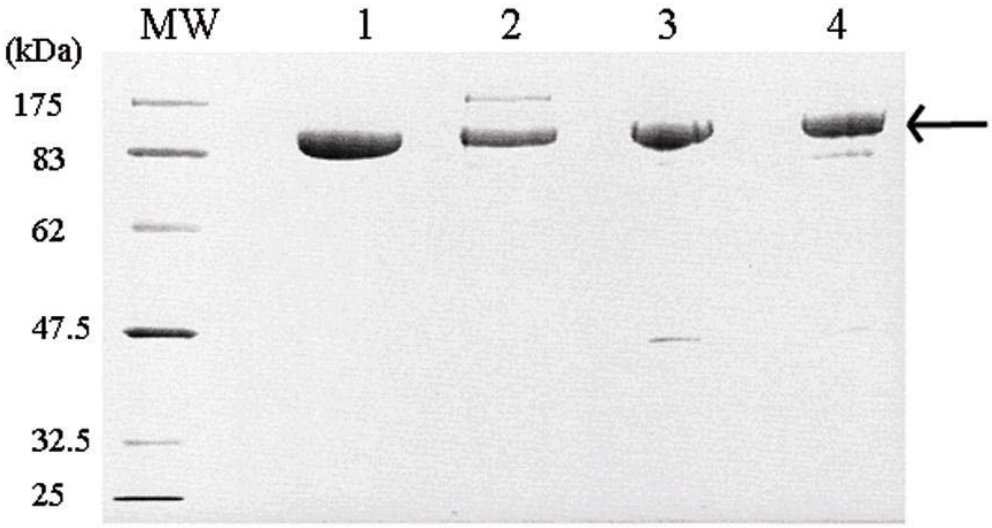

Figure 3.10 SDS-PAGE of three CgIDH mutants.

The three purified CgIDH mutants (~5 μg per lane) were run on a 6% SDS-PAGE. Lane 1 for wild-type IDH, Lane 2 for the S130D mutant, Lane 3 for the K253Q mutant and Lane 4 for the Y416T mutant. The approximate estimated molecular mass of each CgIDH mutant is ~83 kDa as indicated.

3.4.2 Specific activities of the CgIDH mutants

Enzymatic activity of the newly created and purified CgIDH mutants were tested as described in Materials and Methods, except that TEA buffer was replaced by Buffer A [25mM MES (pH 6.2), 2.5 mM $MnSO_4$ and 1mM DTT]. All of the three mutants, S130D, K253Q, and Y416T CgIDH mutants, exhibited much lower specific activities than did wild-type CgIDH. The S130D mutant exhibited ~7% of the wild type; the catalytic activity for the K253Q and Y416T mutants was not detectable.

Ser130 in CgIDH, equivalent to the catalytically important serine (Ser113) in EcIDH, is located at an equivalent position in the active site of the structure of CgIDH. Ser113 in EcIDH interacts with the oxygen atom linked to C5 of isocitrate as well as did the equivalent serine residue in AvIDH. The substitution of the phosphoserine Ser113 with a negatively charged residue inactivated EcIDH. Because of the highly conserved active site between monomeric and homodimeric IDH structures, mutating this serine residue to a negatively charged residue, Asp or

Glu, might be expected to interrupt the interaction of CgIDH with isocitrate, resulting in reduced catalytic activity or even inactivation of CgIDH (LaPorte, 1993; Yasutake *et al.*, 2002). Kinetic assays of the S130D CgIDH mutant revealed that the replacement of this Ser130 residue by a negatively-charged amino acid, Asp, did not completely inactivate CgIDH even though it resulted in ~7% specific activity relative to the wild-type. A significant reduction of the specific activity in the S130D CgIDH mutant still indicates that the serine at position 130 may have an important role in CgIDH activity.

Due to the fact that the *C. glutamiucm* AT13032 genome sequence has recently been reported (Kalinowski *et al*., 2003), a search was performed of the *C. glutamicum* genome for the equivalent enzyme to *E. coli* IDHK/P to verify whether an enzyme for the phosphorylation of CgIDH was present or not. No possible gene or protein homologous to the *E. coli* IDHK/P was found in the database using the BLAST search engine (Altschul *et al*., 1990, 1994). Taken together, with the reduction of the specific activity in the S130D CgIDH mutant, it is presumed that Ser130 may be required for catalysis but may not be regulated by phosphorylation/dephosphorylation to inactivate/activate CgIDH.

Residues analogous to Lys253 and Tyr416 in CgIDH have been reported to play critical roles in PmIDH catalysis since PmIDH activity was reduced by more than 100-fold when analogous Lys and Tyr residues were replaced by Gln or Thr, respectively (Kim *et al*., 2003). In the structure of AvIDH complexed with isocitrate-Mn^{2+}, the equivalent residues were located at the catalytic site and formed hydrogen bonds with isocitrate (Yasutake *et al*., 2002). When the Lys253 in CgIDH was mutated to Met, catalytic activity was not detected (Chen and Yang, 2000). From the amino acid sequence alignment, furthermore, this Lys253 in CgIDH is completely conserved among both homodimeric and monomeric $NADP^+$-dependent IDH enzymes, whereas the Tyr416 is conserved only among $NADP^+$-dependent monomeric IDH enzymes (Figure 3.11). Specific activities for the K253Q and Y416T CgIDH mutants was not detectable, indicating that Lys253 and Tyr416 may be essential for CgIDH activity or may play a critical role in the regulation of its activity.

```
CgIDH 123 RYNAVKGSAVNPVLR----EGNSDRRAPIAVKNFVKKFPHRMGEWSADSK-TNVATMDAN 177
```

```
AvIDH 125 RYDKIKGSAVNPVLR----EGNSDRRAPLSVKNYARKHPHKMGAWSADSK-SHVAHMDNG 189
PmIDH  88 KLKKMWKSP-NGTIRNILGGTVF-REPIICKNIPRLVPGWTKPITIGRH-AHGDQYKATD 144
HcIDH  87 KLKQMWKSP-NGTIRNILGGTVF-REAIICKNIPRLVSGWVKPIIIGRH-AYGDQYRATD 143
EcIDH  94 PVGGGIRSL-NVALRQELDLYICLRPVRYYQGTPSPVKHPELTDMVIFRENSEDIYAGIE 164

CgIDH 237 QVARAKA-EGILFSAHLKATMMKVSDPIIFGHVVRAYFADVFAQYGEQLLAAGLNGENGL 295
AvIDH 239 EIEDAKK-QGVLLSVHLKATMMKVSDPIMFGQIVSEFYKDALTKHAEVLKQIGFDVNNGI 297
PmIDH 197 CFQYAIQ-KKWPLYMSTKNTILKAYD---------GRFKDIFQEIFEKHYKTDFDKYK-- 244
HcIDH 196 SFQMALS-KGWPLYLSTKNTILKKYD---------GRFKDIFQEIYDKQYKSQFEAQK-- 243
EcIDH 213 AIEYAIANDRDSVTLVHKGNIMKFTEG---------AFKDWGYQLAREEFGGELIDGG-- 261

CgIDH 296 AAILSGLESLDNGE--EIKAAFEKGLEDGPDLAMVNSARGITNLHVPSDVIVDASMPAMI 353
AVIDH 298 GDLYARIKTLPEAKQKEIEADIQAVYAQRPQLAMVNSDKGITNLHVPSDVIVDASMPAMI 357
PcIDH 245 ----------------------------------------------IWYEHRLIDDMVAQVL 260
HcIDH 244 ----------------------------------------------IWYEHRLIDDMVAQAM 259
EcIDH 262 --------------------------------PWLKVKNPNTGKEIVIKDVIADAFLQQIL 290

CgIDH 413 AEEYGSHDKTFRIEADGVVQVVSSNGDVLIEHDVEANDIWRACQVKDAPIQDWVKLAVTR 472
AvIDH 417 AEEYGSHDKTFQIPADGVVRVTDESGKLLLEQSVEAGDIWRMCQAKDAPIQDWVKLAVNR 476

CgIDH 533 DTISVTGNVLRDYNTDLFPILELGTSAKMLSVVPLMAGGGLFETGAGGSAPKHVQQVQEE 592
AvIDH 537 DTISVTGNVLRDYLTDLFPIMELGTSAKMLSIVPLMSGGGLFETGAGGSAPKHVQQFLEE 596
PmIDH 273 --------YDGDVQSDILAQG-FGSLGLMTSVLVCPDGKTIEAEAAHGTVTRHYREHQKG 323
HcIDH 272 --------YDGDVQSDSVAQG-YGSLGMMTSVLVCPDGKTVEAEAAHGTVTRHYRMYQKG 322
EcIDH 304 --------LNGDYISDALAAQ---VGGIGIAPGANIGDECALFEATHGTAPKYAGQD--- 349

CgIDH 593 NHLRWDSLGEFLALAESFRHELNNNGNTKAGVLADALDKATEKLLNEEKSPSRKVGEIDN 652
AvIDH 597 GYLRWDSLGEFLALAASLEHLGNAYKNPKALVLASTLDQATGKILDNNKSPARKVGEIDN 656
PmIDH 324 RPTSTNPIASIFAWTRGLEHRGKLDGNQDLIRFAQTLEKVCVETVESGAMTKDLAGCIHG 383
HcIDH 323 QETSTNPIASIFAWTRGLAHRAKLDNNKELAFFANALEEVSIETIEAGFMTKDLAACIKG 382
EcIDH 350 ---KVNPGSIILSAEMMLRHMG-------WTEAADLIVKGMEGAINAKTVTYDFERLMDG 399
```

Figure 3.11 Multiple sequence alignments among monomeric and homodimeric IDH enzymes from different organisms.

Using CLUSTAL W (Higgins *et al*., 1994), portions of the amino acid sequences of monomeric and homodimeric IDH enzymes are aligned and then modified due to the active site residues from the structures. The residues at the $NADP^+$-binding site (blue) and at the isocitrate and divalent metal cation-binding site (pink) are highlighted. Three residues that have been mutated in CgIDH and the equivalent residues are highlighted in red.

3.5 Fluorescence studies to understand the conformational changes in CgIDH

3.5.1 Changes in fluorescence emission for wild type (wt)-CgIDH upon substrate(s) binding.

Both absorption and fluorescence spectroscopic analyses were conducted to examine if any conformational changes can be detected in CgIDH upon its substrate(s) binding. No change in the absorption spectrum was observed for wild type (wt)-CgIDH in the absence and presence of only either isocitrate or $NADP^+$ (data not shown). The relative fluorescence intensity, however, changed when either isocitrate or $NADP^+$ alone was added to the CgIDH solution (Figure 3.12). An approximate 31% quenching of the fluorescence emission was induced when $NADP^+$ was added, whereas an approximate 15% enhanced fluorescence emission occurred in the presence of isocitrate. These changes in the fluorescence emission for wt-CgIDH suggest that a conformational change occurs upon binding of the substrate(s). Furthermore, from the fluorescence spectra, the wavelength of maximum fluorescence intensity did not shift by more than 1-2 nm, indicating that Trp residues in wt-CgIDH were not exposed to water by substrate binding. Thus, the fluorescence emission of wt-CgIDH quenched in the presence of $NADP^+$ and enhanced in the presence of isocitrate, indicate that binding of either $NADP^+$ or isocitrate to wt-CgIDH may induce a conformational change which may not involve the exposure of the Trp residues to water.

(A)

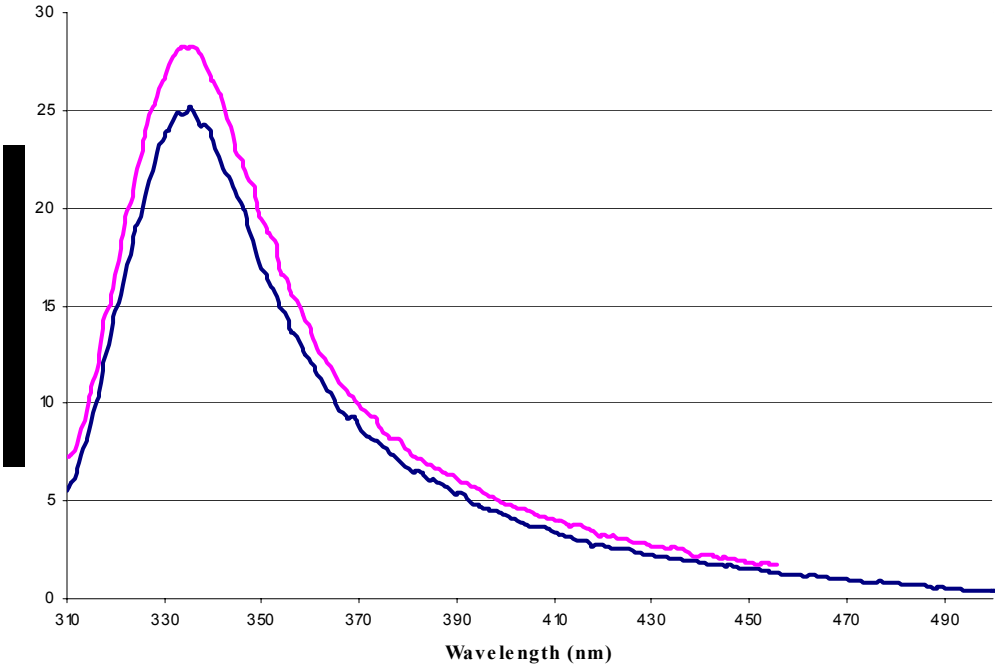

(B)

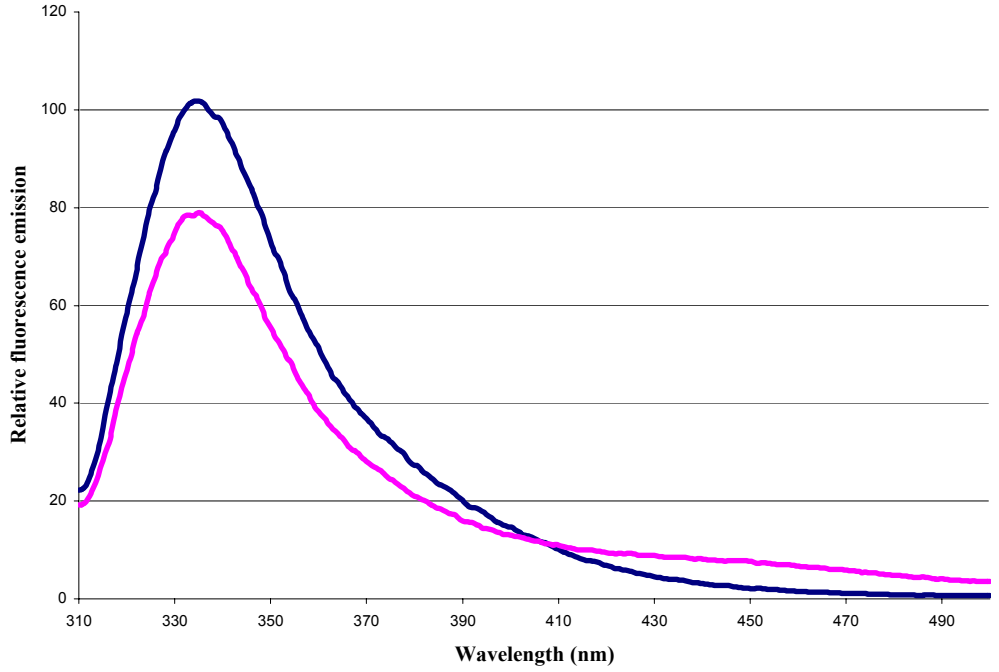

Figure 3.12 Changes in the fluorescence emission for wt-CgIDH upon binding of isocitrate or $NADP^+$.

The relative fluorescence emission was measured from 310 nm to 500 nm after excitation at 297 nm in the absence (blue) and presence (pink) of (A) 1.2 mM isocitrate or (B) 0.08 mM $NADP^+$.

Fluorescence intensity decreased at 335 nm and was enhanced at 450nm by gradual addition of $NADP^+$ to the protein solution (Figure 3.13). The enhanced fluorescence intensity at 450 nm corresponding to the wavelength at which $NADP^+$ fluoresces, increased as more $NADP^+$ was added. The relative fluorescence emission of wt-CgIDH at ~395 nm did not change regardless of the concentrations of $NADP^+$, at which wavelength is termed the isosbestic point (IBP) (Figure 3.13).

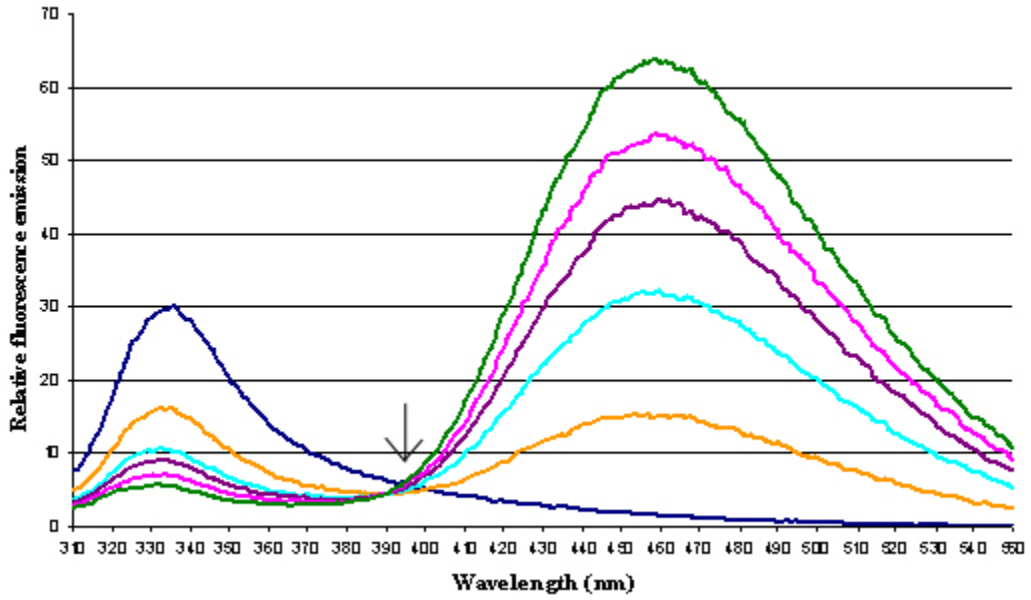

Figure 3.13 The relation between dynamic quenching of wt-CgIDH and the concentration of $NADP^+$.

Wt-CgIDH with no substrates (dark blue) is titrated with $NADP^+$ after adding 0.4 mM isocitrate. $NADP^+$ was added step-by-step to its final concentration: 0.02 mM (yellow), 0.04 mM (sky blue), 0.06 mM (purple), 0.08 mM (pink), and 0.1 mM (green). The enhanced fluorescence at 460 nm corresponds to the fluorescence from NADPH. The isosbestic point at ~395 nm is drawn as a black arrow.

Furthermore, the fluorescence emission of CgIDH was altered regardless of whether isocitrate was added before or after adding $NADP^+$ (Figure 3.14). In the presence of $NADP^+$, the fluorescence emission of CgIDH at 330 nm was reduced by adding isocitrate, and the fluorescence emission at 460 nm (corresponds to the fluorescence of $NADP^+$ and NADPH) was increased. These changes in the fluorescence emission indicate not only that the catalytic reaction is taking place but also that the conformational changes of CgIDH occur in the presence

of both isocitrate and $NADP^+$. From these fluorescence spectroscopic studies, it is suggested that the catalytic reaction and the conformational changes could occur in a reversible manner.

(A)

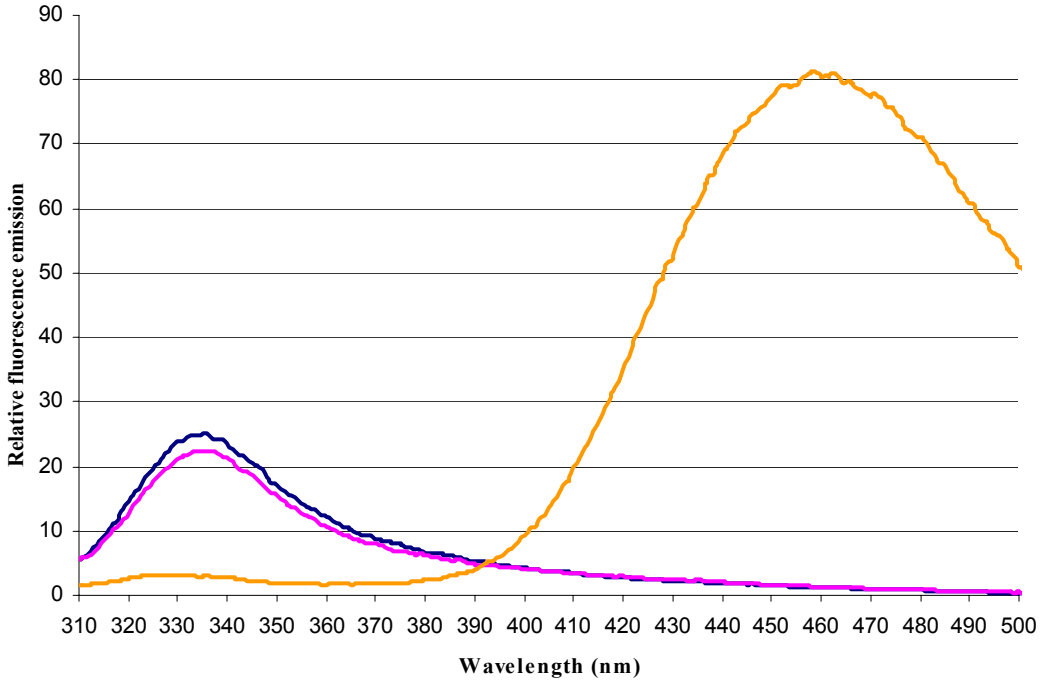

(B)

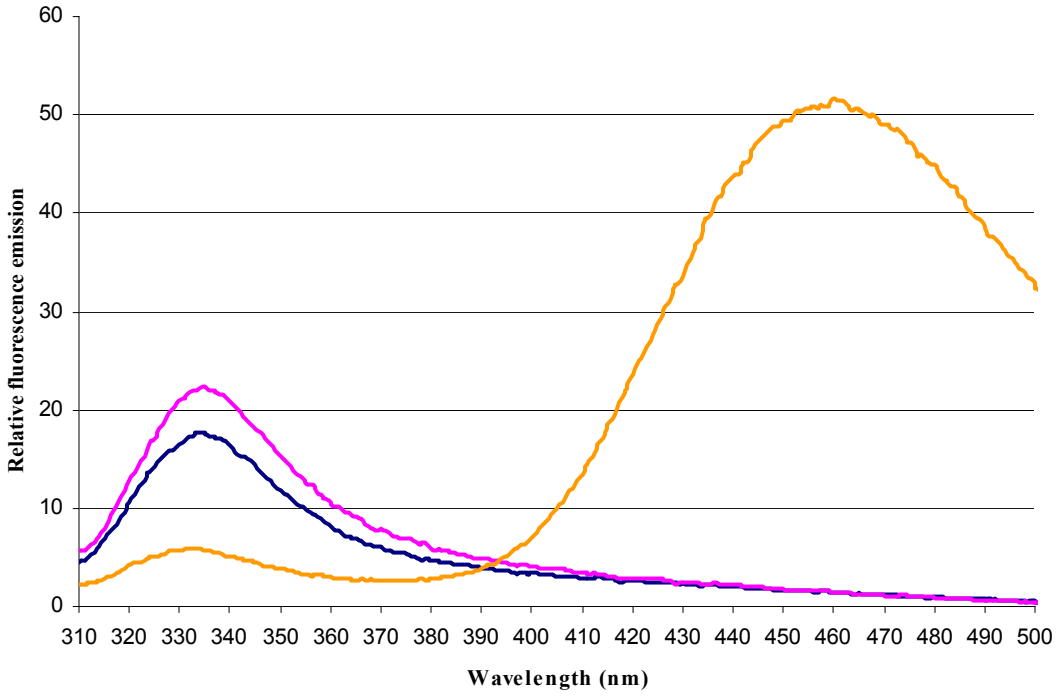

Figure 3.14 The quenching of the fluorescence emission of CgIDH in the presence of $NADP^+$.

The fluorescence emission of CgIDH in the absence of both isocitrate and $NADP^+$ was compared with the one in the presence of $NADP^+$ (A) before and (B) after adding isocitrate to the CgIDH solution. The color codes are; blue for the absence of the substrate(s), pink for the presence of (A) 0.02 mM $NADP^+$ or (B) 0.4 mM isocitrate, and yellow for the presence of both 0.4 mM isocitrate and 0.02 mM $NADP^+$(A and B).

3.5.2 Absorption and fluorescence spectra for CgIDH mutants

Similar absorption and fluorescence spectroscopy studies were performed for the CgIDH mutants in order to examine whether these mutants undergo similar conformational changes upon substrate binding. The absorption spectrum of the S130D mutant changed by adding $NADP^+$ (Figure 3.15), indicating that this mutant could interact with $NADP^+$. On the other hand, unchanged absorption and fluorescence spectra were observed for the same mutant in the presence of isocitrate, which indicates that the S130D mutant could not bind isocitrate (data not shown). Based on the absorption spectrum, it is presumed that the S130D mutant interacts with $NADP^+$ but not with isocitrate. Fluorescence spectroscopic studies also did not indicate that any conformational change occurred in CgIDH in the presence of isocitrate.

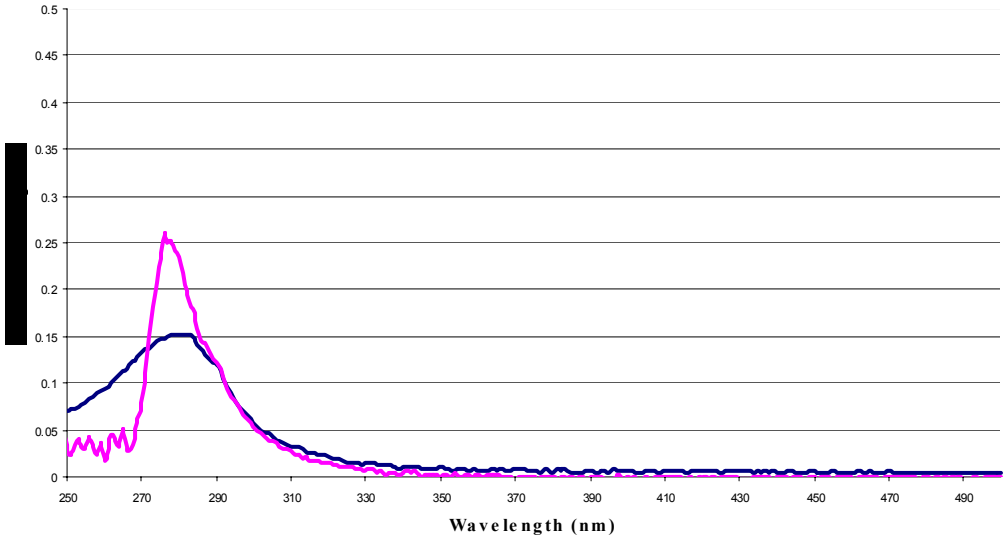

Figure 3.15 Absorption spectra for the S130D CgIDH mutant.

Absorption by the S130D mutant in the presence of 0.4mM $NADP^+$ (pink) is enhanced compared to absorption in the absence of $NADP^+$ (dark blue). Similar absorption spectra occurred for the K253Q and Y416T CgIDH mutants.

Similarly, changes in the absorption spectra were observed for the K253Q and Y416T mutants upon the addition of $NADP^+$, but not isocitrate. Thus, any changes in the fluorescence emission detected in these mutants could not be related to a conformational change upon binding of $NADP^+$ since both the K253Q and Y416T mutants interact with $NADP^+$ prior to the excitation for the fluorescence. Fluorescence spectroscopic analysis, however, showed that the enhanced fluorescence emission for these mutants mediate a conformational change after the addition of isocitrate. More enhanced fluorescence was observed with the K253Q mutant than with the Y416T mutant, indicating that the K253Q mutant may induce more conformational change than does the Y416T mutant in the presence of isocitrate (Figure 3.16). These results suggest that the K253Q and Y416T mutants may still allow a conformational change upon binding of isocitrate, but not of $NADP^+$.

(A)

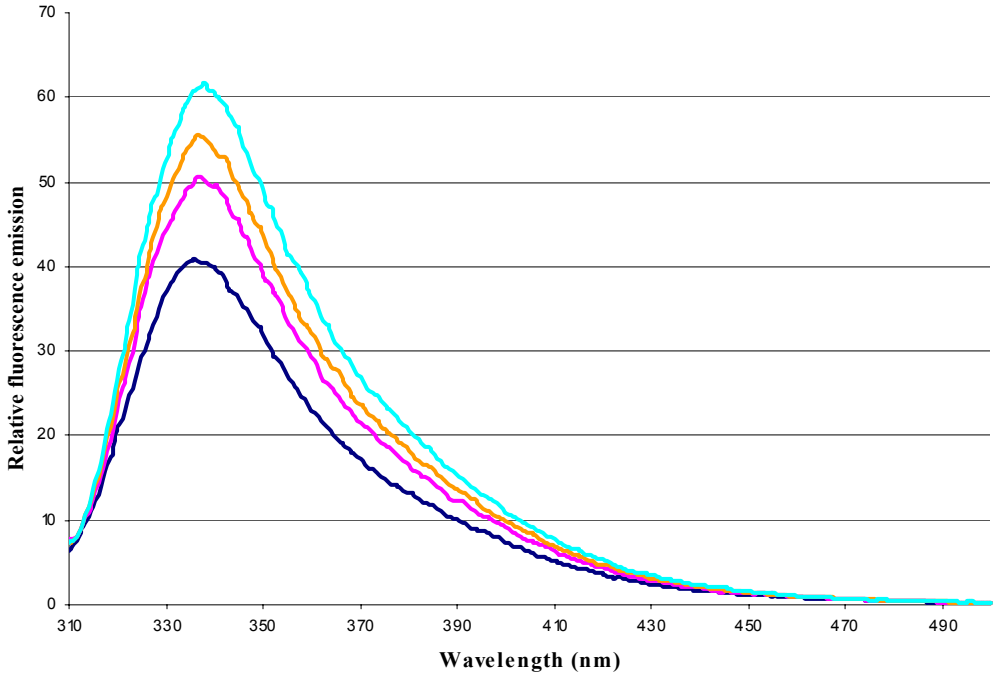

(B)

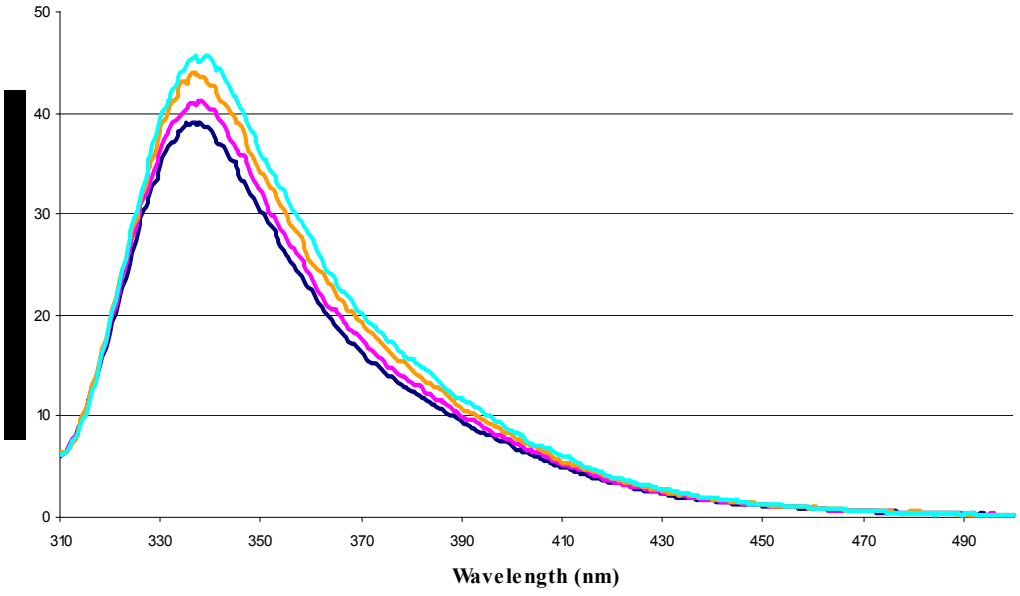

Figure 3.16 Fluorescence spectra for the K253Q and Y416T CgIDH mutants.

The fluorescence emissions of (A) the K253Q and (B) the Y416T CgIDH mutants in the presence of 0 mM (dark blue), 0.4 mM (pink), 0.8mM (orange) and 1.6 mM (sky blue) isocitrate.

Chapter 4 Discussion

4.1 Conformational changes of monomeric IDH upon the substrate(s) binding

4.1.1 Domain movement observed between the structures of CgIDH complexed with Mg^{2+} and AvIDH complexed with isocitrate-Mn^{2+}

The overall secondary and tertiary structures were similar between the structures of CgIDH complexed with Mg^{2+} and of AvIDH complexed with isocitrate-Mn^{2+}. When the structure of CgIDH complexed with Mg^{2+} was superimposed on the structure of AvIDH complexed with isocitrate-Mn^{2+}, using the LSQKAB (Kabsch, 1976) from the CCP4 package (CCP4, 1994), the structure of CgIDH complexed with Mg^{2+} showed a more open conformation than did the structure of AvIDH complexed with isocitrate-Mn^{2+} (Figure 4.1). A large domain (Domain II) appeared to shift more toward the cleft relative to the small domain (Domain I) when isocitrate-Mn^{2+} was bound to AvIDH. The root-mean-square (r.m.s.) difference between the equivalent α-carbon atoms of Domain I and Domain II of the two structures is ~0.8 Å and ~1.8 Å, respectively. Domain I of CgIDH and AvIDH were overlaid by use of LSQKAB, and the rotation angle of Domain II of CgIDH with respect to Domain II of AvIDH complexed with

isocitrate-Mn^{2+} was calculated to be ~ 24˚, which makes Domain II of AvIDH closer to Domain I than Domain II of CgIDH (Figure 4.2).

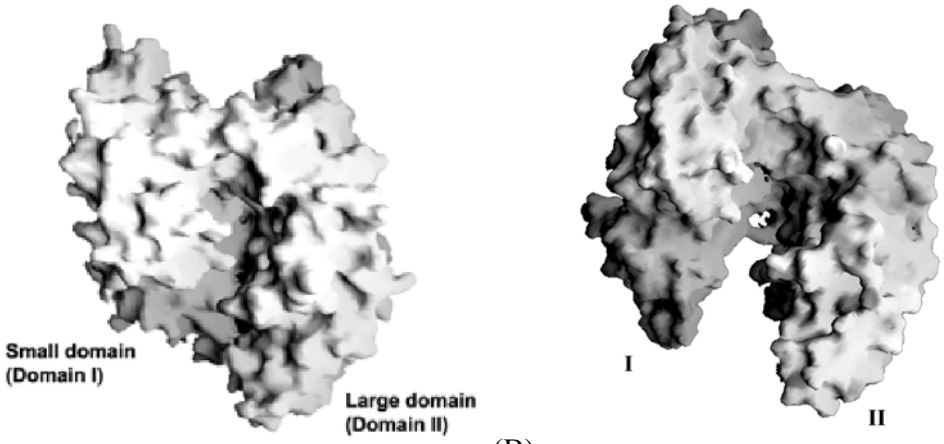

(A) (B)

Figure 4.1 Surface representations of the structures of (A) AvIDH complexed with isocitrate-Mn^{2+} and of (B) CgIDH complexed with Mg^{2+}.

Surface representations of the structures of (A) AvIDH complexed with isocitrate-Mn^{2+} and of (B) CgIDH complexed with Mg^{2+} were adapted and obtained from Yasutake *et al*., 2003, and from the program GRASP (Nicholls *et al*., 1991), respectively. Domain I and Domain II are indicated as I and II in (B), respectively.

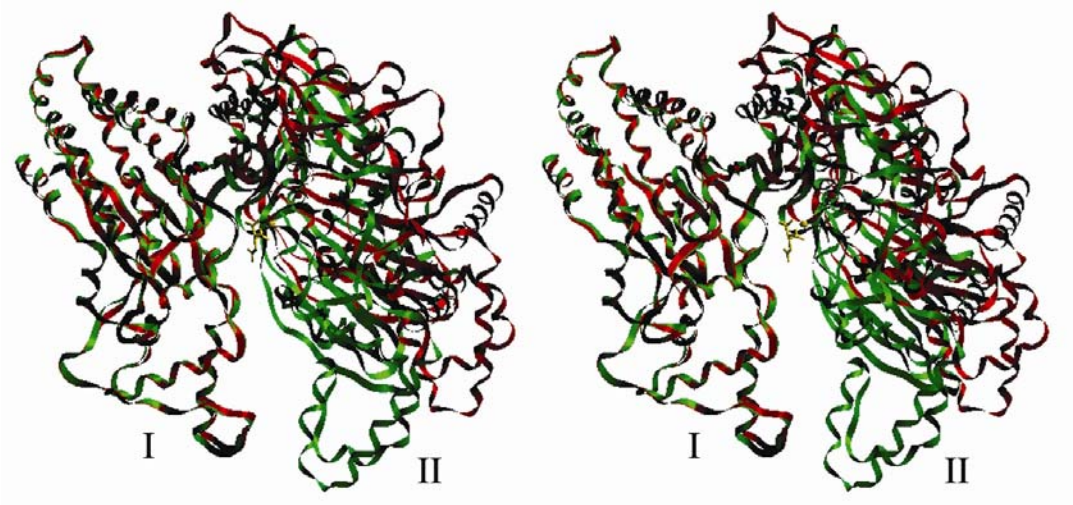

Figure 4.2 Stereo diagram of the superimposed structures of CgIDH complexed with Mg^{2+} and of AvIDH complexed with isocitrate-Mn^{2+}.

Domain I (I) of the structure of CgIDH complexed with Mg^{2+} (red colored ribbon at the left side of the structure) was superimposed onto Domain I of the structure of AvIDH complexed with isocitrate-Mn^{2+} (green colored ribbon) using the LSQKAB from the CCP4 (Kabsch, 1976;

CCP4, 1994). Isocitrate and Mn^{2+} are drawn as yellow stick bonds. The figure was produced using Setor (Evans, 1993).

The superimposed structure of CgIDH complexed with Mg^{2+} onto the structure of AvIDH complexed with isocitrate-Mn^{2+} revealed that the analogous residues at the isocitrate-Mn^{2+} binding site of CgIDH had moved in concert with the domain shift (Figure 4.3). Most residues at the active site are donated from Domain II, especially Arg143, Lys253, Asp346, and Tyr416, were shifted more than 5 Å, compared to the equivalent residues present in AvIDH. Because the domain shift opens up the active site located at the cleft region between the two domains in the structure of CgIDH complexed with Mg^{2+}, these residues were correspondingly further apart. When isocitrate was modeled at the equivalent position in the structure of CgIDH complexed with Mg^{2+}, by superimposing the two enzyme structures, isocitrate would be further away from the analogous active site residues of Domain II in CgIDH. Thus, the analogous active site residues in CgIDH can no longer interact with isocitrate due to the open conformation (Figure 4.4). It is clearly indicated that the open cleft in the structure of CgIDH could no longer mediate interaction of isocitrate with the residues at the active site. These observations lead to the proposal that this open conformation could be a form of CgIDH that allows substrate to enter and then two domains move together to bind substrate at the active site for catalysis to occur.

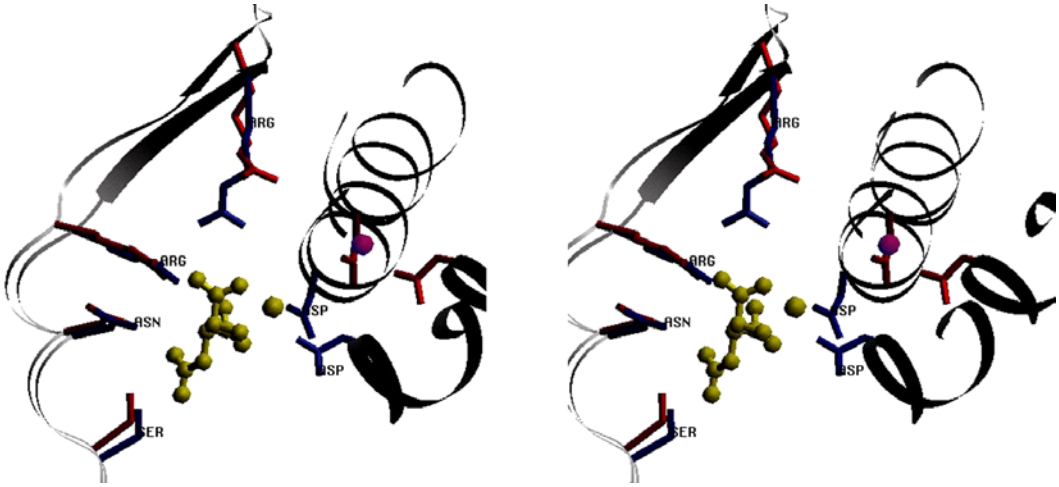

Figure 4.3 Stereo diagram of the movements of the residues at the isocitrate-Mn^{2+} binding site in the structure of CgIDH complexed with Mg^{2+}.

A portion of the backbone of each protein structure of CgIDH complexed with Mg^{2+} and of AvIDH complexed with isocitrate-Mn^{2+} is drawn as gray ribbon, while the labeled residues at the active site are drawn as blue (AvIDH) and as red (CgIDH) sticks. The isocitrate and Mn^{2+} (yellow) are bound at the active site, and the bound Mg^{2+} in CgIDH is drawn as a pink sphere. This picture was produced using Setor.

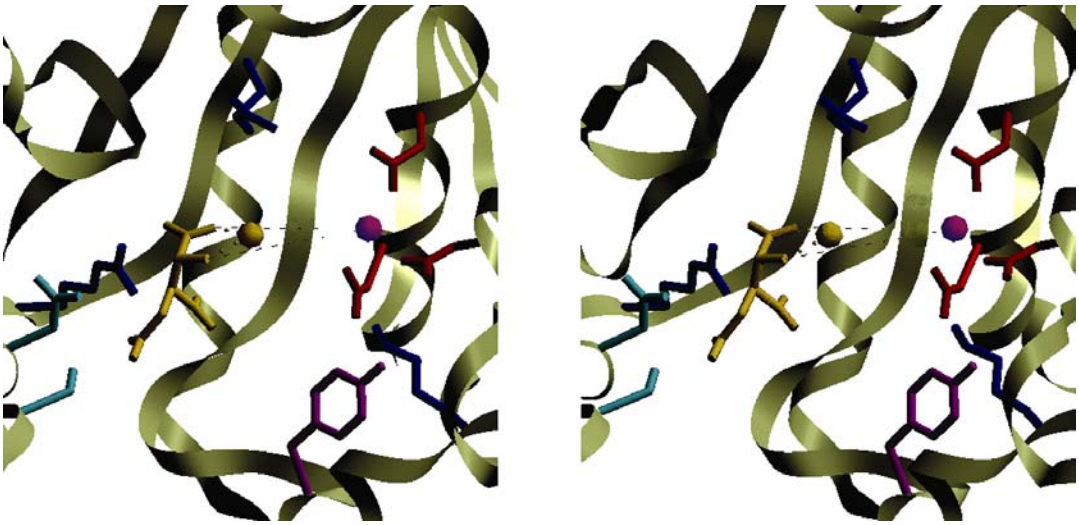

Figure 4.4 Stereo diagram of the structural model of CgIDH complexed with Mg^{2+} and isocitrate-Mn^{2+}.

Isocitrate-Mn^{2+} (yellow) was modeled in the structure of CgIDH complexed with Mg^{2+} (pink sphere) at the equivalent positions of the active site. The active site residues coordinating isocitrate-Mn^{2+} are drawn as colored stick bonds while the light green ribbon represents the backbone of the protein. The dashed lines connect isocitrate and Mg^{2+}.

Due to highly conserved structural features between CgIDH and AvIDH, it is expected that CgIDH could undergo a conformational change when isocitrate is bound to the enzyme. Fluorescence spectroscopic studies showed the changes in the fluorescence emission of CgIDH in the presence of isocitrate, indicating that the conformational changes could be induced upon binding of isocitrate to CgIDH in solution. Taken together with the structural observation, it is suggested that the domain shift in CgIDH could be induced upon binding of isocitrate at the active site.

4.1.2 Coordination geometry of Mg^{2+} and Mn^{2+}

$NADP^+$-dependent IDH is one of the metalloproteins, and it requires either Mg^{2+} or Mn^{2+} for catalysis. One Mg^{2+} was found in the structure of CgIDH in the absence of isocitrate and $NADP^+$. In the structure of CgIDH complexed with Mg^{2+}, Mg^{2+} was hexa-coordinated by side chains of Asp346$O^{\delta1}$, Asp544$O^{\delta2}$, and Asp548$O^{\delta1}$, the carbonyl oxygen of the main chain of Asp544, and two water molecules, whereas Mn^{2+} in the structure of AvIDH complexed with isocitrate-Mn^{2+} was hexa-coordinated by two Asp residues, two water molecules and two oxygen atoms of isocitrate (Figure 4.5 A and B). Because of the absence of isocitrate in the structure of

CgIDH, Mg^{2+} seemed to be coordinated by an extra Asp residue, Asp548, and by the carbonyl oxygen of the main chain of Asp544. Due to the open conformation, the Mg^{2+} was also positioned further way from the corresponding residues that interact with isocitrate in the structure of complex of AvIDH. From the superimposed structure of CgIDH complexed with Mg^{2+} onto the structure of AvIDH complexed with isocitrate-Mn^{2+}, the corresponding distance from Mg^{2+} to one of the oxygen atoms of isocitrate (which coordinates Mn^{2+} in AvIDH) increased from 2.1 Å to ~8.2 Å (Figure 4.6). It is, therefore, proposed that position of Mg^{2+} moves in concert with the conformational change in the presence of isocitrate and then coordinates isocitrate at the active site for catalysis.

Furthermore, previous kinetic studies showed that CgIDH has 10-fold lower K_m value toward isocitrate than homodimeric EcIDH (Chen and Yang, 2000). This specificity of CgIDH toward isocitrate implies that the presence of isocitrate is required to coordinate the divalent metal cation (either Mg^{2+} or Mn^{2+}), which consequently induces a closed conformation and allows the interaction between isocitrate and the divalent metal cation at the active site for catalysis.

(A)

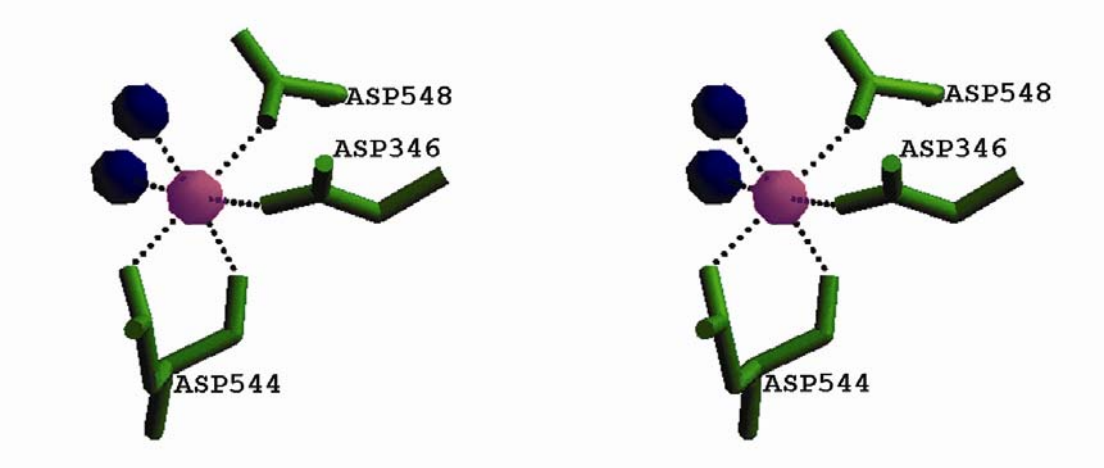

(B)

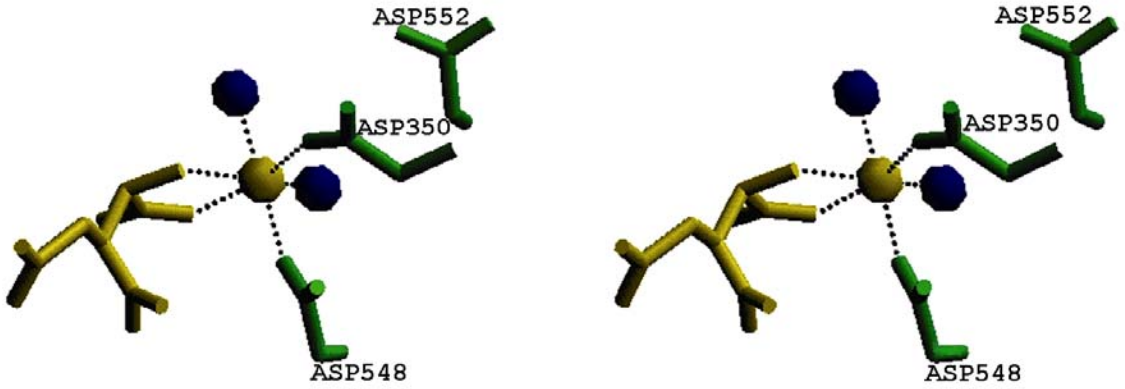

Figure 4.5 Stereo diagrams of the coordination geometries for the divalent metal cations in the structures of (A) CgIDH complexed with Mg^{2+} and of (B) AvIDH complexed with isocitrate-Mn^{2+}.

The coordinating residues are drawn in green, while isocitrate-Mn^{2+} and Mg^{2+} are drawn in yellow and pink, respectively. The blue spheres represent water molecules.

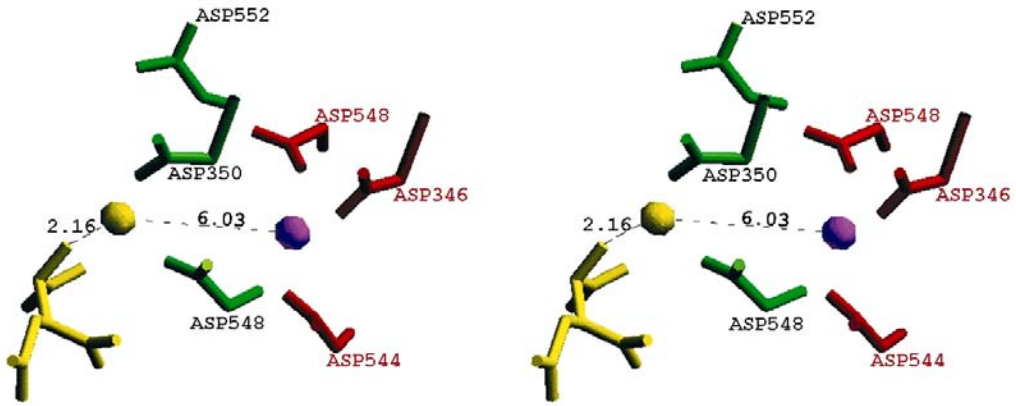

Figure 4.6 Stereo diagram of the superimposed active sites of the structures of CgIDH complexed with Mg^{2+} and AvIDH complexed with isocitrate-Mn^{2+}.

While Mg^{2+} (pink sphere) is coordinated by three Asp residues in CgIDH (red), Mn^{2+} (yellow sphere) is coordinated by two Asp residues (green) and isocitrate (yellow) in AvIDH. Two water molecules coordinating Mg^{2+} or Mn^{2+} are not drawn. The residue names and numbers are written in black for AvIDH and in red for CgIDH. This figure was produced using Setor.

4.1.3 Domain movement induced upon binding of $NADP^+$ in monomeric IDH

A domain shift between the structures of AvIDH complexed with isocitrate-Mn^{2+} and complexed with $NADP^+$ has been proposed (Yasutake *et al*., 2003). When the structure of

CgIDH complexed with Mg^{2+} was superimposed onto the structure of AvIDH complexed with $NADP^+$, Domain II was even more shifted towards Domain I than the one observed in the structure of AvIDH complexed with isocitrate-Mn^{2+} (Figure 4.7). Domain II of the structure of CgIDH complexed with Mg^{2+} appeared to rotate by ~35˚ relative to Domain II of the structure of AvIDH complexed with $NADP^+$. Unlike the residues of Domain I at the isocitrate-Mn^{2+} binding site, the equivalent superimposed residues at the $NADP^+$-binding site of the structure of CgIDH complexed with Mg^{2+} onto those in the structure of AvIDH complexed with $NADP^+$ were correspondingly close in positions (Figure 4.8). The stabilizing loop for the $NADP^+$ binding (described in the structure of AvIDH complexed with $NADP^+$) (Yasutake *et al*., 2003), however, appeared to shift away from the ribose moiety of $NADP^+$ in CgIDH (Figure 4.8). The side chains of Arg600 and Arg649 also seemed to rotate toward the 2'-phosphate moiety in the presence of $NADP^+$, which allows these residues to interact with $NADP^+$. Since these Arg residues at the $NADP^+$-binding site were less affected by a domain shift induced in the presence of isocitrate-Mn^{2+}, binding of $NADP^+$ may result in not only a more closed conformation at the active site but also in the movements of the residues interacting with $NADP^+$ during catalysis.

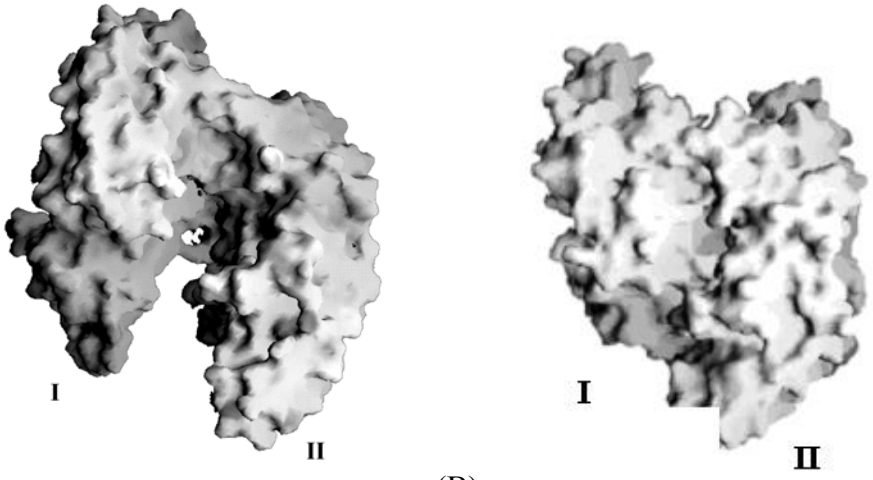

(A) (B)

Figure 4.7 Surface representations of the structures of (A) CgIDH complexed with Mg^{2+} and of (B) AvIDH complexed with $NADP^+$.

The surface representations of the structures of (A) CgIDH complexed with Mg^{2+} and of (B) AvIDH complexed with $NADP^+$ are produced GRASP program (Nicholls *et al*., 1991) and are adapted from the Yasutake *et al*., 2003, respectively. Domain I and Domain II are indicated as I and II, respectively.

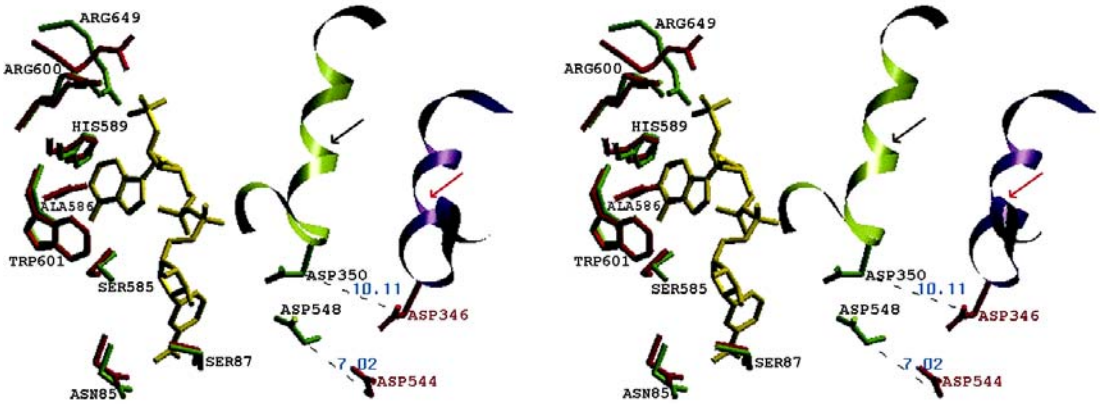

Figure 4.8 Stereo diagram of the $NADP^+$ binding site in the superimposed structure of CgIDH complexed with Mg^{2+} onto the structure of AvIDH complexed with $NADP^+$.

$NADP^+$ (yellow) is bound in the structure of AvIDH (green), which was superimposed onto the structure of CgIDH (pink). The residues to coordinate $NADP^+$ were drawn as green (for AvIDH) and red (for CgIDH) stick bonds. The stabilizing loop in the structure of AvIDH complexed with $NADP^+$ is indicated by a black arrow. The residue names and numbers are written in black for AvIDH and in red for CgIDH.

From fluorescence spectroscopic studies, a significant reduction of the fluorescence emission was observed in CgIDH in the presence of $NADP^+$ than occurs in the presence of isocitrate. The increase in the fluorescence emission indicates that binding of $NADP^+$ could produce a larger conformational change in CgIDH than does binding of isocitrate. Both structural overlay and fluorescence spectroscopic studies agreed that binding of $NADP^+$ to monomeric IDH could induce greater conformational changes than occurred for the binding of isocitrate-Mn^{2+}.

A question raised here is whether this further closed conformation induced upon binding of $NADP^+$ is an active or inactive form. The Asp350 and Asp548 (that coordinate the divalent metal cation) were oriented close to each other in the closed conformation of the structure of AvIDH complexed with $NADP^+$, which could not provide enough space for binding of isocitrate-Ca^{2+}, and therefore the closed conformation could be an inactive form (Yasutake *et al*., 2003). Previous studies have also suggested that CgIDH has 3-fold lower K_m for $NADP^+$ (K_m = 4 μM) than did homodimeric EcIDH (K_m = 11 μM) (Chen and Yang, 2000). Thus, the high affinity of $NADP^+$ for monomeric IDH seems to cause the further closed conformation, to which isocitrate-Ca^{2+} can no longer bind. Isocitrate-Ca^{2+} has lower affinity than $NADP^+$ and isocitrate-Mn^{2+} for AvIDH (Barrera and Jurtshuk, 1970).

Fluorescence spectroscopic studies of CgIDH, on the other hand, showed the quenching of the fluorescence emission when $NADP^+$ was added regardless of the presence of isocitrate in solution (Figure 3.14). It is indicated that binding of $NADP^+$ by itself may induce a further conformational change in CgIDH even in the presence of isocitrate. It is not clear if the additional quenching of the fluorescence emission is directly related to a more closed conformation. The quenching of the fluorescence emission of CgIDH by adding isocitrate in the presence of $NADP^+$ or by adding $NADP^+$ in the presence of isocitrate, suggests that the conformational change could occur in a reversible manner, probably due to the energetic similarity between the open and the closed conformations in CgIDH. It is presumed that the closed conformation induced upon binding of $NADP^+$ could be easily reversed to the partially open conformation, to which isocitrate-Mn^{2+} could bind for catalysis. From both structural observations and fluorescence spectroscopic studies, it is also proposed that the reversible conformational changes could mediate the specificity of monomeric IDH (CgIDH and AvIDH) toward $NADP^+$ and could discriminate between the inhibitor (isocitrate-Ca^{2+} in this case) and the substrate (isocitrate-Mn^{2+}) binding to this enzyme.

4.2 Evolutionary relationship among the IDH family

4.2.1 Two inter-convertible conformations present in the IDH enzyme family

Exhibiting a conformational change is one of the common characteristics of some enzymes during catalysis. Unlike NAD^+-dependent IDH, $NADP^+$-dependent IDH enzymes are not allosterically regulated (Chen and Gadal, 1990). Homodimeric EcIDH is well known to be regulated through the phosphorylation cycle catalyzed by IDHK/P (LaPorte, 1993). When EcIDH is phosphorylated at Ser113, it is inactivated, but a conformational change was not observed between the structures of dephosphorylated and phosphorylated EcIDHs (Hurley *et al*., 1990). It has been suggested, however, that the open conformation could be required in EcIDH for the accessibility of IDHK/P to phosphorylate EcIDH (Finer-Moore *et al*., 1997). From the solved structures, the domain shift by a rotation angle of ~19° was observed only between the substrate-free open conformation and substrate (either isocitrate-Mg^{2+} or $NADP^+$) bound closed conformation in EcIDH (Figure 4.9) (Finer-Moore *et al*., 1997). The superimposed structures of the Ser113Glu EcIDH mutant and of the wild type EcIDH complexed with isocitrate-Mg^{2+}

showed an interdomain rotation by ~ 4º (Hurley *et al*., 1990; Doyle *et al*., 2001), while the rotation angle between the structures of EcIDH complexed with isocitrate-Mg^{2+} and complexed with α-ketoglutarate-Ca^{2+} and $NADP^{+}$ is less than 1º (Hurley *et al*., 1990; Stoddard and Koshland, 1993). Although no significant domain shift was observed between the structures of EcIDH complexed isocitrate-Mg^{2+} and complexed with $NADP^{+}$ (Hurley *et al*., 1991), local conformational changes at the active sites have been reported from the structures of complexes EcIDH and its mutants (LaPorte, 1993; Stoddard and Koshland, 1993). From these studies, it has been proposed that conformational changes may exist in EcIDH to allow the binding of its substrate(s) and to allow phosphorylation of EcIDH by IDHK/P (Finer-Moore *et al*., 1997; Mesecar *et al*., 1998).

Figure 4.9 Stereo diagram of the superimposed structures of the open and closed conformation of EcIDH.

The open conformation of EcIDH in the absence of substrates (red ribbon) was superimposed onto the structure of EcIDH complexed with isocitrate-Mg^{2+} (green ribbon). Only one subunit of the homodimeric EcIDH is presented. The isocitrate and Mg^{2+} are drawn as yellow stick bonds and a sphere, respectively, at the active site. The figure was produced using Setor.

The structures of IMDH that are closely related to EcIDH, have also demonstrated that two conformations could exist, and that a similar domain shift appeared to close the active site (Wallon *et al*., 1997). The domain is rotated by ~16° relative to another domain, which exhibits less rotation of the domain than the rotation angle observed in the structures of wild-type EcIDH, but more than the one between the structures of Ser113Glu EcIDH mutant and of wild-type

EcIDH. The relatively small interdomain rotation angle observed in the structures of IMDH may be due to the fact that the isopropylmalate was absent in the structure of IMDH complexed with Mn^{2+} and SO_4^{2-} (Figure 4.10).

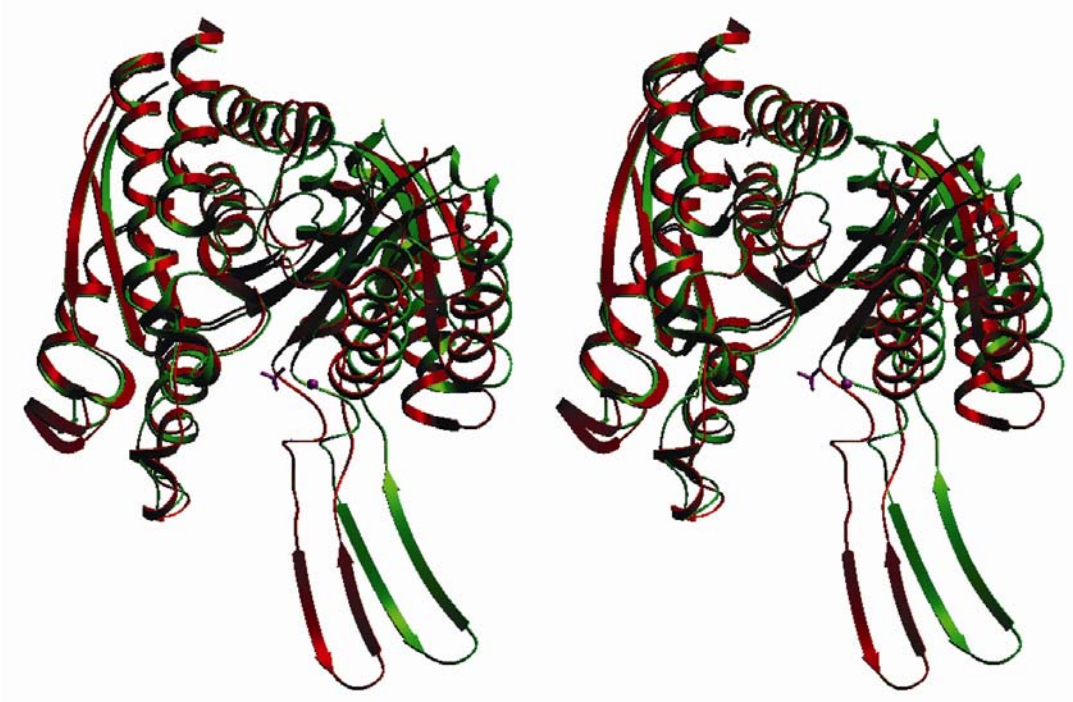

Figure 4.10 Stereo diagram of the superimposed structures of the IMDH in the presence and the absence of Mn^{2+} and SO_4^{2-}.

The structure of EcIMDH in the absence of substrate (green ribbon) was superimposed onto the structure of StIMDH complexed (red ribbon) with Mn^{2+} and SO_4^{2-} (purple sphere and stick bonds, respectively). The figure was produced using Setor.

In addition to prokaryotic homodimeric IDH and the IMDH enzyme family, the mammalian homodimeric IDH seemed to undergo conformational changes. The structure of HcIDH complexed with $NADP^+$ exhibited a more open conformation than did the structure of HcIDH complexed with isocitrate-Ca^{2+} and $NADP^+$ (Xu *et al*., 2004). The domain shift from the structure of HcIDH complexed with isocitrate-Ca^{2+} and $NADP^+$ to the other structure of HcIDH complexed with $NADP^+$, appeared to close the active site by a rotation angle of ~ 27° (Figure 4.11). When the structure of HcIDH complexed with isocitrate-Ca^{2+} and $NADP^+$ was superimposed onto the structure of PmIDH complexed with isocitrate-Mn^{2+}, both structures essentially coincided, indicating that the closed conformation could be the active form in the mammalian homodimeric IDH (Figure 4.12). Because the phosphorylation of the HcIDH has not

been reported up date, it has been proposed that the conformational change of HcIDH could be induced upon binding of isocitrate and could be directly related to the regulation of enzymatic activity in HcIDH (Xu *et al*., 2004).

Figure 4.11 Stereo diagram of the superimposed structures of HcIDH complexed with isocitrate-Ca^{2+} and $NADP^{+}$ and with only $NADP^{+}$.

The structure of HcIDH complexed with isocitrate-Ca^{2+} and $NADP^{+}$ (green ribbon) was superimposed onto the structure of HcIDH complexed with only $NADP^{+}$ (red ribbon), whereas $NADP^{+}$ (yellow stick bonds) is bound at the active site. The figure was produced using Setor.

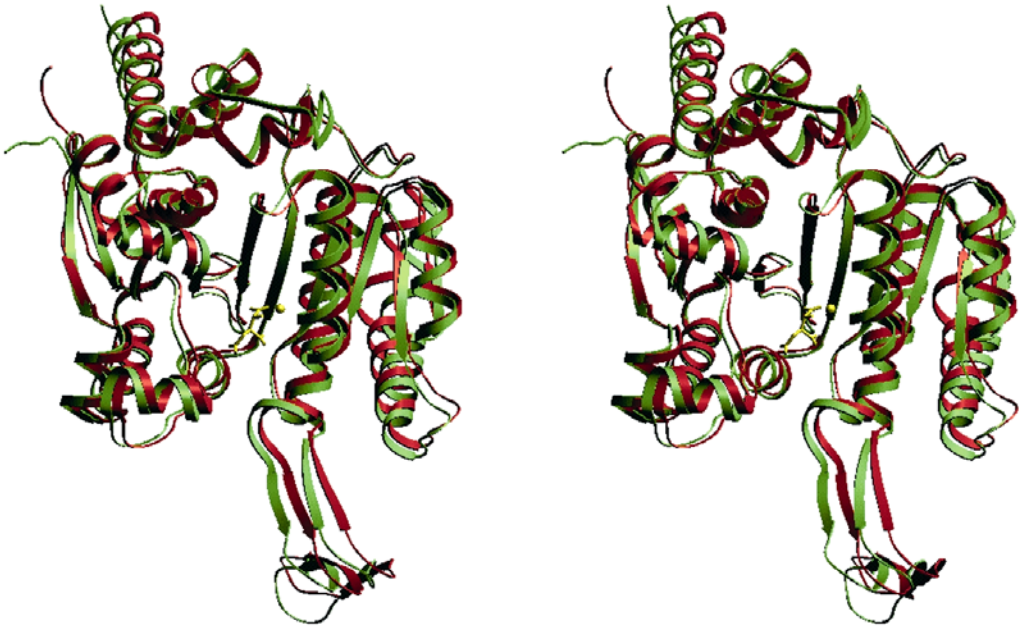

Figure 4.12 Stereo diagram of the superimposed structures of PmIDH complexed with isocitrate-Mn^{2+} and of HcIDH complexed with isocitrate-Ca^{2+} and $NADP^{+}$.

The structure of HcIDH complexed with isocitrate-Ca^{2+} and $NADP^{+}$ (green ribbon) was superimposed onto the structure of PmIDH complexed with isocitrate-Mn^{2+} (red ribbon). Only isocitrate-Mn^{2+} in the structure of PmIDH complexed with isocitrate-Mn^{2+} is drawn in yellow. The figure was produced using Setor.

The domain movement observed from the structure of CgIDH complexed with Mg^{2+} to the structure of complexes of AvIDH (isocitrate-Mn^{2+} and $NADP^{+}$ complexes) appeared to close the cleft region that is homologous to the active site observed in the structures of EcIDH (Figure 4.9), IMDH (Figure 4.10), and HcIDH (Figure 4.11), indicating the similar conformational changes that occur in monomeric and homodimeric IDH enzymes (Figure 4.13). It is also suggested that the closed conformation in monomeric IDH could be the active catalytic form and could be induced upon its substrate(s) binding. These similar conformational changes upon the substrate(s) binding support the hypothesis that both homodimeric and monomeric IDH could have evolved from the same ancestral protein (Chen and Yang, 2000; Yasutake *et al*., 2002, 2003). The rotation angle observed from the domain shifts in monomeric IDH are larger than the rotation angles calculated in the structures of complexes of EcIDH and IMDH, but are similar to the rotation angles between the complex structures of complexes of HcIDH (Table 4.1). The larger rotation angles may be due to more flexibility of monomeric IDH and homodimeric HcIDH than of homodimeric EcIDH and IMDH. The similar rotation angles observed from the

domain shift in the structures of monomeric IDH and homodimeric HcIDH also suggest that monomeric IDH may be more closely related to mammalian homodimeric HcIDH rather than to prokaryotic homodimeric EcIDH and IMDH. Based on the similar topological features among homodimeric IMDH, homodimeric IDH, and monomeric IDH enzymes, it is proposed that the open and the closed forms of monomeric CgIDH could be energetically inter-convertible during substrate binding and catalysis.

(A)

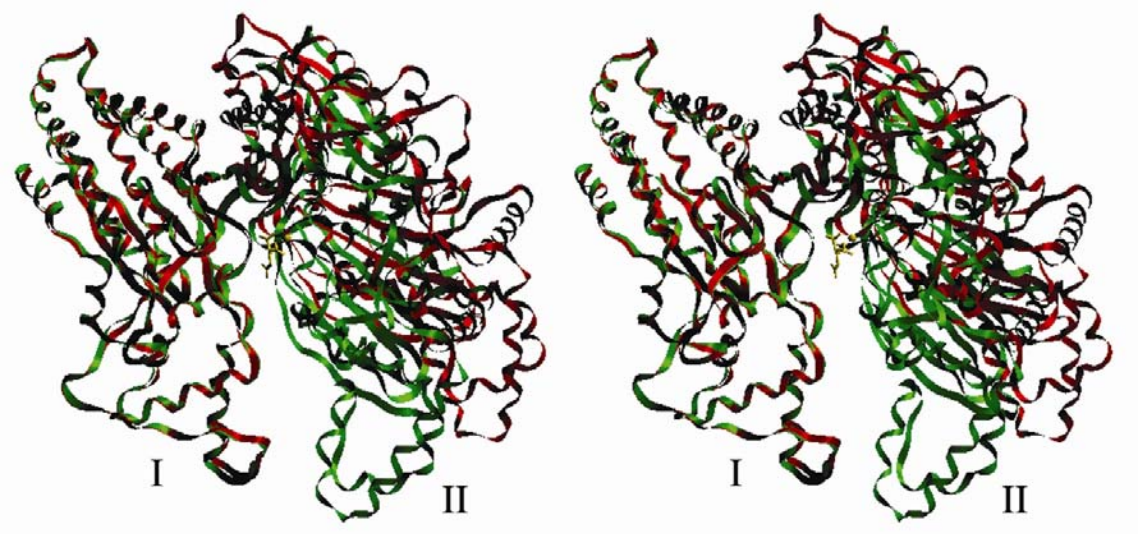

(B)

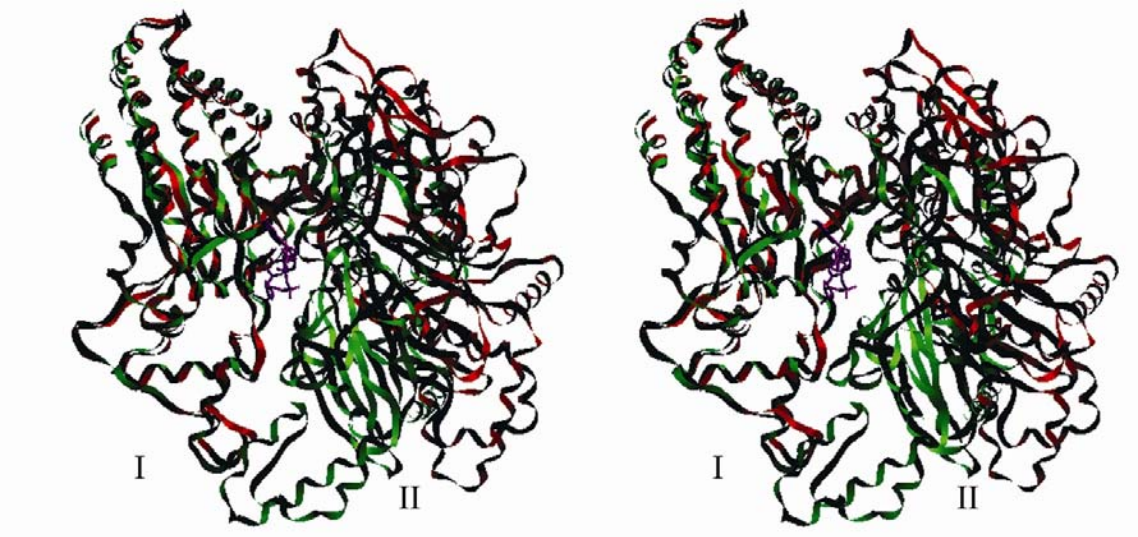

Figure 4.13 Stereo diagrams of the overlaid structures of CgIDH complexed with Mg^{2+} and the structures of AvIDH complexed (A) with isocitrate-Mn^{2+} or (B) with $NADP^{+}$.

(A) The structure of CgIDH complexed with Mg^{2+} was superimposed onto the structures of AvIDH complexed with isocitrate-Mn^{2+} (green ribbon). Isocitrate and Mn^{2+} are drawn as yellow stick bonds at the active site. (B) The structure of CgIDH complexed with Mg^{2+} was superimposed onto the structures of AvIDH complexed with $NADP^{+}$ (green ribbon). $NADP^{+}$ is drawn as pink stick bonds at the active site. These diagrams were produced using Setor.

A pair of the domain in the protein structures compared		Rotation angle (°) calculated
1AI2	5ICD	0.65
1HJ6	5ICD	4.1
1SJS	5ICD	19.3
1CNZ	1CM7	15.7
1TO9	1TOL	27.2
1J1W	1ITW	12.6
CgIDH	1ITW	23.9
CgIDH	1J1W	35.2

Table 4.1 Rotation angles observed in the structures of homodimeric IDH, homodimeric IMDH and monomeric IDH enzymes.

The rotation angle of the domain between two structures was calculated using the LSQKAB from the CCP4 package (Kabsch, 1976; CCP4, 1994). The accession codes for PDB files are 1AI2 (the structure of EcIDH complexed with isocitrate-Ca^{2+} and $NADP^{+}$), 5ICD (the structure of EcIDH complexed with isocitrate-Mg^{2+}), 1HJ6 (the structure of the Ser113Glu EcIDH mutant complexed with isopropylmalate-Mg^{2+}), 1CNZ (the structure of StIMDH complexed with Mn^{2+} and SO_4^{2-}), 1CM7 (the structure of EcIMDH in the absence of substrate), 1TO9 (the structure of HcIDH complexed with isocitrate-Ca^{2+} and $NADP^{+}$), 1TOL (the structure of HcIDH complexed with $NADP^{+}$), 1ITW (the structure of AvIDH complexed with isocitaret-Mn^{2+}) and 1J1W (the structure of AvIDH complexed with $NADP^{+}$). The structure of CgIDH complexed with Mg^{2+} is indicated as CgIDH.

4.2.2 Conserved isocitrate and a divalent metal cation binding sites among the IDH enzyme family

Regardless of the amino acid sequence alignments that show less than 10% identity between homodimeric EcIDH and monomeric IDH, isocitrate and a divalent metal cation binding site were well conserved among the structures of EcIDH and monomeric IDH complexes as well as in PmIDH and HcIDH complexes. The equivalent residue to Ser113 in EcIDH was identified from the structures of complexes of CgIDH and AvIDH, which is completely conserved among monomeric IDH enzymes from other sources (Figure 3.10). The equivalent residue to Lys230′ in EcIDH, Lys253 in CgIDH, was also completely conserved in both homodimeric and monomeric IDH (Figure 3.10).

The coordination geometries of isocitrate and Mn^{2+} in the structure of the complex of AvIDH were similar to those in the structures of complexes of EcIDH, PmIDH, and HcIDH. Isocitrate is coordinated by equivalent Ser, Arg, Lys, and Tyr residues, and the divalent metal cation is coordinated by the equivalent Asp residues, two water molecules, and two oxygen atoms of isocitrate (Figure 4.14). One major difference is the absence of the second active site in monomeric IDH due to the lack of the domain that is equivalent to Domain A′ in the second subunit of homodimeric IDH (Figure 1.16). Beside the absence of the second active site, the structures of both homodimeric and monomeric IDH established that the well-conserved active site could be formed for the identical catalysis even though their primary structures were < 10% identical. These conserved active sites imply not only the evolutionary relationship among homodimeric and monomeric IDH enzymes but also similar tertiary structures for the proteins

that catalyze the identical reaction but have minimal identity of amino acid sequence to other members of the enzyme family.

(A)

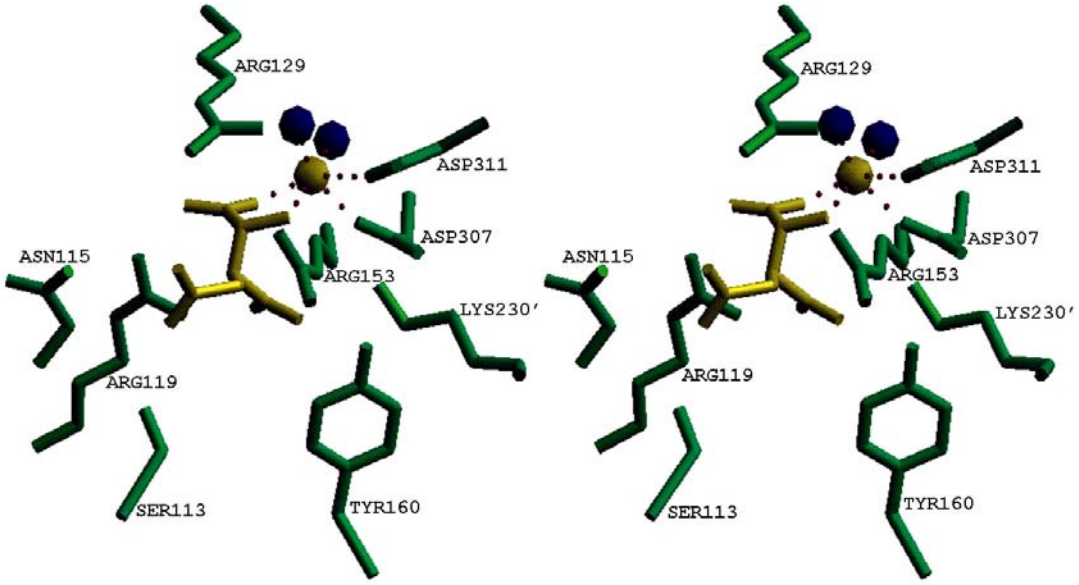
ARG129
ASP311
ASP307
ASN115
ARG153
LYS230′
ARG119
SER113
TYR160
ARG129
ASP311
ASP307
ASN115
ARG153
LYS230′
ARG119
SER113
TYR160

(B)

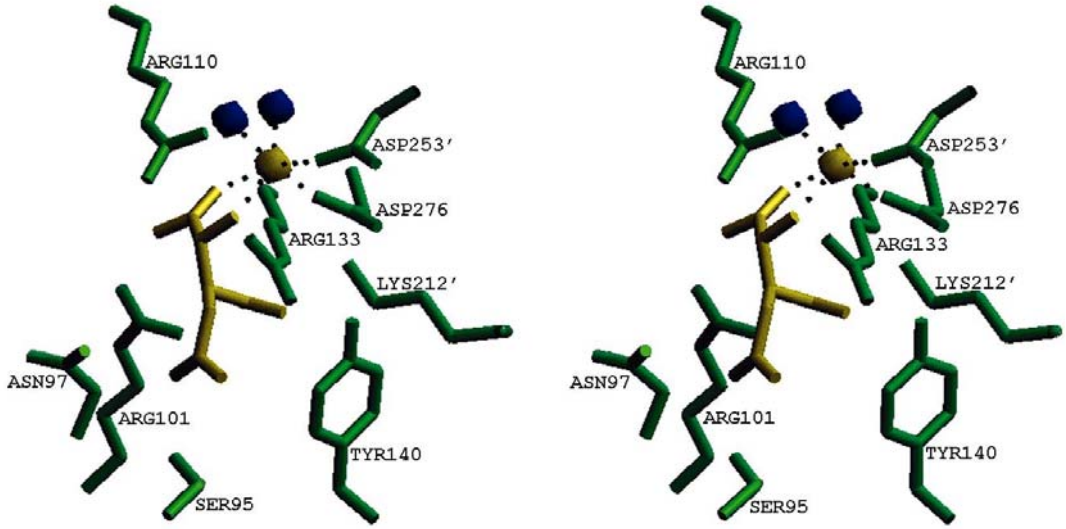
ARG110
ASP253′
ASP276
ARG133
LYS212′
ASN97
ARG101
TYR140
SER95
ARG110
ASP253′
ASP276
ARG133
LYS212′
ASN97
ARG101
TYR140
SER95

(C)

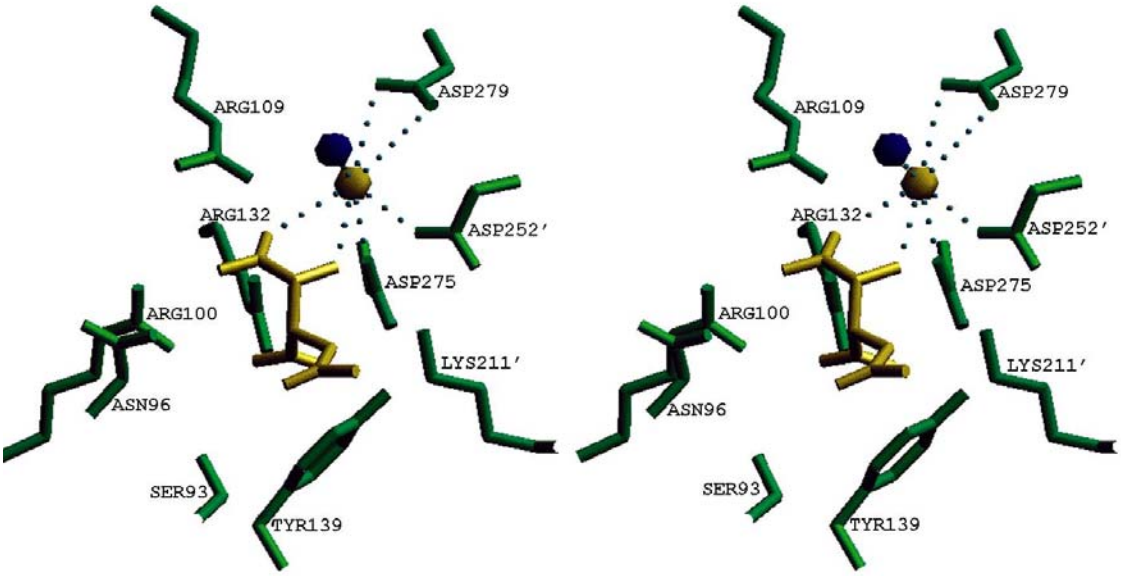

(D)

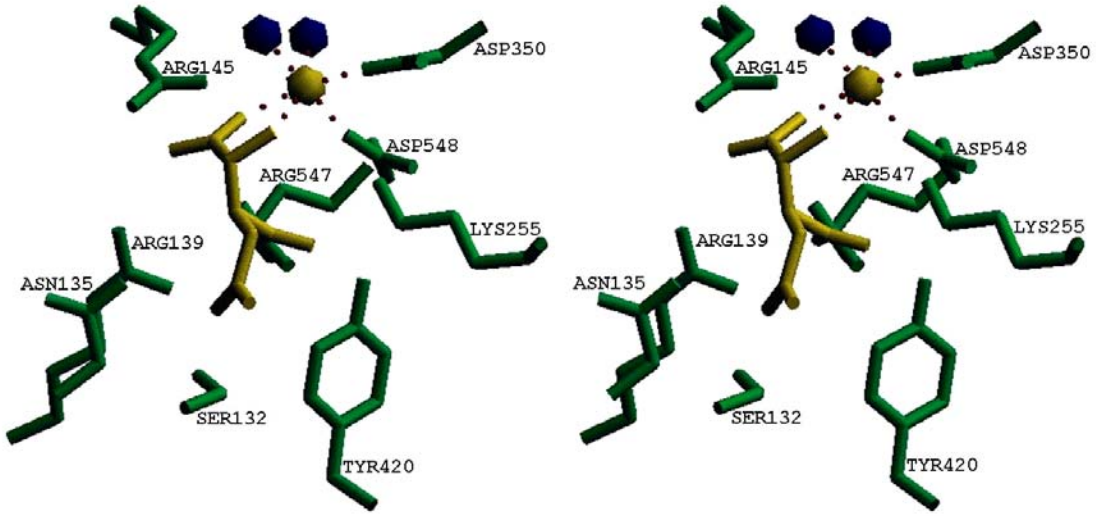

Figure 4.14 Stereo diagrams of the conserved isocitrate and a divalent metal cation binding sites among the structures of homodimeric and monomeric IDH.

Isocitrate and a divalent metal cation binding site in each structure of (A) EcIDH complexed with isocitrate-Mg^{2+}, of (B) PmIDH complexed with isocitrate-Mn^{2+}, of (C) HcIDH complexed with isocitrate-Ca^{2+}, and of (D) AvIDH complexed with isocitrate-Mn^{2+}. The residues at the active site are drawn in green, while the isocitrate and a divalent metal cation are drawn in yellow. The blue spheres represent water molecules.

4.2.3 The unique stabilizing loop at the $NADP^+$-binding sites in monomeric IDH

The structure of AvIDH complexed with $NADP^+$ revealed that the residues at the $NADP^+$ binding site observed from the structure of complex of AvIDH were well conserved among monomeric IDH from other sources including CgIDH, but were different from the residues in homodimeric EcIDH (Yasutake *et al*., 2003). It has been suggested that the $NADP^+$ binding site in monomeric AvIDH could be more similar to the one in HcIDH rather than to the one in EcIDH (Yasutake *et al*., 2003). The residues identified to coordinate the moieties of $NADP^+$ in the structures of AvIDH, HcIDH, and EcIDH complexed with $NADP^+$ are summarized in Table 4.2. While Tyr345 and Tyr391 have been suggested as critical residues to coordinate the 2'-phosphate moiety of $NADP^+$, His and Arg residues coordinated the $NADP^+$ at the equivalent positions in the structures of complexes of both AvIDH and HcIDH (His589 and Arg649 in AvIDH, and His315 and Arg314 in HcIDH) (Figure 3.10). Three continuous non-charged amino acid residues, Gly-Ser (Thr in HcIDH)-Ala (Val in HcIDH), also stabilized the ribose and diphosphate moieties in both of these structures. Two Ser residues also coordinated the nicotinamide moiety of $NADP^+$ in the structure of AvIDH complexed with $NADP^+$, as did two Thr residues in HcIDH (Yasutake *et al*., 2003; Xu *et al*., 2004).

Moiety of $NADP^+$	EcIDH	HcIDH	AvIDH

Adenine	Tyr345	His309	Trp601
	Gly321	Val312	
	Asn392	Thr327	
	Asp352	Asn328	Asp602
2'-phosphate	Tyr391	Arg314	Arg649
	Tyr345	His315	His589
	Arg395		Arg600
Ribose		Leu288	
and diphosphate		Gly310	Gly584
		Thr311	Ser585
	Ala342	Val312	Ala586
Nicotinamide	Thr104	Thr311	Ser585
		Thr75	Ser87
		Lys72	
		Arg82	
		Asn96	Asn85

Table 4.2 The equivalent interacting residues for $NADP^+$ in EcIDH, HcIDH, and AvIDH.

The equivalent residues to coordinate $NADP^+$ were identified from the structures of EcIDH (Hurley *et al*., 1991), HcIDH (Xu *et al*., 2004), and AvIDH (Yasutake *et al*., 2003) complexed with $NADP^+$. The red highlighted residues were those in each of the complex structures that coordinate 2'-phosphate of $NADP^+$ specific recognition. The semi-conserved residues between HcIDH and AvIDH to coordinate the ribose and diphosphate are highlighted in blue.

The structure of HcIDH complexed with $NADP^+$ also revealed that the hydrogen bonding between Ser95 and Asp279 was formed in the absence of isocitrate-Ca^{2+}, and that Arg314 could extend its side chain toward $NADP^+$ when isocitrate-Ca^{2+} was bound (Xu *et al*., 2004). The similar reorientation of the equivalent Arg residue(s) at the $NADP^+$ binding site was observed when the closed conformation of AvIDH complexed with $NADP^+$ was superimposed onto the open conformation of CgIDH complexed with Mg^{2+} (Figure 4.15). The side chains of two Arg residues (Arg600 and Arg649 in AvIDH) seemed to rotate toward $NADP^+$ when it is bound.

Thus, it is consistent that binding of $NADP^+$ could induce the reorientation of the equivalent Arg residues(s) in HcIDH and in monomeric IDH (AvIDH and CgIDH).

(A)

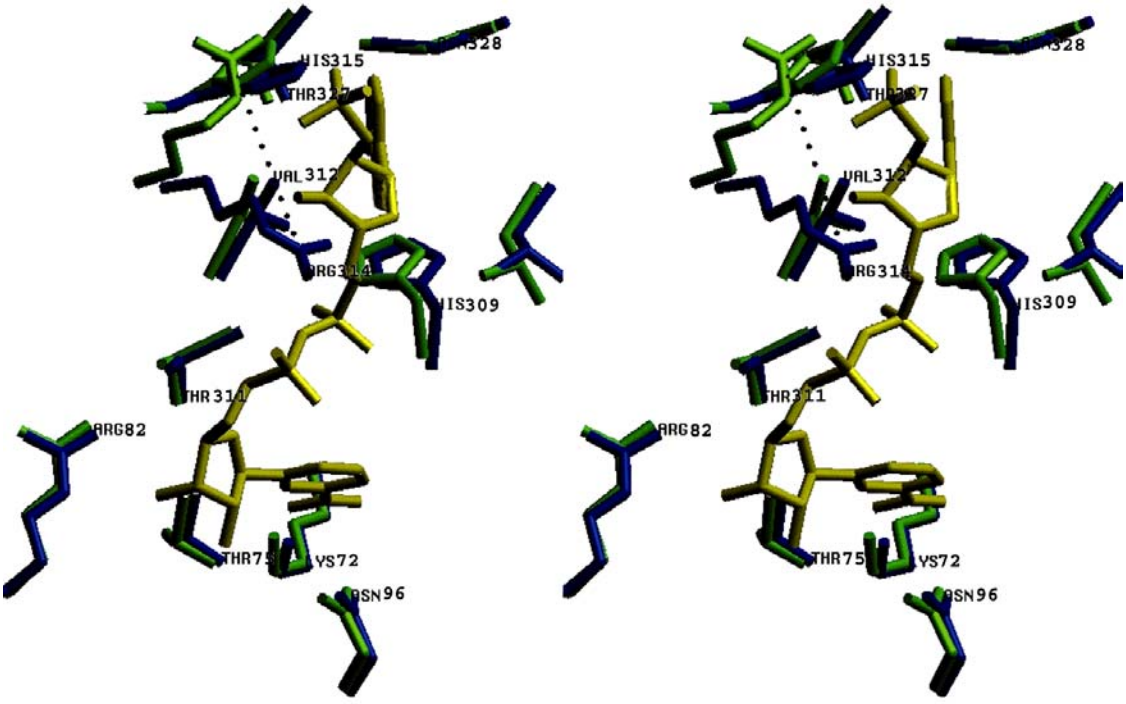
HIS315
VAL312
ARG314
HIS309
THR311
ARG82
LYS72
ASN96
HIS315
VAL312
ARG314
HIS309
THR311
ARG82
ASN96

(B)

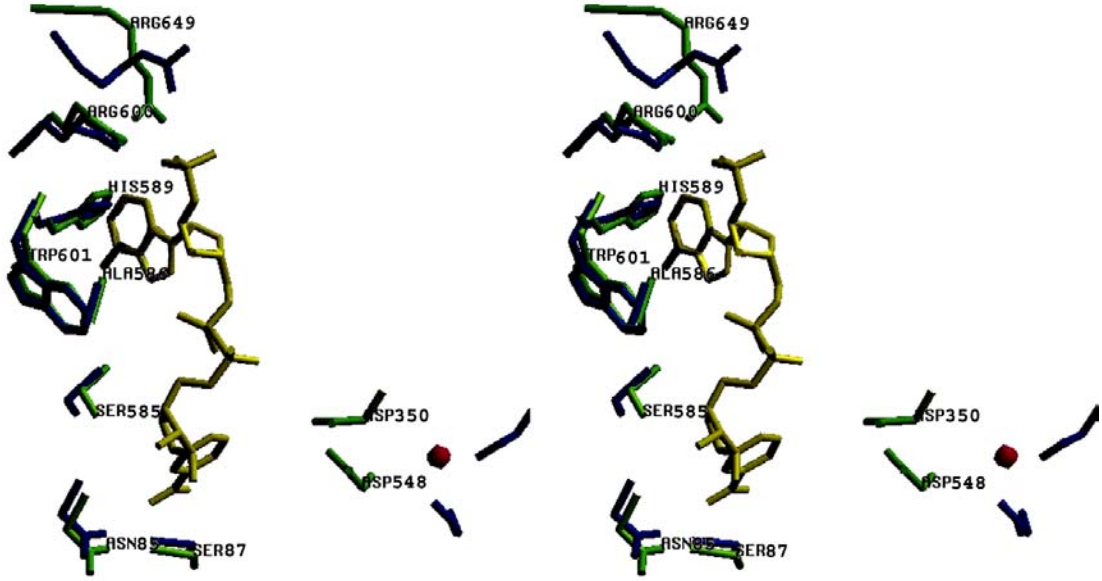
ARG649
HIS589
TRP601
SER585
ASP350
ASP548
SER87
ARG649
HIS589
TRP601
SER585
ASP350
ASP548
SER87

Figure 4.15 Stereo diagrams of the reorientation of Arg residue at the $NADP^+$ binding site in structures of HcIDH and AvIDH complexed with $NADP^+$.

(A) The structure of HcIDH complexed with $NADP^+$ (green) was superimposed onto the structure of HcIDH complexed with isocitrate-Ca^{2+} and $NADP^+$ (blue). The Arg residue that is rotated is indicated by dashed line, while $NADP^+$ is drawn in yellow color. (B) The structure of CgIDH complexed with Mg^{2+} (blue) was superimposed onto the structure of AvIDH complexed with $NADP^+$ (green). The two Arg residues are indicated as arrows, while $NADP^+$ and Mg^{2+} are drawn in yellow and pink colors.

In terms of the overall structures, however, the structure of AvIDH complexed with $NADP^+$ exhibited a closed conformation, while an inactive open conformation was observed from the structure of HcIDH complexed with $NADP^+$. There are two possible explanations to observe two different conformations in the structures complexed with $NADP^+$. It is noteworthy that the crystallization for this AvIDH complex has been carried out in the presence of both $NADP^+$ and isocitrate-Ca^{2+}, not in the presence of $NADP^+$ only as was done for the crystallization of the HcIDH complex. The presence of both $NADP^+$ and isocitrate-Ca^{2+} for crystallization of this AvIDH complex probably could exclude isocitrate-Ca^{2+} from binding to the closed conformation of AvIDH complexed with $NADP^+$, resulting in an inhibition of AvIDH. Thus, the crystallization conditions could affect the conformation of the protein in the crystal. Another possibility for the closed conformation of AvIDH complexed with $NADP^+$ is that AvIDH may have a unique mechanism to regulate the binding of $NADP^+$, which makes this enzyme more specific toward $NADP^+$. Previous studies showed that CgIDH had a highly specific affinity for $NADP^+$ (Chen and Yang, 2000). Due to the completely conserved residues at the $NADP^+$ binding site and similar topological features between AvIDH and CgIDH, $NADP^+$ could be coordinated in an identical manner in these monomeric IDH enzymes and could possess the similar high specificity toward $NADP^+$. The superimposed structures of CgIDH complexed with Mg^{2+} onto AvIDH complexed with $NADP^+$ revealed that the stabilizing loop for $NADP^+$ could be shifted along with the domain movement (Figure 4.8), whereas this stabilizing loop was absent in EcIDH and HcIDH (Yasutake *et al*., 2003; Xu *et al*., 2004). Thus, the presence of this unique stabilizing loop for $NADP^+$ indicates that $NADP^+$ could bind to the active site better in monomeric IDH than in homodimeric EcIDH and HcIDH.

Fluorescence spectroscopic studies of CgIDH also agreed that the conformational change occurred in the presence of either $NADP^+$ or isocitrate. Taken together with the observation of the two inter-convertible conformations in homodimeric and monomeric IDH, it is proposed that

monomeric IDH could have a closed conformation when either $NADP^+$ or isocitrate is bound due to the specificity of this enzyme toward $NADP^+$ and isocitrate. Therefore, the $NADP^+$ binding site in monomeric IDH was similar to the one in mammalian homodimeric HcIDH but in addition may have a unique stabilizing loop that could allow $NADP^+$ to bind better and to induce conformational changes for stabilization of $NADP^+$ at the active site in monomeric IDH. Similarly, binding of isocitrate and a divalent metal cation (Mg^{2+} or Mn^{2+}) could cause conformational changes in monomeric and homodimeric IDH enzymes.

4.3 Kinetic properties of monomeric IDH

4.3.1 Regulation of enzymatic activity in monomeric IDH

The structure of CgIDH complexed with Mg^{2+} revealed the open conformation, compared to the structures of AvIDH complexed with isocitrate-Mn^{2+} and with $NADP^+$. If the open conformation is a form that allows the substrate(s) to enter, and if the coordinating residues of the substrate(s) are shifted along with the domain movement, the domain shift observed in these structures of complexes of CgIDH and AvIDH may be involved in the regulation of the enzymatic activity in monomeric IDH. In the presence of isocitrate or $NADP^+$, monomeric IDH could assume the closed conformation, where this enzyme can interact with the substrate at the active site. Similar to homodimeric HcIDH, the open and closed conformations of monomeric IDH could be energetically inter-convertible, and monomeric IDH might display different conformations depending on the presence of certain substrates or inhibitors. The specificity of isocitrate and $NADP^+$ proposed in CgIDH could be due to the sensitivity of the domain shift on the substrate(s). Thus, CgIDH could form the active conformation possibly in the presence of isocitrate-Mn^{2+}/ isocitrate- Mg^{2+} or $NADP^+$, but not in the presence of Mn^{2+}/ Mg^{2+} only or inhibitor(s) that have lower affinity to the enzyme. The binding of $NADP^+$ could result in regulation of the enzyme activity.

The phosphorylation cycle to control the enzymatic activity has been reported only in homodimeric EcIDH among homodimeric and monomeric IDH enzymes (LaPorte, 1993). The site-directed mutagenesis studies on CgIDH showed that the equivalent residue to Ser113 in EcIDH, Ser130 in CgIDH, could not completely inactivate CgIDH even when it was replaced by a negatively charged Asp. Rather, the K253Q and Y416T CgIDH mutants appeared to inactivate

CgIDH, indicating that these residues may play critical roles in the enzymatic activity of CgIDH. The presence of the detectable 7% enzymatic activity in the S130D CgIDH mutant but not in the K253Q and the Y416T CgIDH mutants suggest that the activity in CgIDH may not be regulated by phosphorylation. Since both the equivalent Lys and Tyr residues have been suggested to be critical for the enzymatic activity of PmIDH, the kinetic studies of these CgIDH mutants also support the hypothesis that CgIDH (monomeric IDH) may be more similar to the homodimeric HcIDH and PmIDH than to homodimeric EcIDH, in terms of the regulation of their enzymatic activities.

The enhanced fluorescence emission observed in the K253Q and Y416T CgIDH mutants in the presence of isocitrate suggest that these mutants may cause some different conformational changes when isocitrate is bound. The types of the conformational changes for these mutants could not be determined from the fluorescence spectroscopy studies. Because these Lys253 and Tyr416 residues were observed to be shifted further away from the closed to the open conformations in monomeric IDH, and because the substitution of Lys or Tyr by Asp or Thr, respectively, shortens the side chain at each position, it is expected that these mutant proteins may be unable to form the active conformation of CgIDH, resulting in the inactivation of these mutants. The absence of any changes in the fluorescence emission for the S130D CgIDH mutant, on the other hand, indicates that this mutant may bind to isocitrate but may not undergo any conformational changes. Since Ser130 was identified to interact with isocitrate like Ser113 in EcIDH, the mutation of this Ser residue could interfere with proper binding of isocitrate to the enzyme, which results in not only a decrease in the enzymatic activity but also the absence of the conformational change that occurs when isocitrate is bound. From these structural analyses together with fluorescence spectroscopic and site-directed mutagenesis studies of CgIDH, it is proposed that the conformational changes in the presence of substrate(s) may have essential roles in the regulation of enzymatic activity of monomeric IDH since these active site residues would be reoriented to interact with the substrate by the domain movement.

4.3.2 The proposed reaction mechanism in monomeric IDH

Based on the structures of complexes of homodimeric EcIDH, two steps in the oxidation of isocitrate have been suggested in EcIDH (Figure 1.1) (Hurley *et al*., 1991; Dean and Koshland, 1993). The similar catalytic mechanism has been postulated for homodimeric PmIDH (Kim *et*

al., 2003). Due to the well conserved active site between homodimeric and monomeric IDH, it is conceivable that monomeric IDH catalyzes the decarboxylation of isocitrate in two steps (Figure 4.16). First, a proton is removed from isocitrate by a general base, and a hydride ion is transferred to $NADP^+$, resulting in the formation of oxalosuccinate. Then, the β-carboxylate of oxalosuccinate is lost by releasing CO_2, followed by the protonation of the β-carbon of α-ketoglutarate. Either Mg^{2+} or Mn^{2+} stabilizes the α-carboxylate and the C2 enolate ion of isocitrate throughout catalysis.

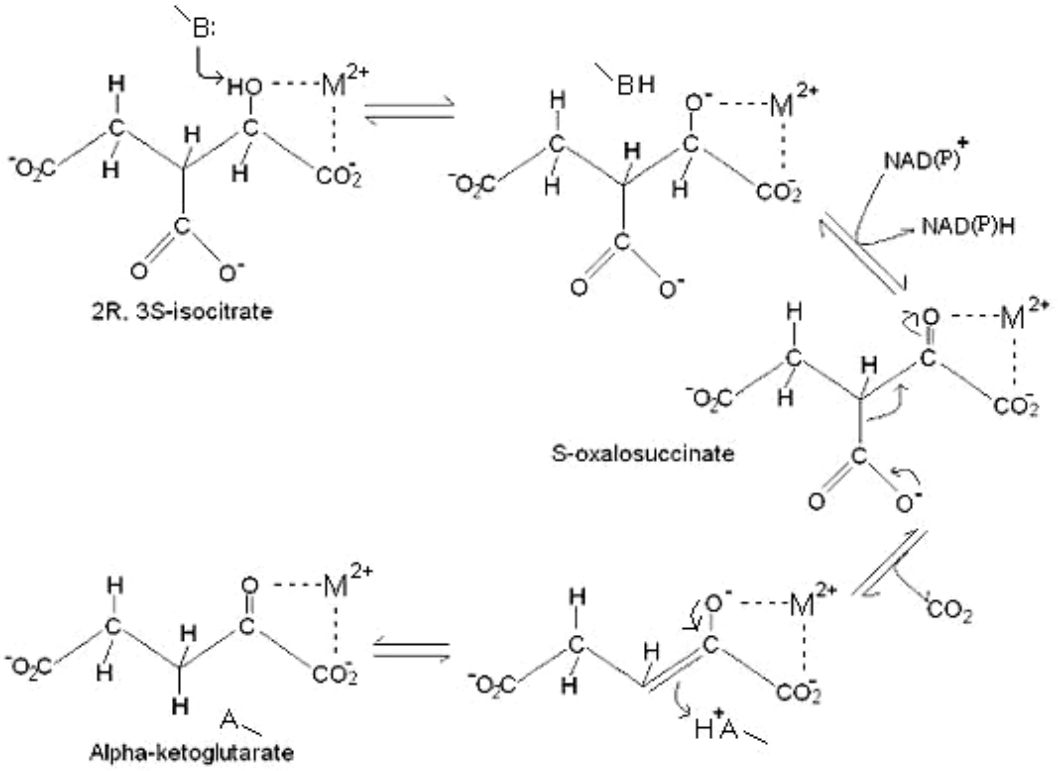

Figure 4.16 The proposed reaction mechanism for monomeric IDH.

Two steps in the decarboxylation of isocitrate are proposed as the catalytic reaction mechanism in CgIDH. The half-arrows represent the directions of the catalytic reaction and the release of products (NADPH and CO_2), and the full-arrows indicate the movements of electrons in the reaction. The coordination of the divalent metal cation (M^{2+}), Mg^{2+} or Mn^{2+}, is drawn as a dashed line. A general base (B) and a general acid (A) are active site residues from CgIDH.

The mechanism of the interaction between monomeric IDH and the substrate(s) is similar to the one described for homodimeric EcIDH (Dean and Koshland, 1993). Either isocitrate or

$NADP^+$ can bind to monomeric IDH and solely induce a closed conformation. Then, another remaining substrate can bind to the enzyme in the altered conformation since these closed conformations seemed to be energetically similar to each other as well as to the open conformation (Figure 4.17). It is not clear if the conformation of monomeric IDH can be further altered in the presence of both isocitrate and $NADP^+$ during catalysis. Based on fluorescence spectroscopic studies of CgIDH, this enzyme appeared to induce further conformational changes in the presence of both isocitrate and $NADP^+$. It is presumed, therefore, that the conformation of monomeric IDH may be variable depending on the presence of substrate(s) or inhibitor(s), which may play a critical role to control its enzymatic activity.

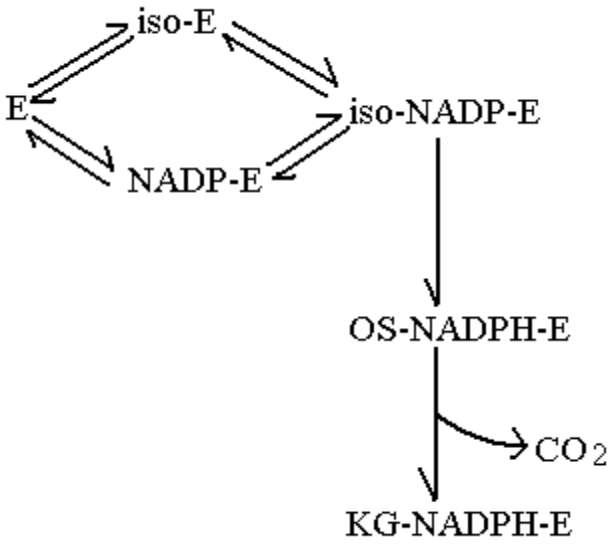

Figure 4.17 The proposed mechanism of the interaction between monomeric IDH and its substrate(s).

Monomeric IDH is labeled as 'E' while isocitrate, $NADP^+$, oxalosuccinate, and α-ketoglutarate are presented as 'iso', 'NADP', 'OS', and 'KG', respectively. The half-arrows indicate the interaction between monomeric IDH and its substrate(s), whereas a release of carbon dioxide is drawn in a full arrow.

Chapter 5 Conclusion and future work

5.1 Summary of the research project

Based on previous preliminary studies, the purification of CgIDH was modified in order to minimize the purification steps while purity of the protein was maintained (Figure 3.1) (Bai *et al*., 1999). The optimizations of crystallization and of cryocrystallography were successfully done to diffract the CgIDH crystal at higher resolution with lower crystal mosaicity (Table 3.1). The CgIDH crystal in the absence of isocitrate and $NADP^+$ diffracted at 1.75 Å resolution. The structure was solved using MR and was refined using CNS (Brünger *et al*., 1998). The structure of CgIDH complexed with Mg^{2+} is composed of two domains, and the active site is formed at the cleft region between two domains (Figure 3.5). One magnesium ion was hexa-coordinated by three Asp residues and two water molecules in an octahedral geometry at the active site in CgIDH. When the structure of CgIDH complexed with Mg^{2+} was superimposed onto the structures of AvIDH complexed with isocitrate-Mn^{2+} or complexed with $NADP^+$, the domain shift was observed, which causes the closure of the active site located between two domains (Figures 4.1, 4.2, 4.7, and 4.13). Fluorescence spectroscopic studies suggested that the conformational changes occurred in CgIDH by its substrate(s) binding (Figures 3.11). Similar domain shifts have been reported in the structures of homodimeric EcIDH, IMDH, and HcIDH (Figure 4.9-11). From these observations, it is proposed that the IDH enzyme family could exist in the open and the closed conformations that are energetically inter-convertible for catalysis. Although the closed conformation was suggested as an active form induced in the presence of isocitrate and $NADP^+$, the closed conformation was observed in the structure of AvIDH complexed with only $NADP^+$. Fluorescence spectroscopic studies of CgIDH agreed that the conformational change could be induced solely by the binding of $NADP^+$ (Figure 3.14). The conformational changes observed between the structures of CgIDH complexed with Mg^{2+} and of AvIDH complexed with $NADP^+$, as well as in the quenching of the fluorescence emission in CgIDH in the presence of $NADP^+$, presumably explain the specificity and high affinity of CgIDH toward $NADP^+$ for catalysis. Yet, it is not clear if isocitrate-Mn^{2+} may bind to CgIDH prior to binding of $NADP^+$ or may bind to CgIDH in the closed conformation induced after binding of $NADP^+$.

From both site-directed mutagenesis and the fluorescence spectroscopy studies, three newly generated CgIDH mutants (S130D, K253Q and Y416T mutants) appeared to have reduced and

non-existent specific activities compared to the wild-type enzyme. While the S130D CgIDH mutant did not exhibit any conformational changes in the presence of isocitrate, conformational changes in the K253Q and Y416T mutants seemed to be induced in the presence of isocitrate (Figure 3.15). It is therefore presumed that the mutations of these residues at the active site in CgIDH could affect not only the specific activities but also the conformational changes that are induced in the presence of isocitrate. It is also proposed that the conformational change in the presence of substrate(s) may be involved in the regulation of CgIDH activity; therefore, the substitutions of the active site residues could cause the mutant protein not to assemble the active conformation properly in the presence of substrate(s). The structural analysis of CgIDH compared with homodimeric IDH agreed with the similar topological features between CgIDH and homodimeric IDH. The conserved active sites support the hypothesis that both monomeric and homodimeric IDH could be evolved from the same ancestral protein. It is also proposed that monomeric IDH is more closely related to mammalian homodimeric PmIDH and HcIDH rather than to prokaryotic homodimeric EcIDH since the $NADP^+$ binding site in AvIDH and CgIDH was more similarly formed to the one in HcIDH (Figure 4.15), and since the binding of isocitrate and/or $NADP^+$ could mediate conformational changes in AvIDH, CgIDH, and HcIDH (Figures 4.9-13). Thus, monomeric IDH, like mammalian homodimeric IDH, may be regulated by the self-assembly of the active conformation in the presence of its substrate(s), while the phosphorylation cycle controls the enzymatic activity in EcIDH.

5.2 Future work

The structural aspects of CgIDH together with site-directed mutagenesis and fluorescence spectroscopic studies revealed that the conformational changes could occur in CgIDH when its substrate(s) is(are) bound. From the collected diffraction data sets, the complex CgIDH crystals belonged to the same space group, *C*2, but had different unit cell dimensions, suggesting that the substrate was likely bound to the enzyme. Hence, the structures of CgIDH complexed with each of $NADP^+$, NAD^+, and isocitrate-NAD^+ should be solved, in order to display variable conformations in the presence of different substrate(s). Yet, it is not known if CgIDH mediates different conformations in the presence of inhibitor such as isocitrate-Ca^{2+} or in the presence of its product(s) such as α-ketoglutarate. Furthermore, because the conformational changes were indicated for the K253Q and Y416T CgIDH mutants in the presence of isocitrate, the solving of

crystal structures of these mutants complexed with isocitrate-Mn^{2+}/Mg^{2+} or isocitrate-Ca^{2+} should verify whether these mutants would assemble in different conformations or not.

The domain shift observed from the open to the closed conformation in the absence and the presence of $NADP^+$, respectively, revealed that two Arg residues could be rotated toward $NADP^+$ along with the domain shift. Since Arg600 is a unique residue at the $NADP^+$-binding site in monomeric AvIDH (Yasutake *et al*., 2003), the mutation of the equivalent Arg residue in CgIDH may elucidate the detailed role of this Arg residue for binding of $NADP^+$ in monomeric IDH. Because His589 in the structure of AvIDH complexed with $NADP^+$ was also identified as an equivalent to His315 in the structure of HcIDH complexed with $NADP^+$ and interacts with $NADP^+$, and because the mutation of this His residue in PmIDH and HcIDH has been reported to reduce the binding affinity of homodimeric IDH for $NADP^+$ (Huang *et al*., 2002), the mutation of the equivalent His residue (His584) in CgIDH may confirm the hypothesis that the $NADP^+$-binding site in CgIDH could be similar to the one in mammalian homodimeric IDH rather than to the one in prokaryotic homodimeric EcIDH.

References

Altschul, S.F., Gish, W., Miller, W., Myers, E.W., and Lipman, D.J. (1990). Basic local alignment search tool. J. Mol. Biol. *215*, 403-410.

Altschul, S.F., Boguski, M.S., Gish, W., and Wootton, J.C. (1994). Issues in searching molecular sequence databases. Nature Genet. *6*, 119-129.

Audette, G.F., Quail, J.W., Hayakawa, K., Bai, C., Chen, R.D., and Delbaere, L.T.J. (1999). Crystallization and preliminary X-ray diffraction studies of monomeric isocitrate dehydrogenase from *Corynebacterium glutamicum*. Acta Crystallogr. D. *55*, 1584-1585.

Bai, C., Fernandez, E., Yang, H., Chen, R.D. (1999). Purification and stabilization of a monomeric isocitrate dehydrogenase from *Corynebacterium glutamicum*. Protein Expr. Purif. *15*, 344-348.

Barrera, C.R., and Jurtshuk, P. (1970) Characterization of the highly active isocitrate ($NADP^+$) dehydrogenase of *Azobacter vinelandii*. Biochim. Biophys. Acta *220*, 416-429.

Belfiore, F., and Iannello, S. (1995). Fatty acid synthesis from glutamate in the adipose tissue of normal subjects and obese patients: an enzyme study. Biochem. Mol. Med. *54*, 19-25.

Benderdour, M., Charron, G., DeBlois, D., Comte, B., and Des Rosiers, C. (2003). Cardiac mitochondrial $NADP^+$-isocitrate dehydrogenase is inactivated through 4-hydroxynonenal adduct formation: an event that precedes hypertrophy development. J. Biol. Chem. *278*, 45154-45159.

Bhat, T.N. (1988). Calculation of an OMIT map. J. Appl. Crystallogr. *21*, 279-281.

Birnboim, H.C., and Doly, J. (1979). A rapid alkaline extraction procedure for screening recombinant plasmid DNA. Nucleic Acids Res. *7*, 1513-1523.

Bradford, M.M. (1976). A rapid and sensitive method for the quantization of microgram quantities of protein utilizing the principle of protein-dye binding. Anal. Biochem. *72*, 248-254.

Bragg, W.L. (1913). The diffraction of short electromagnetic waves by a crystal. Proc. Camb. Phil. Soc. *17*, 43-57.

Bröer, S., and Krämer, R. (1991). Lysine excretion by *Corynebacterium glutamicum*. 1. Identification of a specific secretion carrier system. Eur. J. Biochem. *202*, 131-135.

Brünger, A.T., Krukowski, A., and Erickson, J.W. (1990). Slow-cooling protocols for crystallographic refinement by simulated annealing. Acta Crystallogr. A. *46*, 585-593.

Brünger, A.T. (1992). Free R value: a novel statistical quantity for assessing the accuracy of crystal structures. Nature (Lond.) *355*, 472-475.

Brünger, A.T. (1997). Patterson Correlation Search and Refinement. In Methods in Enzymology, Carter, C. W. Jr. and Sweet, R.M., eds. (San Diego; Academic Press), pp 558-580.

Brünger, A.T., Adams, P.D., Clore, G.M., DeLano, W.L., Gros, P., Grosse-Kunstleve, R.W., Jiang, J.-S., Kuszewski, J., Nilges, N., Pannu, N.S., Read, R.J., Rice, L.M., Simonson, T., and Warren, G.L. (1998). Crystallography and NMR system (CNS): A new software system for macromolecular structure determination. Acta Crystallogr. D. *54*, 905-921.

Brünger, A.T., Kuriyan, J., and Karplus, M. (1987). Crystallographic R Factor Refinement by Molecular Dynamics. Science *235*, 458-460.

Brünger, A.T. (1992). X-PLOR Version 3.1. A System for X-ray Crystallography and NMR (New Haven; Yale University Press).

Carter, C.W. Jr. (1999). Experimental design, quantitative analysis, and the cartography of crystal growth. In Crystallization of Nucleic Acids and Proteins; A Practical Approach. 2nd Ed. Ducruix, A., and Giegé, R., eds. (New York; Oxford University Press Inc.), pp 75-120.

Ceccarelli, C., Grodsky, N.B., Ariyaratne, N., Colman, R.F., and Bahnson, B.J. (2002). Crystal structure of porcine mitochondrial $NADP^+$-dependent isocitrate dehydrogenase complexed with Mn^{2+} and isocitrate. Insights into the enzyme mechanism. J. Biol. Chem. *277*, 43454-434562.

Chayen, N. E. (1997). The Role of Oil in Macromolecular Crystallisation. Structure (Camb.) *5*, 1269-1274.

Chen, R.D., and Gadal, P. (1990). Structure, functions and regulation of NAD- and NADP-dependent isocitrate dehydrogenase in higher plants and other organisms. Plant Physiol. Biochem. *28*, 411-427.

Chen, R.D., and Yang, H. (2000). A highly specific monomeric isocitrate dehydrogenase from *Corynebacterium glutamicum*. Arch. Biochem. Biophys. *383*, 238-245.

Cherbavaz, D.B., Lee, M.E., Stroud, R.M., and Koshland, D.E. Jr. (2000). Active site water molecules revealed in the 2.1 Å resolution structure of a site-directed mutant of isocitrate dehydrogenase. J. Mol. Biol. *295*, 377-385.

CCP4 (1994). The CCP4 Suite: Programs for Protein Crystallography. Acta Crystallogr. D. *50*, 760-763.

Comte, B., Vincent, G., Bouchard, B., Benderdour, M., and Des Rosiers, C. (2002). Reverse flux through cardiac $NADP^+$-isocitrate dehydrogenase under normoxia and ischemia. Am. J. Physiol. Heart. Circ. Physiol. *283*, H1505-1514.

Cortay, J.C., Bleicher, F., Rieul, C., Reeves, H.C., and Cozzone, A.J. (1988). Nucleotide sequence and expression of the *ace*K gene coding for isocitrate dehydrogenase kinase/phosphatase in *Escherichia coli*. J. Bacteriol. *170*, 89-97.

Cudney, R., Patel, S., Weisgraber, K., Newhouse, Y., and McPherson, A. (1994). Screening and optimization strategies for macromolecular crystal growth. Acta Crystallogr. A. *50*, 414-423.

Dean, A.M., Lee, M.H., and Koshland, D.E. Jr. (1989). Phosphorylation inactivates *Escherichia coli* isocitrate dehydrogenase by preventing isocitrate binding. J. Biol. Chem. *264*, 20482-20486.

Dean, A.M., and Koshland, D.E. Jr. (1990). Electrostatic and steric contributions to regulation at the active site of isocitrate dehydrogenase. Science *249*, 1044-1046.

Dean, A.M., and Koshland, D.E. Jr. (1993). Kinetic mechanism of *Escherichia coli* isocitrate dehydrogenase. Biochemistry *32*, 9302-9309.

Doyle, S.A., Beernink, P.T., and Koshland, D.E. Jr. (2001). Structural basis for a change in substrate specificity: crystal structure of S113E isocitrate dehydrogenase in a complex with isopropylmalate, Mg^{2+}, and NADP. Biochemistry *40*, 4234-4241.

Ducruix, A., and Giegé, R. (1992). Methods of crystallization. In Crystallization of Nucleic Acids and Proteins; A Practical Approach. 2nd Ed. Ducruix, A., and Giegé, R., eds. (New York; Oxford University Press Inc.), pp 121-145.

Eftink, M.R., and Shastry, M.C. (1997). Fluorescence methods for studying kinetics of protein-folding reactions. Methods Enzymol. *278*, 258-286.

Eikmanns, B.J., Rittmann, D., and Sahm, H. (1995). Cloning, sequence analysis, expression, and inactivation of the *Corynebacterium glutamicum icd* gene encoding isocitrate dehydrogenase and biochemical characterization of the enzyme. J. Bacteriol. *177*, 774-782.

Evans, S.V. (1993). SETOR: hardware lighted three dimentional solid model representations of macromolecules. J. Mol. Graphics. *11*, 134-138.

Finer-Moore, J.F., Tsutakawa, S.E., Cherbavaz, D.R., LaPorte, D.C., Koshland, D.E. Jr., and Stroud, R.M. (1997). Access to phosphorylation in isocitrate dehydrogenase may occur by domain shifting. Biochemistry *36*, 13890-13896.

Florio, W., Bottai, D., Batoni, G., Esin, S., Pardini, M., Maisetta, G., and Campa, M. (2002). Identification, molecular cloning, and evaluation of potential use of isocitrate dehydrogenase II of *Mycobacterium bovis* BCG in serodiagnosis of tuberculosis. Clin. Diagn. Lab. Immunol. *9*, 846-851.

Fremont, D.H., Hendrickson, W.A., Marrack, P., and Kappler, J. (1996). Structures of an MHC Class II Molecule with covalently bond single peptides. Science *272*, 1001-1004.

Fukunaga, N., Imagawa, S., Sahara, T., Ishii, A., and Suzuki, M. (1992). Purification and characterization of monomeric isocitrate dehydrogenase with $NADP^+$-specificity from *Vibrio parahaemolyticus*Y-4. J. Biochem. (Tokyo) *112*, 849-855.

Garcia-Ruiz, J.M., Garvira, J.A., López-Jaramillo, F.J., and Otalora, F. (2001). Crystallization screening directly in electrophoresis gels. J. Cryst. Growth. *232*, 596-602.

Garman, E.F., and Schneider, T.R. (1997). Macromolecular Cryocrystallography. J. Appl. Cryst. *30*, 211-237.

Garnak, M., and Reeves, H.C. (1979). Purification and properties of phosphorylated isocitrate dehydrogenase of *Escherichia coli*. J. Biol. Chem. *254*, 7915-7920.

Gerstmeir, R., Wendisch, V.F., Schnicke, S., Ruan, H., Farwick, M., Reinscheid, D., and Eikmanns, B.J. (2003). Acetate metabolism and its regulation in *Corynebacterium glutamicum*. J. Biotechnol. *104*, 99-122.

Grodsky, N.B., Soundar, S., and Colman, R.F. (2000). Evaluation by site-directed mutagenesis of aspartic acid residues in the metal site of pig heart NADP-dependent isocitrate dehydrogenase. Biochemistry *39*, 2193-2200.

Harding, M.M. (2001). Geometry of metal-ligand interactions in proteins. Acta Crystallogr. D. *57*, 401-411.

Harding, M.M. (2004). The architecture of metal coordination groups in proteins. Acta Crystallogr. D. *60*, 849-859.

Hartmut, M. (1991). Crystallization of membrane proteins. Hartmut, M., ed. (Boca Raton; CRC Press).

Haselbeck, R.J., Colman, R.F., and McAlister-Henn, L. (1992). Isolation and sequence of a cDNA encoding porcine mitochondrial NADP-specific isocitrate dehydrogenase. Biochemistry *31*, 6219-6223.

Higgins, D.G, Thompson, J.D., and Gilson, T.J. (1994). CLUSTAL W: improving the sensitivity of progressive multiple sequence alignment through sequence weighting, position-specific gap penalties and weight matrix choice. Nucleic Acid Res. *22*, 4673-4680.

Hodel, A., Kim, S.-H., and Brünger, A.T. (1992). Model bias in macromolecular crystal structures. Acta Crystallogr. A. *48*, 851-858.

Holms, W.H., and Nimmo, H.G. (1982). Reversible inactivation of isocitrate dehydrogenase in *Escherichia coli*. Biochem. Soc. Trans. *10*, 319-320.

Hope, H. (1988). Cryocrystallography of biological macromolecules: a generally applicable method. Acta Crystallogr. B. *44*, 22-26.

Huang, Y.C., and Colman, R.F. (2002). Evaluation by mutagenesis of the roles of His309, His315, and His319 in the coenzyme site of pig heart NADP-dependent isocitrate dehydrogenase. Biochemistry *41*, 5637-5643.

Huang, Y.C., Grodsky, N.B., Kim, T.K., and Colman, R.F. (2004). Ligands of the Mn^{2+} bound to porcine mitochondrial NADP-dependent isocitrate dehydrogenase, as assessed by mutagenesis. Biochemistry *43*, 2821-2828.

Hurley, J.H., Thorsness, P., Ramalingham, V., Halmers, N., Koshland, D. E. Jr., and Stroud, R. M. (1989). Structure of a bacterial enzyme regulated by phosphorylation, isocitrate dehydrogenase. Proc. Natl. Acad. Sci. USA. *86*, 8635-8639.

Hurley, J.H., Dean, A.M., Sohl, J.L., Koshland, D.E. Jr., and Stroud, R.M. (1990). Regulation of an enzyme by phosphorylation at the active site. Science *249*, 1012-1016.

Hurley, J.H., Dean, A.M., Koshland, D.E. Jr., and Stroud, R.M. (1991). Catalytic mechanism of $NADP^+$-dependent isocitrate dehydrogenase: implications from the structures of magnesium-isocitrate and $NADP^+$ complexes. Biochemistry *30*, 8671-8678.

Ishii, A., Ochiai, T., Imagawa, S., Fukunaga, N., Sasaki, S., Minowa, O., Mizuno, Y., and Shiokawa, H. (1987). Isozymes of isocitrate dehydrogenase from an obligately psychrophilic bacterium, *Vibrio sp*. strain ABE-1: purification, and modulation of activities by growth conditions. J. Biochem. (Tokyo) *102*, 1489-1498.

Jetten, M.S., Follettie, M.T., and Sinskey, A.J. (1994). Metabolic engineering of *Corynebacterium glutamicum*. Ann. N. Y. Acad. Sci. *721*, 12-29.

Jo, S.H., Son, M.K., Koh, H.J., Lee, S.M., Song, I.H., Kim, Y.O., Lee, Y.S., Jeong, K.S., Kim, W.B., Park, J.W., Song, B.J., Huh, T.L., and, and Huhe, T. L. (2001). Control of mitochondrial redox balance and cellular defense against oxidative damage by mitochondrial $NADP^+$-dependent isocitrate dehydrogenase. J. Biol. Chem. *276*, 16168-16176.

Kabsch, W. (1976). A solution for the best rotation to relate two sets of vectors. Acta Crystallogr. A. *32*, 922-923.

Kalinowski, J., Bathe, B., Bartels, D., Bischoff, N., Bott, M., Burkovski, A., Dusch, N., Eggeling, L., Eikmanns, B.J., Gaigalat, L., Goesmann, A., Hartmann M, Huthmacher, K., Kramer, R., Linke, B., McHardy, A.C., Meyer, F., Mockel, B., Pfefferle, W., Puhler, A., Rey, D.A., Ruckert, C., Rupp, O., Sahm, H., Wendisch, V.F., Wiegrabe, I., and Tauch, A. (2003). The complete *Corynebacterium glutamicum* ATCC 13032 genome sequence and its impact on the production of L-aspartate-derived amino acids and vitamins. J. Biotechnol. *104*, 5-25.

Kiefer, P., Heinzle, E., Zelder, O., and Wittmann, C. (2004). Comparative metabolic flux analysis of lysine-producing *Corynebacterium glutamicum* cultured on glucose or fructose. Appl. Environ. Microbiol. *70*, 229-239.

Kim, T.-K., Lee, P., and Colman, R. F. (2003). Critical Role of Lys212 and Tyr140 in Porcine NADP-dependent Isocitrate Dehydrogenase. J. Biol. Chem. *278*, 49323-49331.

Kleywegt, G.J. and Brunger, A.T. (1996). Checking your imagination: Applications of the free R value. Structure (Camb.) *4*, 897-904.

Kleywegt, G.J., and Jones, T.A. (!998). Databases in protein crystallography. Acta Crystallogr. D. 54, 1119-31

Kwong, P.D., and Liu, Y. (1999). Use of cryoprotectants in combination with immiscible oils for flash cooling macromolecular crystals. J. Appl. Cryst. *32*, 102-105.

LaPorte, D.C., and Koshland, D.E. Jr. (1983). Phosphorylation of isocitrate dehydrogenase as a demonstration of enhanced sensitivity in covalent regulation. Nature *305*, 286-290.

LaPorte, D.C., and Chung, T. (1985). A single gene codes for the kinase and phosphatase which regulate isocitrate dehydrogenase. J. Biol. Chem. *260*, 15291-15297.

LaPorte, D.C., Thorsness, P.E., and Koshland, D.E. Jr. (1985). Compensatory phosphorylation of isocitrate dehydrogenase. A mechanism for adaptation to the intracellular environment. J. Biol. Chem. *260*, 10563-10568.

LaPorte, D.C. (1993). The isocitrate dehydrogenase phosphorylation cycle: regulation and enzymology. J. Cell. Biochem. *51*, 14-18.

Laskowski, R.A., MacArthur, M.W., Moss, D.S., and Thornton, J.M. (1993). PROCHECK: a program to check the stereochemical quality of protein structures. J. Appl. Cryst. *26*, 283-291.

Lee, J.H., Yang, E.S. and Park, J.-W. (2003). Inactivation of $NADP^+$-dependent Isocitrate Dehydrogenase by Perosynitrite. Implications for cytotoxicity and alcohol-induced liver injury. J. Biol. Chem. *278*, 51360-51371.

Lee, M.E., Dyer, D.H., Klein, O.D., Bolduc, J.M., Stoddard, B.L., and Koshland, D.E. Jr. (1995). Mutational analysis of the catalytic residues lysine 230 and tyrosine 160 in the $NADP^+$-dependent isocitrate dehydrogenase from *Escherichia coli*. Biochemistry *34*, 378-384.

Lee, P., and Colman, R.F. (2002). Implication by site-directed mutagenesis of Arg314 and Tyr316 in the coenzyme site of pig mitochondrial NADP-dependent isocitrate dehydrogenase. Arch. Biochem. Biophys. *401*, 81-90.

Lee, S.M., Koh, H.J., Huh, T.L., and Park, J.W. (1999). Radiation sensitivity of an *Escherichia coli* mutant lacking $NADP^+$-dependent isocitrate dehydrogenase. Biochem. Biophys. Res. Commun. *254*, 647-650.

Lee, S.M., Huh, T.L., and Park, J.W. (2001). Inactivation of $NADP^+$-dependent isocitrate dehydrogenase by reactive oxygen species. Biochimie. *83*, 1057-1065.

Lee, S.M., Koh, H.J., Park, D.C., Song, B.J., Huh, T.L., and Park, J.W. (2002). Cytosolic $NADP^+$-dependent isocitrate dehydrogenase status modulates oxidative damage to cells. Free Radical Biol. Med. *32*, 1185-1196.

Lopez-Jaramillo, F.J., Gracia-Ruiz, J.M., Gevira, J.A., and Otalora, F. (2001). Crystallization and cryocrytallography inside X-ray cappillaries. J. Appl. Cryst. *34*, 365-370.

Luzzatti, P.V. (1952). Traitement Statistique des Erreurs dans la Determination des Structures Cristallines. Acta Crystallog. *5*, 802-810.

Matthews, B.W. (1968). Solvent content of protein crystals. J. Mol. Biol. *33*, 491-497.

McCammon, M.T., Epstein, C.B., Przybyla-Zawislak, B., McAlister-Henn, L., and Butow, R.A. (2003). Global transcription analysis of Krebs tricarboxylic acid cycle mutants reveals an alternating pattern of gene expression and effects on hypoxic and oxidative genes. Mol. Biol. Cell. *14*, 958-972.

McRee, D.E. (1993). Practical Protein Crystallography. McRee, D.E. ed. (San Diego; Academic Press), pp21-28, 37-61, 145-166, and 172-180.

Merelo, J.J., Andrade, M.A. , Prieto, A., and Morán, F. (1994). Proteinotopic Feature Maps. Neurocomputing *6*, 443-454.

Mesecar, A.D., Stoddard, B.L., and Koshland, D.E. Jr. (1997). Orbital steering in the catalytic power of enzymes: small structural changes with large catalytic consequences. Science *277*, 202-206.

Miller, J.H. (1972) Experiments in Molecular Genetics. Cold Spring Harbor Laboratory, Cold Spring Harbor, NY.

Nelson, M., and McClelland, M. (1992). Use of DNA methyltransferase/endonuclease enzyme combinations for megabase mapping of chromosomes. Methods Enzymol. *216*, 279-303.

Nicholls, A., Sharp, K., and Honig, B., (1991). Protein Folding and Association: Insights From the Interfacial and Thermodynamic Properties of Hydrocarbons. Proteins *11*, 281-96

Norman, F.M.H, and Lonsdale, K. (1976). International Tables for X-ray Crystallography, Volume I Symmetry Groups, Norman, F.M.H, and Lonsdale, K. eds. 3rd ed. (Birmingham, England; The Kynoch Press), pp 6-12.

Ochiai, T., Fukunaga, N., and Sasaki, S. (1979). Purification and some properties of two $NADP^+$-specific isocitrate dehydrogenases from an obligately psychrophilic marine bacterium, *Vibrio sp.*, strain ABE-1. J. Biochem. (Tokyo) *86*, 377-384.

Ohman, R., and Ridell, M. (1996). Purification and characterisation of isocitrate dehydrogenase and malate dehydrogenase from *Mycobacterium tuberculosis* and evaluation of their potential as suitable antigens for the serodiagnosis of tuberculosis. Tubercule. Lung Dis. *77*, 454-461.

Ohnishi, J., Mitsuhashi, S., Hayashi, M., Ando, S., Yokoi, H., Ochiai, K., and Ikeda, M. (2002). A novel methodology employing *Corynebacterium glutamicum* genome information to generate a new L-lysine-producing mutant. Appl. Microbiol. Biotechnol. *58*, 217-223.

Otwinowski, Z., and Minor, W. (1997). Processing of X-Ray Diffraction Data Collected in Oscillation Mode. In Methods in Enzymology; Macromolecular Crystallography Part A, Carter, C.W.Jr., and Sweet R.M., eds. (San Diego, Academic Press), pp 307-325.

Ramakrishnan, C., and Ramachandran, G.N. (1965). Stereochemical criteria for polypeptide and protein chain conformations. II. Allowed conformations for a pair of peptide units. Biophys. J. *5*, 909-933.

Read, R.J. (1986). Improved Fourier coefficients for maps using phases from partial structures with errors. Acta Crystallogr. A. *42*, 140-149.

Reeves, H.C., and Malloy, P.J. (1982). The phosphorylation of isocitrate dehydrogenase in *Escherichia coli*. Biochem. Soc. Trans. *10*, 321-322.

Riboldi-Tunnicliffe, A., and Hilgenfeld, R. (1999). Crystallography with oil -an old idea revived-. J. Appl. Cryst. *32*, 1003-1005.

Roussel, A., Fontecilla-Camps, J.C., and Cambillau, C. (1990). TURBO-FRODO: A new program for protein crystallography and modelling. Acta Crystallogr. A. *46*, C66.

Robert, M.-C., Vidal, O., Garcia-Ruiz, J.-M., and Otalora, F. (1999). Crystallization in gels and related methods. In Crystallization of Nucleic Acids and Proteins; A Practical Approach. 2nd Ed. Ducruix, A., and Giegé, R., eds. (New York; Oxford University Press Inc.), pp 149-177.

Sahara, T., Takada, Y., Takeuchi, Y., Yamaoka, N., and Fukunaga, N. (2002). Cloning, sequencing, and expression of a gene encoding the monomeric isocitrate dehydrogenase of the nitrogen-fixing bacterium, *Azotobacter vinelandii*. Biosci. Biotechnol. Biochem. *66*, 489-500.

Seery, V.L., and Farrell, H.M. Jr. (1990). Spectroscopic evidence for ligand-induced conformational change in $NADP^+$:isocitrate dehydrogenase. J. Biol. Chem. *265*, 17644-176448.

Soundar, S., Danek, B.L., and Colman, R.F. (2000). Identification by mutagenesis of arginines in the substrate binding site of the porcine NADP-dependent isocitrate dehydrogenase. J. Biol. Chem. *275*, 5606-5612.

Sousa, R. (1995). Use of glycerol, polyols and other protein structure stabilizing agents in protein crystallization. Acta Crystallogr. A. *51*, 271-277.

Steen, I.H., Madsen, M.S., Birkeland, N.K., and Lien, T. (1998). Purification and characterization of a monomeric isocitrate dehydrogenase from the sulfate-reducing bacterium *Desulfobacter vibrioformis* and demonstration of the presence of a monomeric enzyme in other bacteria. FEMS Microbiol. Lett. *160*, 75-79.

Stoddard, B.L., and Koshland, D.E. Jr. (1993). Structure of isocitrate dehydrogenase with alpha-ketoglutarate at 2.7-Å resolution: conformational changes induced by decarboxylation of isocitrate. Biochemistry *32*, 9317-9322.

Stoddard, B.L., Dean, A.M., and Koshland, D.E. Jr. (1993). Structure of isocitrate dehydrogenase with isocitrate, nicotinamide adenine dinucleotide phosphate, and calcium at 2.5-Å resolution: a pseudo-Michaelis ternary complex. Biochemistry *32*, 9310-9316.

Stueland, C.S., Eck, K.R., Stieglbauer, K.T., and LaPorte, D.C. (1987). Isocitrate dehydrogenase kinase/phosphatase exhibits an intrinsic adenosine triphosphatase activity. J. Biol. Chem. *262*, 16095-16099.

Suzuki, M., Sahara, T., Tsuruha, J., Takada, Y., and Fukunaga, N. (1995). Differential expression in *Escherichia coli* of the *Vibrio sp*. strain ABE-1 *icd*I and *icd*II genes encoding structurally different isocitrate dehydrogenase isozymes. J. Bacteriol. *177*, 2138-2142.

Tauch, A., Homann, I., Mormann, S., Ruberg, S., Billault, A., Bathe, B., Brand, S., Brockmann-Gretza, O., Ruckert, C., Schischka, N., Wrenger, C., Hoheisel, J., Mockel, B., Huthmacher, K., Pfefferle, W., Puhler, A., and Kalinowski J. (2002). Strategy to sequence the genome of *Corynebacterium glutamicum* ATCC 13032: use of a cosmid and a bacterial artificial chromosome library. J. Biotechnol. *95*, 25-38.

Thorsness, P.E., and Koshland, D.E. Jr. (1987). Inactivation of isocitrate dehydrogenase by phosphorylation is medeiated by the negative charge of the phosphate. J. Biol. Chem. *262*, 10422-10425.

Wallon, G., Lovett, S.T., Magyar, C., Svingor, A., Szilagyi, A., Zavodszky, P., Ringe, D., and Petsko, G.A. (1997) Sequence and homology model of 3-isopropylmalate dehydrogenase from the psychrotrophic bacterium *Vibrio* sp. I5 suggest reasons for thermal instability. Protein Eng. *10*, 665-672.

Wang, W., and Malcolm, B.A. (1999). Two-stages PCR protocol allowing introduction of multiple mutations, deletions and insertions using Quickchange site directed mytagenesis. Biotechnol. Tech. *26*, 680-682.

Weber, P.C. (1997). Overview of Protein Crystallization Methods. In Methods in Enzymology; Macromolecular Crystallography Part A. Carter, C. W. Jr. and Sweet R. M., eds. (San Diego; Academic Press), pp13-22.

Xu, X., Zhao, J., Xu, Z., Peng, B., Huang, Q., Arnold, E., and Ding, J. (2004). Structures of human cytosolic NADP-dependent isocitrate dehydrogenase reveal a novel self-regulatory mechanism of activity. J. Biol. Chem. *279*, 33046-33957.

Yang, E.S., Richter, C., Chun, J.S., Huh, T.L., Kang, S.S., and Park, J.W. (2002). Inactivation of $NADP^+$-dependent isocitrate dehydrogenase by nitric oxide. Free Radical Biol. Med. *33*, 927-937.

Yasutake, Y., Watanabe, S., Yao, M., Takada, Y., Fukunaga, N., and Tanaka, I . (2002). Structure of the monomeric isocitrate dehydrogenase. Evidence of a protein monomerization by a domain duplication. Structure (Camb.) *10*, 1637-1648.

Yasutake, Y., Watanabe, S., Yao, M., Takada, Y., Fukunaga, N., and Tanaka, I. (2003). Crystal structure of the monomeric isocitrate dehydrogenase in the presence of $NADP^+$; insight into the cofactor recognition, catalysis and evolution. J. Biol. Chem. *278*, 36897-36904.

Yoshihara, T., Hamamoto, T., Munakata, R., Tajiri, R., Ohsumi, M., and Yokota, S. (2001). Localization of cytosolic NADP-dependent isocitrate dehydrogenase in the perioxisomes of rat liver cells; Biochemical and immunocytochemical studies. J. Histochem. Cytochem. *49*, 1123-11131.